International Benchmark on Pressurised Water Reactor Sub-channel and Bundle Tests

Volume III: Departure from nucleate boiling

OECD

BETTER POLICIES FOR BETTER LIVES

NEA

NUCLEAR ENERGY AGENCY

Nuclear Science
Nuclear Safety and Regulation

International Benchmark based on Pressurised Water Reactor Sub-channel and Bundle Tests

Volume III: Departure from Nucleate Boiling

ORGANISATION FOR ECONOMIC CO-OPERATION AND DEVELOPMENT

The OECD is a unique forum where the governments of 34 democracies work together to address the economic, social and environmental challenges of globalisation. The OECD is also at the forefront of efforts to understand and to help governments respond to new developments and concerns, such as corporate governance, the information economy and the challenges of an ageing population. The Organisation provides a setting where governments can compare policy experiences, seek answers to common problems, identify good practice and work to co-ordinate domestic and international policies.

The OECD member countries are: Australia, Austria, Belgium, Canada, Chile, the Czech Republic, Denmark, Estonia, Finland, France, Germany, Greece, Hungary, Iceland, Ireland, Israel, Italy, Japan, Korea, Luxembourg, Mexico, the Netherlands, New Zealand, Norway, Poland, Portugal, the Slovak Republic, Slovenia, Spain, Sweden, Switzerland, Turkey, the United Kingdom and the United States. The European Commission takes part in the work of the OECD.

OECD Publishing disseminates widely the results of the Organisation's statistics gathering and research on economic, social and environmental issues, as well as the conventions, guidelines and standards agreed by its members.

NUCLEAR ENERGY AGENCY

The OECD Nuclear Energy Agency (NEA) was established on 1 February 1958. Current NEA membership consists of 31 countries: Australia, Austria, Belgium, Canada, the Czech Republic, Denmark, Finland, France, Germany, Greece, Hungary, Iceland, Ireland, Italy, Japan, Korea, Luxembourg, Mexico, the Netherlands, Norway, Poland, Portugal, Russia, the Slovak Republic, Slovenia, Spain, Sweden, Switzerland, Turkey, the United Kingdom and the United States. The European Commission also takes part in the work of the Agency.

The mission of the NEA is:

– to assist its member countries in maintaining and further developing, through international co-operation, the scientific, technological and legal bases required for a safe, environmentally friendly and economical use of nuclear energy for peaceful purposes;

– to provide authoritative assessments and to forge common understandings on key issues, as input to government decisions on nuclear energy policy and to broader OECD policy analyses in areas such as energy and sustainable development.

Specific areas of competence of the NEA include the safety and regulation of nuclear activities, radioactive waste management, radiological protection, nuclear science, economic and technical analyses of the nuclear fuel cycle, nuclear law and liability, and public information.

The NEA Data Bank provides nuclear data and computer program services for participating countries. In these and related tasks, the NEA works in close collaboration with the International Atomic Energy Agency in Vienna, with which it has a Co-operation Agreement, as well as with other international organisations in the nuclear field.

Foreword

The need to refine models for best-estimate calculations, based on good-quality experimental data, has been expressed in many recent meetings in the field of nuclear applications. The needs arising in this respect should not be limited to the currently available macroscopic methods but should be extended to next-generation analysis techniques that focus on more microscopic processes. One of the most valuable databases identified for the thermal-hydraulics modelling was developed by the Nuclear Power Engineering Corporation (NUPEC), Japan, which includes sub-channel void fraction and departure from nucleate boiling (DNB) measurements in a representative Pressurised Water Reactor (PWR) fuel assembly. Part of this database has been made available for this international benchmark activity entitled "NUPEC PWR Sub-channel and Bundle Tests (PSBT) benchmark". This international project has been officially approved by the Japanese Ministry of Economy, Trade, and Industry (METI), the US Nuclear Regulatory Commission (NRC) and endorsed by the NEA.

The JNES has made available the PWR NUPEC database for the purposes of the NEA/NRC PSBT international benchmark and has asked PSU to organise and conduct this benchmark activity. The NEA/NRC PSBT benchmark was announced at the sixth and last workshop for the NEA/NRC Benchmark based on NUPEC BWR Full-size Fine-mesh Bundle Tests (BFBT-6), which was held on 27-28 April 2009 in University Park/State College, PA, US. The presentation of the new benchmark included the benchmark database, specification and schedule. Three PSBT workshops have taken place since then. The first workshop (PSBT-1) was hosted by the San Piero a Grado Nuclear Research Group, University of Pisa, Italy in April 2010. The PSBT-2 workshop was hosted by the Royal Institute of Technology (Kungliga Tekniska Högskolan, KTH), Sweden in April 2011. The third and last workshop (PSBT-3) was held in conjunction with the 14th International Topical Meeting on Nuclear Reactor Thermal Hydraulics (NURETH-14), Toronto, Canada on 25 September 2011.

Volume I of the NEA/NRC PSBT Benchmark: *Experimental Database and Final Problem Specifications* was distributed to the benchmark participants and the NEA in January 2010. The NEA/NRC PSBT was designed to provide a data set for evaluation of the abilities of existing sub-channel, system, and Computational Fluid Dynamics (CFD) thermal-hydraulics codes to predict void distribution and Departure from Nucleate Boiling (DNB) in PWRs under steady-state and transient conditions. The benchmark consists of seven exercises divided into two phases, a void distribution benchmark and a DNB benchmark. A specification was created to distribute experimental information to the participants. In addition, two studies were performed to determine the reliability of the experimental data.

Volume II of the NEA/NRC PSBT Benchmark: *Benchmark Results for the Void Distribution Phase* summarises the results of Phase I, which was focused on an assessment and validation of void generation and distribution models in CFD codes; sub-channel thermal-hydraulic codes and system thermal-hydraulic codes.

Volume III of the NEA/NRC PSBT Benchmark: *Benchmark Results for the Departure from Nucleate Boiling Phase* summarises the results of Phase II, which was designed to assess and validate the models for DNB prediction under steady-state and transient PWR conditions.

Acknowledgements

Table of contents

List of figures

List of tables

Executive summary

This report summarised the second phase of the Nuclear Energy Agency (NEA) and the Nuclear Regulatory Commission (NRC) Benchmark Based on NUPEC PWR Sub-channel and Bundle Tests (PSBT), which was intended to provide data for the verification of Departure from Nucleate Boiling (DNB) prediction in existing thermal-hydraulics codes and provide direction in the development of future methods. This phase was composed of three exercises; Exercise 1: fluid temperature benchmark, Exercise 2: steady-state rod bundle benchmark and Exercise 3: transient rod bundle benchmark.

The experimental data provided to the participants of this benchmark is from a series of void measurement tests using full-size mock-up tests for both BWRs and PWRs. These tests were performed from 1987 to 1995 by the Nuclear Power Engineering Corporation (NUPEC) in Japan and made available by the Japan Nuclear Energy Safety Organisation (JNES) for the purposes of this benchmark, which was organised by Pennsylvania State University.

Nine institutions from seven countries participated in this benchmark. Nine different computer codes were used in Exercise 1, 2 and 3. Among the computer codes were porous-media, sub-channel and systems thermal-hydraulic code.

The improvement between FLICA-OVAP (sub-channel) and FLICA (sub-channel) was noticeable. The main difference between the two was that FLICA-OVAP implicitly assigned flow regime based on drift flux, while FLICA assumes single phase flows. In Exercises 2 and 3, the codes were generally able to predict the Departure from Nucleate Boiling (DNB) power as well as the axial location of the onset of DNB (for the steady-state cases) and the time of DNB (for the transient cases). It was noted that the codes that used the Electric-Power-Research-Institute (EPRI) Critical-Heat-Flux (CHF) correlation had the lowest mean error in Exercise 2 for the predicted DNB power.

Chapter 1
Introduction

1.1 Introduction

Recently, the need to refine models for best-estimate calculations based on good-quality experimental data has arisen for various nuclear applications. One of the most extensive and valuable databases available was developed by the Nuclear Power Engineering Corporation (NUPEC) of Japan, consisting of both void distribution and Departure from Nucleate Boiling (DNB) data for a representative Pressurised Water Reactor (PWR) fuel assembly. A part of this database has been made available for the PWR Sub-channel and Bundle Tests (PSBT) benchmark. This benchmark follows the highly successful BWR Full-size Fine-mesh Bundle Tests (BFBT) benchmark.

1.2 Benchmark Objective

The objective of the benchmark was twofold. First, the benchmark aimed to evaluate currently available computational approaches in an effort to understand the strengths and weaknesses of current thermal-hydraulic codes. Second, the benchmark was intended to encourage the development of the next generation of approaches that focus more on microscopic processes.

1.3 Definition of Benchmark Phases

The PSBT benchmark was divided into two separate phases, with each consisting of individual exercises. Table 1.3-1 presents the structure of the benchmark phases and a map showing which test series are included in each exercise.

Table 1.3-1 PSBT Benchmark

Items of Data	Test Series
Void fraction measurements data	
- Steady-state void fraction in sub-channel by CT measurement	1, 2, 3, 4
- Steady-state void distribution image in sub-channel by CT measurement	1, 2
- Steady-state void fraction in rod bundle by chordal measurement	5, 6, 7, 8
- Steady-state void distribution image in rod bundle by chordal measurement	5, 6, 7, 8
- Transient void fraction in rod bundle by chordal measurement	5T, 6T, 7T
DNB measurements data	
- Steady-state DNB data in rod bundle	0, 2, 3, 4, 8, 13
- Steady-state DNB detected location in rod bundle	4, 8, 13
- Steady-state fluid temperature distribution in rod bundle	1
- Transient DNB data in rod bundle	11T, 12T

1.3.1 Phase I – Void Distribution Benchmark

Exercise 1 – Steady-state single sub-channel benchmark. These test cases involved predicting void distribution in a single sub-channel under steady-state conditions.

Exercise 2 – Steady-state bundle benchmark. These test cases involved predicting void distribution in a bundle under steady-state conditions.

Exercise 3 – Transient bundle benchmark. These test cases involved predicting void distribution in a bundle under transient conditions.

Exercise 4 – Pressure drop benchmark. These test cases involved predicting the axial pressure drop across a bundle.

1.3.2 Phase II – Departure from Nucleate Boiling (DNB) Benchmark

Exercise 1 – Steady-state fluid temperature benchmark. These test cases involved predicting fluid temperatures at the exit of the heated section of a bundle.

Exercise 2 – Steady-state DNB benchmark. These test cases involved predicting DNB in a bundle under steady-state conditions.

Exercise 3 – Transient DNB benchmark. These test cases involved predicting DNB in a bundle under transient conditions.

1.4 Benchmark Team and Sponsorship

The benchmark activities were performed as an international project supported by USNRC and METI (Japan), and endorsed by the NEA. The benchmark team is organised based on the collaboration between the US and Japan as shown in Figure 1.4-1.

Figure 1.4-1 PSBT Benchmark Team
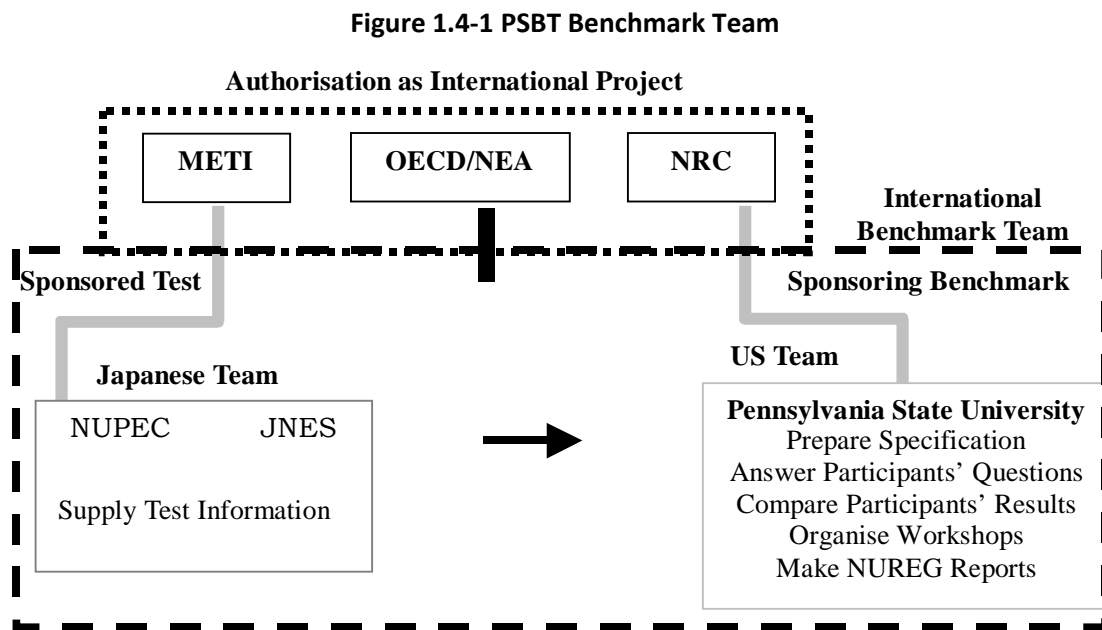
There were a total of nine (9) participants in Phase II. Table 1.4-1 summarises these participants, as well as the exercises in which they participated. It should be noted that some participants submitted results for multiple codes, which are summarised in each exercise.

Table 1.4-1 List of Phase I Participants

Participant	Abbreviation	Country	Exercise II-1	Exercise II-2	Exercise II-3
Commissariat à l'énergie atomique et aux énergies alternatives (Grenoble)	CEA-Grenoble	France	Yes	Yes	No
Commissariat à l'énergie atomique et aux énergies alternatives (Saclay)	CEA-Saclay	France	Yes	Yes	Yes
Électricité de France	EDF	France	Yes	Yes	Yes
Korea Atomic Energy Research Institute	KAERI	Korea	Yes	Yes	Yes
Karlsruhe Institute of Technology	KIT	Germany	Yes	Yes	Yes
Kungliga Tekniska högskolan	KTH	Sweden	No	Yes	Yes
McMaster University	McMaster	Canada	Yes	Yes	Yes
Nuclear Research Institute Rex plc	NRI	Czech Republic	Yes	Yes	Yes
Paul Scherrer Institut	PSI	Switzerland	Yes	Yes	Yes

1.5 Report Outline

This report presents the final results of the three exercises of Phase II: Departure from Nucleate Boiling of the NEA/NRC PSBT benchmark.

Chapter 1 discusses the main objectives of the international NEA/NRC PSBT benchmark. A definition of the benchmark phases and exercises is provided.

Chapter 2 discusses the NUPEC PWR PSBT facility and the specific methods used in the DNB measurements.

Chapter 3 presents comparative analyses of submitted final results for the three exercises of Phase II: fluid temperature results, steady-state DNB results, and transient DNB results.

Chapter 4 concludes the activities performed on the DNB benchmark and discusses the major observations.

Appendix I contains the full set of code-to-data comparisons for Exercise I-1: Steady-state single sub-channel benchmark.

Appendix II contains the full set of code-to-data comparisons for Exercise I-2: Steady-state bundle benchmark.

Appendix III contains the full set of code-to-data comparisons for Exercise I-3: Transient bundle benchmark.

Appendix IV gives detailed description of the modelling approaches utilised by the participants.

Chapter 2
Departure from Nucleate Boiling (DNB) Benchmark

2.1 General

The second phase of the PSBT Benchmark was intended to provide data for the verification of DNB prediction in existing thermal-hydraulics codes and provide direction in the development of future methods. This phase was composed of three exercises: a fluid temperature benchmark, a steady-state rod bundle benchmark, and a transient rod bundle benchmark.

2.2 Test Facility

The void distribution and DNB measurements took place at the NUPEC test facility shown in Figure 2.2-1. The facility is able to simulate the conditions found in PWRs. The same test loop was used for both benchmark phases, but different test sections were constructed to simulate single sub-channels and complete rod bundles. The range of operating conditions for the facility is given in Table 2.2-1 and the operating conditions for the four transient scenarios are given in Table 2.2-2.

Figure 2.2-1 NUPEC Test Facility
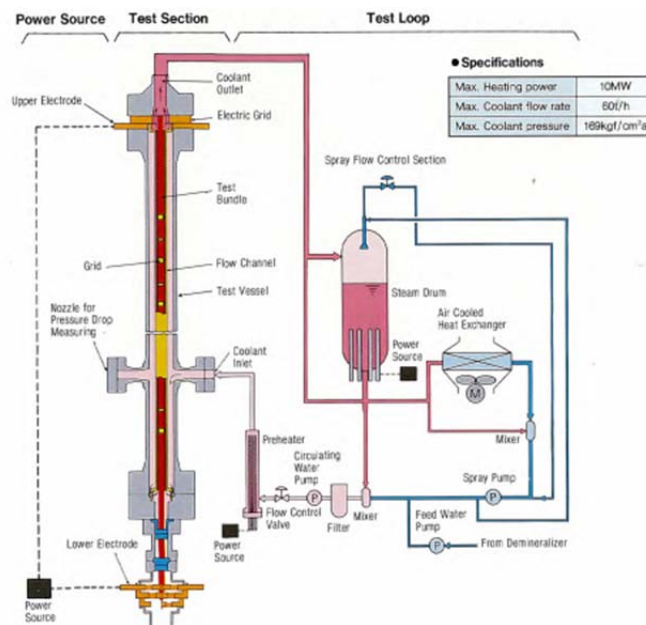
Table 2.2-1 Range of NUPEC PWR Test Facility Operating Conditions

Quantity	Range
Pressure	4.9 – 16.6 MPa
Mass Velocity	550 – 4150 kg/m²s
Inlet Coolant Temperature	140 – 345°C

Table 2.2-2 Transient Parameters of NUPEC PWR Test Facility

Transient Scenario	Transient Change
Depressurisation	-0.03 MPa/s
Temperature Increase	1°C/s
Flow Reduction	-25%/s
Power Increase	15%/s

2.2.1 Rod Bundle Test Section and Assemblies

Figure 2.2.1-1 shows the test section used for the bundle void distribution and DNB measurements. The heated section is 3.658 m long, beginning 630 mm above the bottom of the pressure vessel, with measurement locations at 2.216 m, 2.669 m, and 3.177 m from the start of the heated section. The coolant flows horizontally into the section inlet, then down through a downcomer section before turning vertically up through the test section.
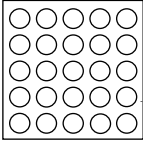
According to experimental data, the area between the downcomer and test section was fully insulated so there would not be heat transfer between the two flows.

Table 2.2.1-1, Table 2.2.1-2, and Table 2.2.1-3 provide information about the assemblies used in the DNB portion of the benchmark. The spacer grids and heater rods used in these assemblies are the same as those used in the assemblies for the void distribution benchmark (see Figure 2.2.1.1-1, Figure 2.2.1.1-2, Figure 2.2.1.1-3, Figure 2.2.1.2-1).

Figure 2.2.1-1 Test Section for Rod Bundle Void Distribution and DNB Measurement
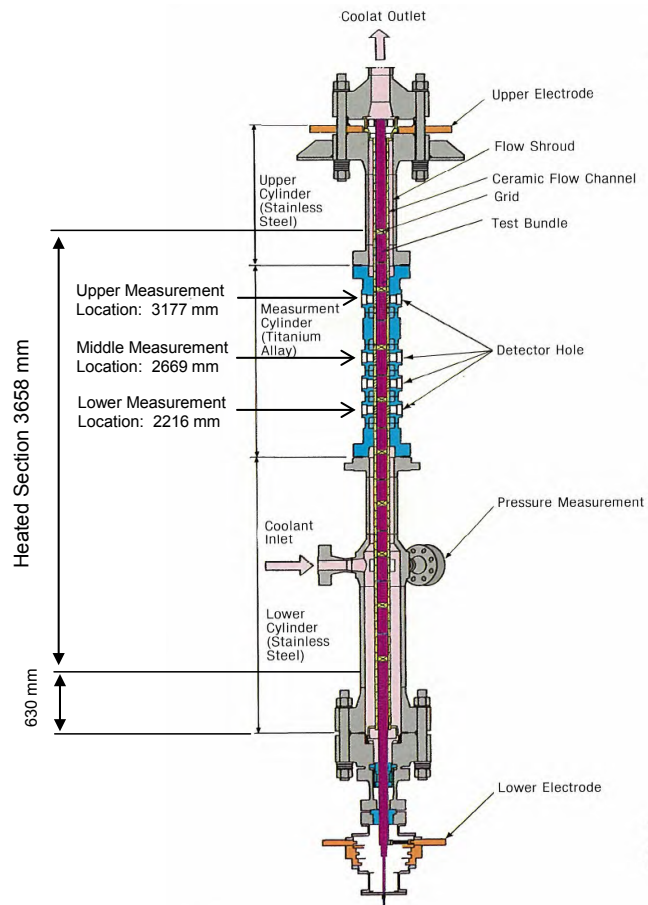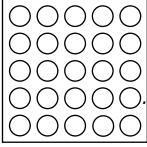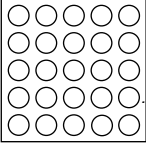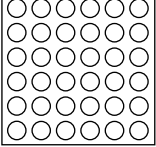
Table 2.2.1-1 Assembly Data for Assembly A0

Item	Data
Assembly	**A0**
Rods array	5×5
Number of heated rods	25
Number of thimble rods	0
Heated rod outer diameter (mm)	9.50
Thimble rod outer diameter (mm)	-
Heated rods pitch (mm)	12.60
Axial heated length (mm)	3658
Flow channel inner width (mm)	64.9
Radial power shape	A
Axial power shape	Uniform
Number of MV spacers	5
Number of NMV spacers	2
Number of simple spacers	6
MV spacer location (mm)	610, 1219, 1829, 2438, 3048
NMV spacer location (mm)	0, 3658
Simple spacer location (mm)	305, 914, 1524, 2134, 2743, 3353
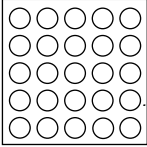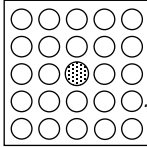
◯ : Heated rod ⊛Thimble rod MV: Mixing vane, NMV: No mixing vane

Spacer location is distance from bottom of heated length to spacer bottom face.

Table 2.2.1-2 Assembly Data for Assemblies A1, A2, A3

Item	Data		
Assembly	A1	A2	A3
Rods array	5×5	5×5	6×6
Number of heated rods	25	25	36
Number of thimble rods	0	0	0
Heated rod outer diameter (mm)	9.50	9.50	9.50
Thimble rod outer diameter (mm)	-	-	-
Heated rods pitch (mm)	12.60	12.60	12.60
Axial heated length (mm)	3658	3658	3658
Flow channel inner width (mm)	64.9	64.9	77.5
Radial power shape	C	A	D
Axial power shape	Uniform	Uniform	Uniform
Number of MV spacers	7	7	7
Number of NMV spacer	2	2	2
Number of simple spacers	8	8	8
MV spacer location (mm)	457, 914, 1372, 1829, 2286, 2743, 3200		
NMV spacer location (mm)	0, 3658		
Simple spacer location (mm)	229, 686, 1143, 1600, 2057, 2515, 2972, 3429		

Table 2.2.1-3 Assembly Data for Assemblies A4, A8, A11, A12

Item	Data	
Assembly	A4, A11	A8, A12
Rods array	5×5	5×5
Number of heated rods	25	24
Number of thimble rods	0	1
Heated rod outer diameter (mm)	9.50	9.50
Thimble rod outer diameter (mm)	-	12.24
Heated rods pitch (mm)	12.60	12.60
Axial heated length (mm)	3658	3658
Flow channel inner width (mm)	64.9	64.9
Radial power shape	A	B
Axial power shape	Cosine	Cosine
Number of MV spacers	7	7
Number of NMV spacer	2	2
Number of simple spacers	8	8
MV spacer location (mm)	471, 925, 1378, 1832, 2285, 2739, 3247	
NMV spacer location (mm)	2.5, 3755	
Simple spacer location (mm)	237, 698, 1151, 1605, 2059, 2512, 2993, 3501	

Figure 2.2.1-2 Radial Power Distribution A

0.85	0.85	0.85	0.85	0.85
0.85	1.00	1.00	1.00	0.85
0.85	1.00	1.00	1.00	0.85
0.85	1.00	1.00	1.00	0.85
0.85	0.85	0.85	0.85	0.85

Figure 2.2.1-3 Radial Power Distribution B

0.85	0.85	0.85	0.85	0.85
0.85	1.00	1.00	1.00	0.85
0.85	1.00	0.00	1.00	0.85
0.85	1.00	1.00	1.00	0.85
0.85	0.85	0.85	0.85	0.85

Figure 2.2.1-4 Radial Power Distribution C

1.00	1.00	0.25	0.25	0.25
1.00	1.00	1.00	0.25	0.25
1.00	1.00	0.25	0.25	0.25
1.00	1.00	1.00	0.25	0.25
1.00	1.00	0.25	0.25	0.25

Figure 2.2.1-5 Radial Power Distribution D

0.85	0.85	0.85	0.85	0.85	0.85
0.85	1.00	1.00	1.00	1.00	0.85
0.85	1.00	1.00	1.00	1.00	0.85
0.85	1.00	1.00	1.00	1.00	0.85
0.85	1.00	1.00	1.00	1.00	0.85
0.85	0.85	0.85	0.85	0.85	0.85

Table 2.2.1-4 Cosine Axial Power Distribution

Node	Relative Power
(*Bottom*)	
1	0.42
2	0.47
3	0.56
4	0.67
5	0.80
6	0.94
7	1.08
8	1.22
9	1.34
10	1.44
11	1.51
12	1.55
13	1.55
14	1.51
15	1.44
16	1.34
17	1.22
18	1.08
19	0.94
20	0.80
21	0.67
22	0.56
23	0.47
24	0.42
(*Top*)	

2.2.1.1 Spacer Grid Data

There were three types of spacers instrumented along the axial length: simple spacer (SS), spacer with no mixing vanes (NMV), and spacer with mixing vanes (MV). The simple spacer has only dimples while NMV and MV have dimples and springs. The grids straps are made out of Inconel 600 alloy. Detailed geometrical description of the grids used in the experiment was not available to the

benchmark. As a result, the benchmark team, with the assistance of a benchmark participant, was forced to develop a grid model based on the understanding that the grids used in the experiments were similar to grids for which data was readily available. Table 2.2.1.1-1 summarises the grid data that was available as part of the benchmark. Figure 2.2.1.1-1, Figure 2.2.1.1-2 and Figure 2.2.1.1-3 provide three-dimensional views of the simple spacer, non-mixing vane, and mixing vane grids. The simple spacer has dimples while the mixing vane and non-mixing vane grids have both dimples and springs. These dimples provide a gap (~0.1) around each heating rod, which prevents bowing of these rods when they linearly expand at high temperatures.

Table 2.2.1.1-1 provides the bundle average spacer pressure loss coefficients for the three types of grids. Depending on the participants' computer code, and using the provided spacer data, each participant may choose the sub-channel grids loss coefficients or other required input values.

Figure 2.2.1.1-1 View of Simple Spacer Grid
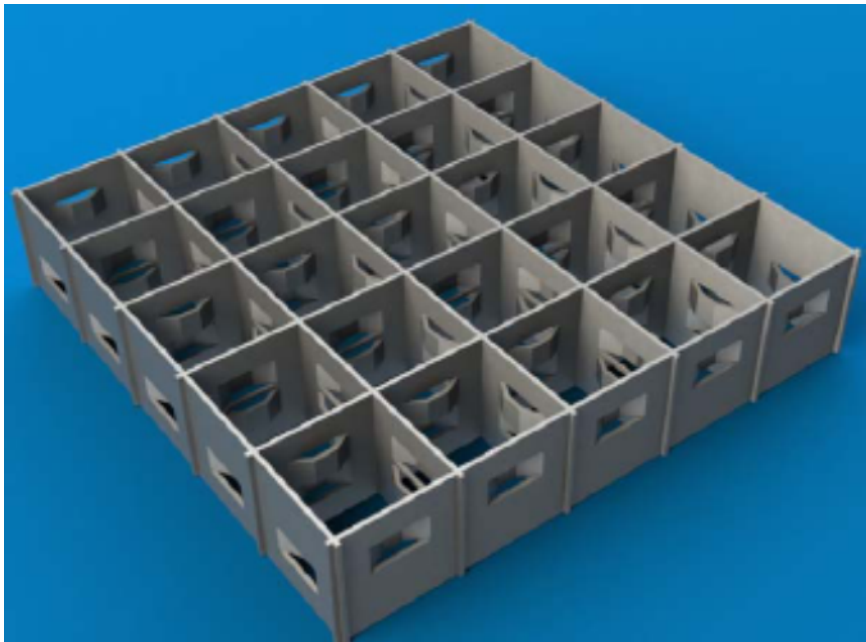
Figure 2.2.1.1-2 View of Non-Mixing Vane Spacer Grid
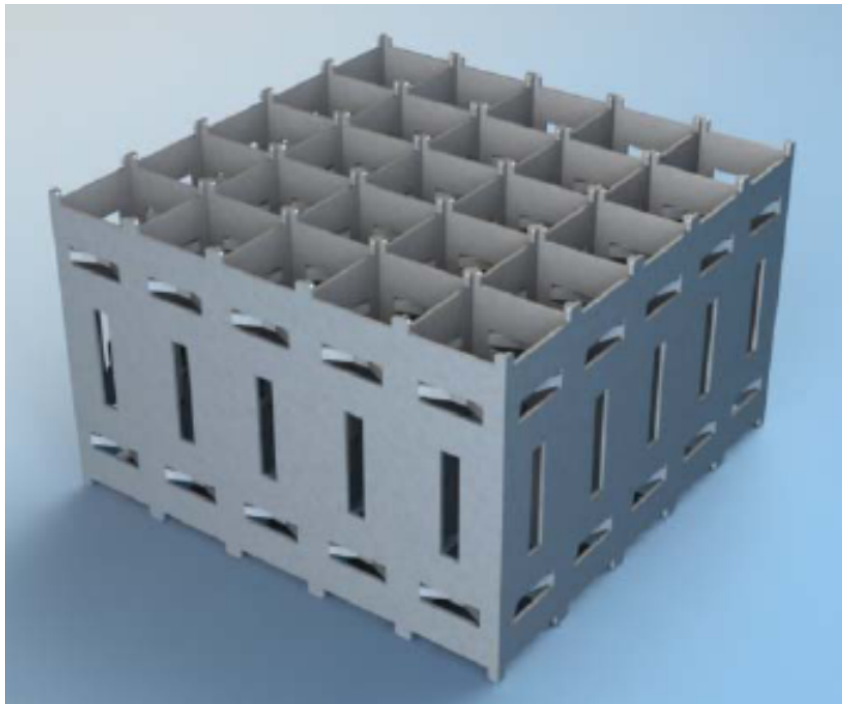
Figure 2.2.1.1-3 View of Mixing Vane Spacer Grid
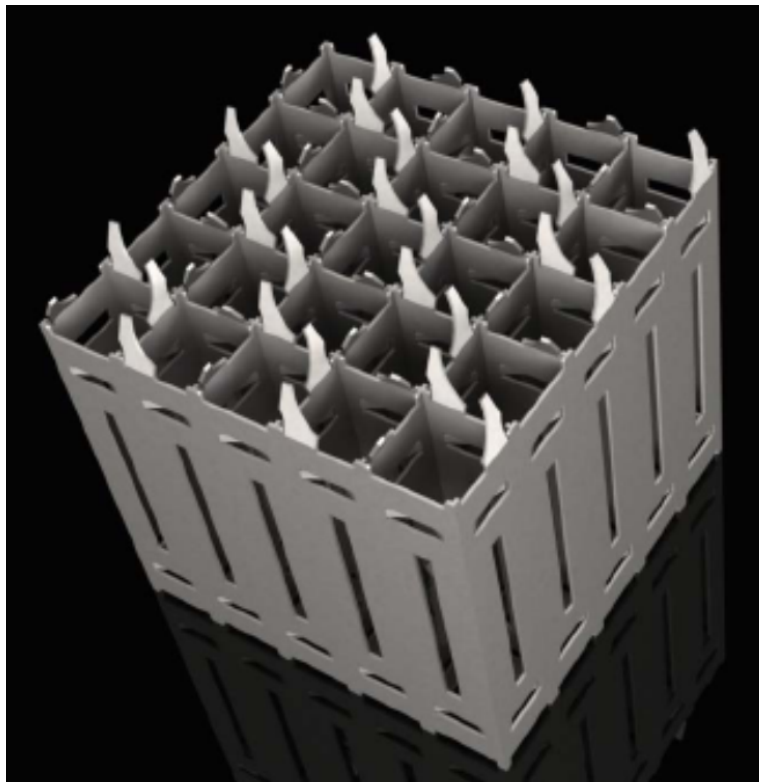
Table 2.2.1.1-1 Bundle Average Spacer Pressure Loss Coefficients

Spacer Type	Loss Coefficient
Simple Spacer (SS)	0.4
Non-Mixing Vanes Spacer (NMV)	0.7
Mixing Vanes Spacer (MV)	1.0

2.2.1.2 Heater Rod Data

Table 2.2.1.2-1 summarises the material and geometrical properties of the heater rods used in the rod bundle tests. Figure 2.2.1.2-1 provides a cross-sectional view of the heater rods and gives dimensions.

Table 2.2.1.2-1 Properties of Heater Rods

Item		Data
Heater	Outer diameter (mm)	9.5
	Thickness (mm)	0.65
	Material	Inconel 600
	Heating Method	Direct Heating
Insulator	Outer diameter (mm)	8.2
	Inner diameter (mm)	5.8
	Material	Alumina

Figure 2.2.1.2-1 Cross-sectional View of Heater Rod
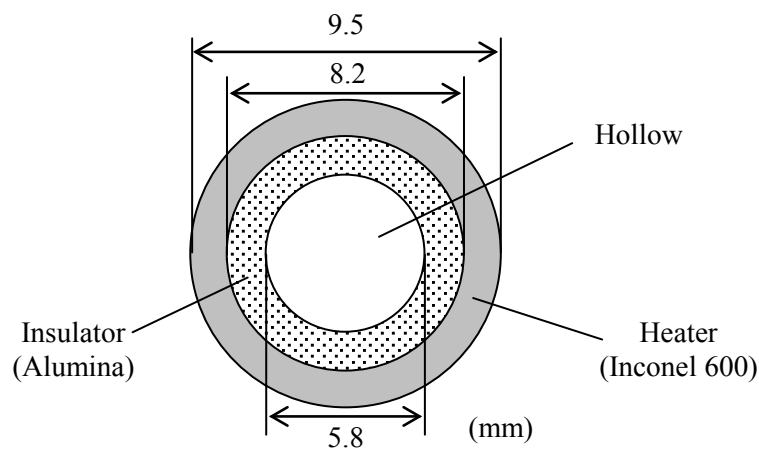
2.2.2 Measurement Techniques

The bundle power was gradually increased in fine steps to the expected vicinity of DNB, which was based on previous analysis operator experience. The onset of DNB was confirmed by a rod temperature rise greater than 11°C (20°F) as measured by the thermocouples seen in Figure 2.2.2-1. The DNB power is defined as the power corresponding to the step immediately preceding the step in which this temperature rise is seen. The accuracy of the process parameters involved in this process is seen in Table 2.2.2-1. The exit fluid temperatures were measured by the thermocouples shown in Figure 2.2.2-2.

Figure 2.2.2-1 Locations of Thermocouples for Test Assemblies
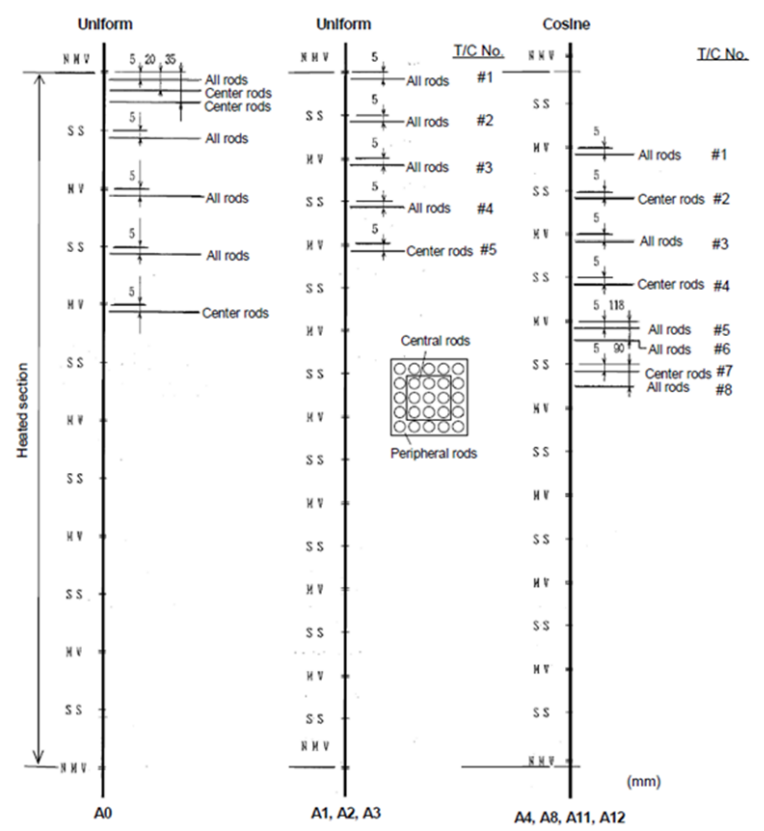
Figure 2.2.2-2 Diagram of Fluid Temperature Measurement Set-up
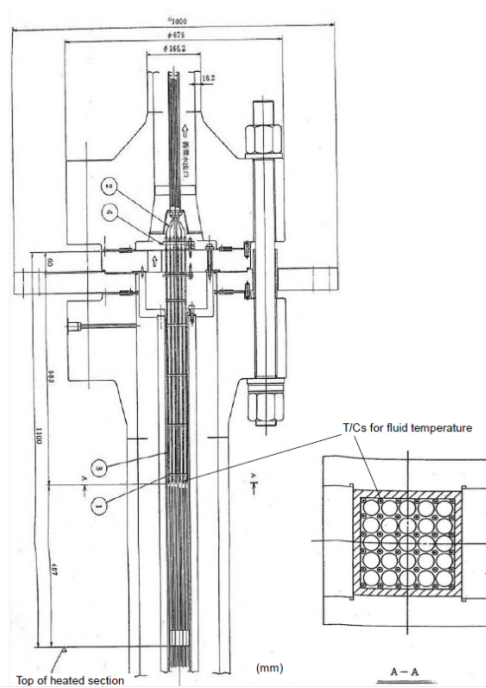
Table 2.2.2-1 Accuracy of Process Parameters in DNB Measurement

Quantity	Accuracy
Process parameters	
Pressure	1%
Flow	1.5%
Power	1%
Fluid temperature	1 Celsius

Chapter 3
Comparative Analysis of Submitted Final Results for DNB

3.1 General

Table 3.1-1 summarises the test series used in the DNB portion of the benchmark.

Table 3.1-1 Test Series for DNB Measurements

Test series	Test section	Assembly	Test mode		Measurement	
			Steady-State	Transient	DNB	Fluid temperature
0		A0	Y		Y	
1	5×5	A1	Y			Y
2		A2	Y		Y	
3	6×6	A3	Y		Y	
4		A4	Y		Y	
8		A8	Y		Y	
11T	5×5	A11		Y	Y	
12T		A12		Y	Y	
13		A4	Y		Y	

3.2 Exercise 1 – Fluid Temperature

3.2.1 Selected Exercise Cases and Requested Computational Results

The available data for this exercise consisted of fluid temperature measurements taken at the exit of the test section using the thermocouples shown in Figure 2.2.2-2. These temperatures were taken for each sub-channel in the bundle assembly.

The selected exercise test cases for the steady-state fluid temperature distribution are given in Table 3.2.1-1.

The requested outputs for this exercise were the fluid temperatures at the exit of the bundle for each sub-channel.

Table 3.2.1-1 Test Conditions for Steady-State Fluid Temperature Measurements

Test number	Pressure (kg/cm^2)*	Mass flux (10^6 kg/m^2 hr)	Inlet temperature (°C)	Power (MW)
01-5343	150.3	5.03	165.3	1.25
01-5342	150.0	1.92	164.5	0.52
01-5215	150.3	10.95	282.9	2.09
01-5125	150.3	10.94	289.2	1.50
01-5237	150.1	16.95	229.4	3.23
01-6232	169.1	2.10	251.5	0.42
01-6233	169.1	4.90	254.0	1.02
01-1237	50.2	17.00	86.0	3.44
01-5252	150.0	1.95	113.9	0.41

*$1kg/cm^2 = 98,066.5\ Pa$

3.2.2 Participation and Submitted Results

There were a total of seven (7) participants for Exercise 1. Table 3.2.2-1 lists these participants, as well as the codes for which results were submitted.

Table 3.2.2-1 Phase II Exercise 1 Participants

Participant	Code	Code Type
EDF	THYC	Porous media
CEA-Saclay	FLICA-OVAP	Sub-channel
KAERI	MATRA	Sub-channel
KIT	SUBCHANFLOW	Sub-channel
McMaster	ASSERT-PV	Sub-channel
PSI	FLICA	Sub-channel
NRI	VIPRE	Sub-channel
CEA-Grenoble	CATHARE 3	System

The questionnaires that were submitted by the participants can be found in Appendix IV.

The codes for which questionnaires and results were submitted vary in the mixing models used in the calculations. MATRA calculated diversion cross-flow using the lateral momentum equation and used a turbulent mixing model. TRACE (KTH) does not model cross-flow for a one-dimensional component. FLICA (PSI) calculated turbulent mixing based on a mixing length approach, while ASSERT-PV used Carlucci to determine the cross-flow and the Rogers and Tahir correlation for single-phase turbulent mixing.

3.2.3 Statistical Methodology

The mean error, calculated as:

$$\overline{\alpha} = \frac{1}{N} \sum_{n=1}^{N} (\alpha_{code}^{n} - \alpha_{exp}^{n})$$

Where N is the total number of test cases, it was determined for each sub-channel type for each test case for each code.

3.2.4 Comparative Analysis of Participant Results

Table 3.2.4-1 and Table 3.2.4-2 show the fluid temperature error for each code for each code type.

3.2.5 Discussion on the Predicted Fluid Temperature

In several cases, the codes were unable to accurately model the fluid temperature at the right side of the bundle, either overpredicting or underpredicting significantly. These cases generally involved a high pressure, high inlet temperature, high mass flow, and moderate-to-high power or a very low pressure, high mass flow, low inlet temperature, and high power. These conditions, coupled with the strong power gradient (seen in Figure 2.2.1-4) across the bundle, create an environment that is difficult for the codes to model accurately.

3.3 Exercise 2 – Steady-State Rod Bundle

3.3.1 Selected Exercise Cases and Requested Computational Results

The available data for this exercise consisted of the powers at which DNB could be confirmed.

The selected exercise test cases for the steady-state fluid temperature distribution are given in Table 3.2.1-1.

The requested outputs were the axial and radial locations of DNB in the bundle, as well as the power at which DNB first occurred.

Table 3.2.4-1 Fluid Temperature Error (°C) by Sub-channel Type

T(calc) - T(meas)		CEA-Grenoble (CATHARE 3)	CEA-Saclay (FLICA-OVAP)	EDF (THYC)	KAERI (MATRA)
Test Case 01-5343	Corner	0.375	-0.622	-1.925	-0.285
	Central	0.888	0.648	-1.188	0.784
	Side	-0.513	-1.172	-2.731	-1.114
Test Case 01-5342	Corner	3.100	0.945	-7.375	2.100
	Central	3.450	2.128	-3.937	3.164
	Side	1.881	0.134	-6.994	0.986
Test Case 01-5215	Corner	1.570	1.168	1.975	2.025
	Central	0.116	0.467	0.531	0.901
	Side	0.611	0.423	0.975	1.078
Test Case 01-5125	Corner	-0.085	0.111	0.200	0.150
	Central	-1.569	-1.122	-1.200	-1.038
	Side	-0.791	-0.515	-0.469	-0.534
Test Case 01-5237	Corner	-2.438	-2.907	-2.825	5.160
	Central	-3.039	-3.186	-3.406	5.075
	Side	-3.225	-3.589	-3.638	4.417
Test Case 01-6232	Corner	2.310	1.190	-3.100	1.685
	Central	0.453	-0.344	-3.725	0.236
	Side	0.933	-0.050	-3.825	0.356
Test Case 01-6233	Corner	0.280	-0.252	-1.375	-0.135
	Central	-1.609	-1.837	-3.113	-1.629
	Side	-0.576	-0.998	-2.175	-0.959
Test Case 01-1237	Corner	-4.365	-5.828	-4.275	-4.600
	Central	-5.814	-5.151	-5.600	-5.321
	Side	-6.498	-6.982	-6.331	-6.619
Test Case 01-5252	Corner	6.640	4.353	1.300	5.585
	Central	-0.407	-1.222	-3.313	-0.500
	Side	2.365	0.783	-1.788	1.451

Table 3.2.4-2 Fluid Temperature Error (°C) by Sub-channel Type (Continued)

T(calc) - T(meas)		KIT (SUBCHANFLOW)	NRI (VIPRE)	PSI (FLICA)	McMaster (ASSERT)	Prediction Mean
Test Case 01-5343	Corner	0.110	0.265	-6.149	-2.162	-1.299
	Central	0.836	1.073	1.459	-0.561	0.492
	Side	-0.745	-0.556	-4.852	-2.835	-1.815
Test Case 01-5342	Corner	3.355	2.303	-4.783	0.728	0.046
	Central	3.865	2.359	1.186	2.143	1.795
	Side	2.171	0.927	-4.232	-0.246	-0.671
Test Case 01-5215	Corner	2.180	2.000	-5.419	1.595	0.887
	Central	0.781	0.570	-0.643	0.705	0.429
	Side	1.179	0.986	-4.218	0.809	0.230
Test Case 01-5125	Corner	0.365	0.065	-2.731	1.590	-0.042
	Central	-1.041	-1.323	-0.599	0.561	-0.916
	Side	-0.351	-0.649	-2.303	0.947	-0.583
Test Case 01-5237	Corner	-2.710	-3.035	-7.106	-3.660	-2.440
	Central	-3.205	-3.481	-2.091	-3.408	-2.093
	Side	-3.525	-3.834	-6.100	-4.313	-2.976
Test Case 01-6232	Corner	2.320	1.015	-2.933	1.715	0.525
	Central	0.561	-0.663	-0.822	0.530	-0.472
	Side	0.956	-0.305	-3.060	0.482	-0.564
Test Case 01-6233	Corner	0.170	-0.750	-4.776	-0.220	-0.882
	Central	-1.583	-2.468	-1.496	-1.346	-1.885
	Side	-0.672	-1.582	-4.019	-0.933	-1.489
Test Case 01-1237	Corner	-4.200	-4.330	-10.425	-5.645	-5.458
	Central	-5.469	-5.561	-3.523	-6.098	-5.317
	Side	-6.295	-6.420	-10.166	-7.584	-7.112
Test Case 01-5252	Corner	7.090	6.487	0.123	4.058	4.455
	Central	0.188	-0.282	-1.420	-2.156	-1.139
	Side	2.850	2.303	-2.535	-0.034	0.674

Table 3.3.1-1 Test Conditions for Steady-State DNB Measurements

Test number	Pressure (kg/cm^2)	Mass flux (10^6 kg/m^{2}hr)	Inlet Temperature (°C)
<u>00-5350</u>	150.1	11.23	252.9
<u>00-4440</u>	125.6	8.09	202.4
<u>00-4460</u>	125.4	14.20	202.0
<u>00-5450</u>	150.7	11.13	223.4
<u>00-6470</u>	169.8	17.16	238.6
<u>00-6240</u>	168.9	8.12	295.4
<u>00-6230</u>	169.2	5.12	296.2
<u>00-5170</u>	150.8	17.80	321.4
<u>00-3352</u>	100.2	10.93	211.7

* 1kg/cm^2 = 98,066.5 Pa

3.3.2 Participation and Submitted Results

There were a total of seven (7) participants for Exercise 2. Table 3.2.2-1 lists these participants, as well as the codes for which results were submitted.

Table 3.3.2-1 Phase II Exercise 2 Participants

Participant	Code	Code Type
EDF	THYC	Porous media
CEA-Saclay	FLICA-OVAP	Sub-channel
KAERI	MATRA	Sub-channel
KIT	SUBCHANFLOW	Sub-channel
McMaster	ASSERT-PV	Sub-channel
PSI	FLICA	Sub-channel
NRI	VIPRE	Sub-channel
CEA-Grenoble	CATHARE 3	System
KTH	TRACE	System

The questionnaires submitted for each code can be found in Appendix IV.
The codes used in this exercise varied widely in the DNB modelling approach used. ASSERT-PV, TRACE (KTH), CATHARE 3, and FLICA (PSI) all used Groeneveld look-up tables, while MATRA used the EPRI CHF correlation and FLICA-OVAP used the Shah correlation.

3.3.3 Statistical Methodology

Mean error and standard deviation were calculated for each code for each test series. The mean error (where N is the total number of test cases) was represented as:

$$\overline{\alpha} = \frac{\sum_{n=1}^{N} \alpha^n}{N}$$

where the void fraction error for test case "n" is represented as:

$$\alpha^n = (\alpha_{code}^n - \alpha_{\exp}^n).$$

The standard deviation was given as:

$$\sigma = \pm\sqrt{\frac{\sum_{n=1}^{N}(\alpha^n - \overline{\alpha})^2}{N-1}}.$$

3.3.4 Comparative Analysis of Participant Results

Appendix II contains the complete set of participant results for Exercise 2. Figure 3.3.4-1 shows the mean error of each code for DNB power for each test series. Figure 3.3.4-2 shows the standard deviation of each code for DNB power for each test series.

Figure 3.3.4-1 Mean Error of Predicted DNB Power
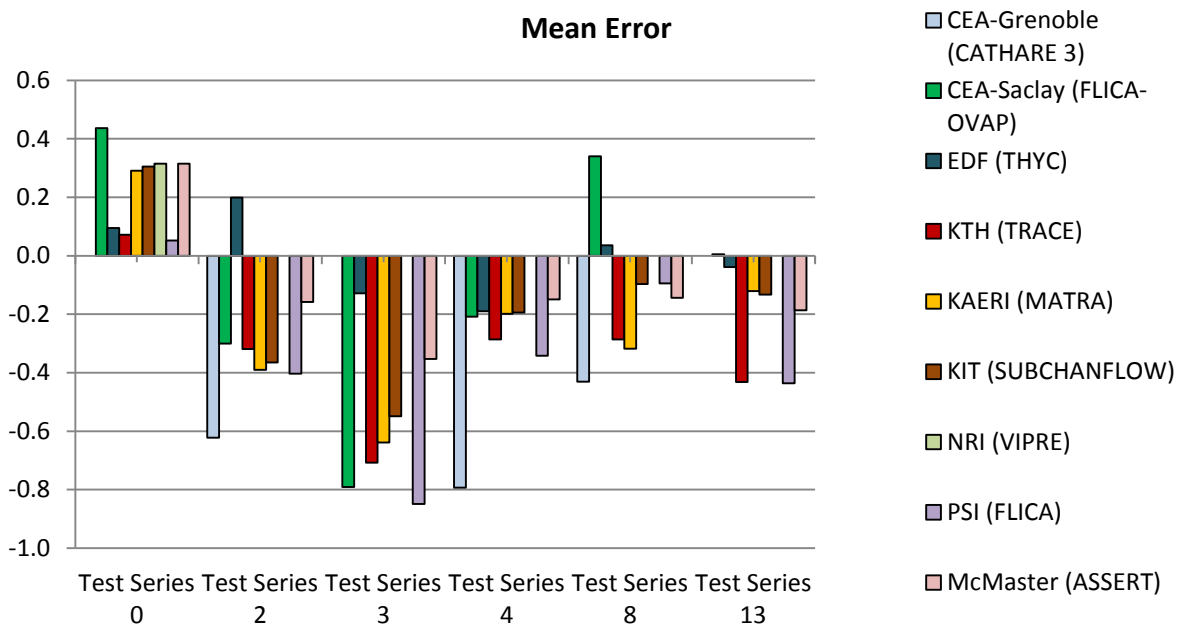
Figure 3.3.4-2 Standard Deviation of Predicted DNB Power
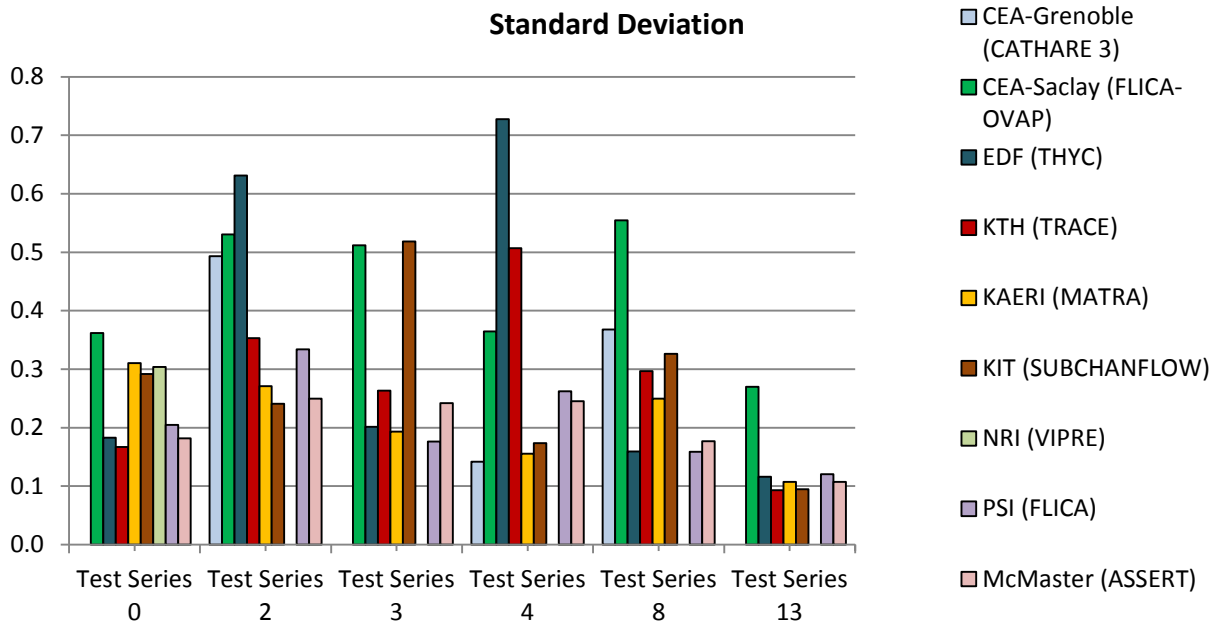
3.3.5 Discussion on the Predicted DNB Power and Elevation of DNB

The codes were generally able to calculate the DNB power satisfactorily and there was no observable bias across test series. The DNB power was consistently overpredicted in Test Series 0, while it was underpredicted in Test Series 2, 3, 4, and 13. There was also considerable variation in the predictions of axial elevation of first detected DNB. It should be noted that the measured data represent the first thermocouple at which DNB was detected. Therefore, it is the latest (axially speaking) that the onset of DNB would have occurred, and is not an exact value, as DNB could have occurred lower on the bundle.

3.4 Exercise 3 – Transient Rod Bundle

3.4.1 Selected Exercise Cases and Requested Computational Results

The available data for this exercise consisted of the transient time at which DNB was first detected in the rod bundle. It was also requested that participants should submit the power at which DNB was confirmed for code-to-code comparisons.

Four transient scenarios (temperature increase, power increase, depressurisation, and flow reduction) were used in this exercise for each test series, yielding eight total test cases. The boundary conditions for test series 11T are shown in Figure 3.4.1-1, Figure 3.4.1-2, Figure 3.4.1-3, and Figure 3.4.1-4. Similar boundary conditions are given for test series 12T in the benchmark specification.

The requested outputs were the time of detected DNB and the predicted DNB power.

Figure 3.4.1-1 Variation of Properties for Test Case 11T (Power Increase)
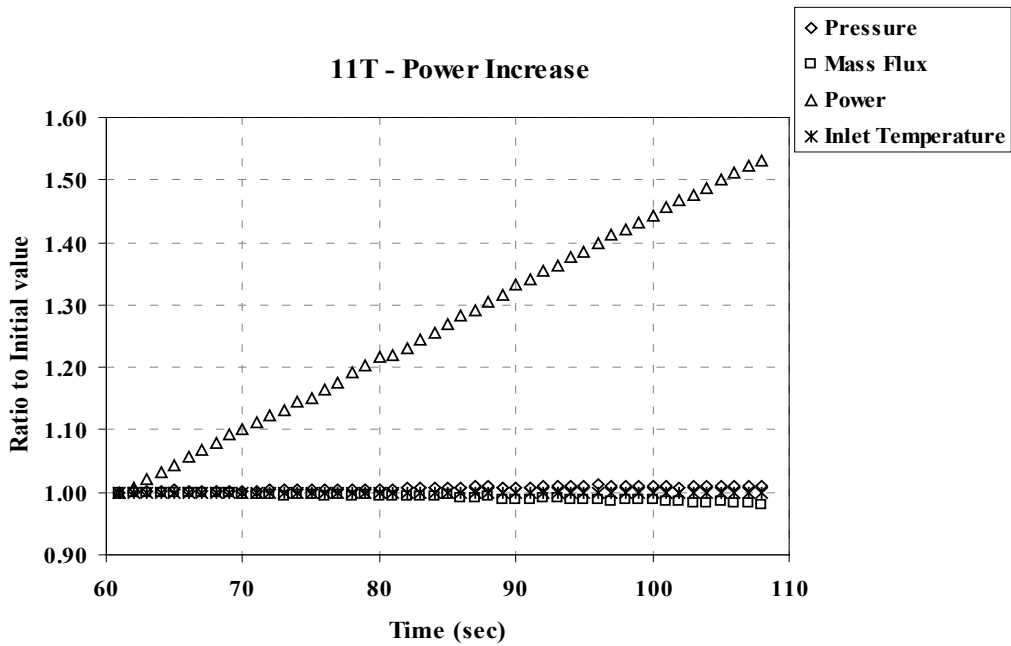
Figure 3.4.1-2 Variation of Properties for Test Case 11T (Flow Reduction)
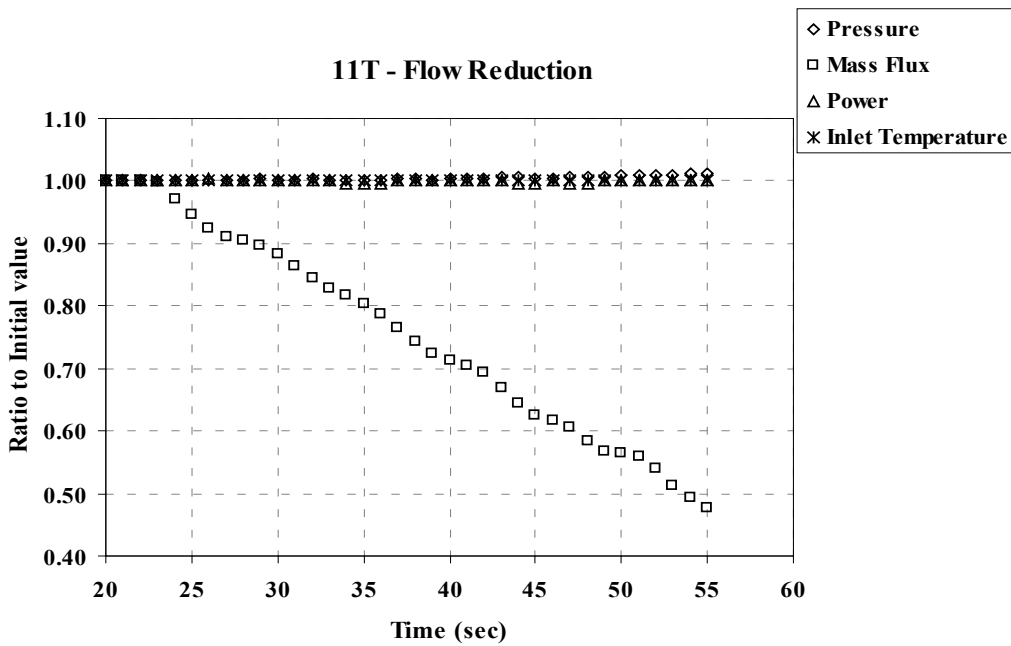
Figure 3.4.1-3 Variation of Properties for Test Case 11T (Depressurisation)

11T - Depressurization
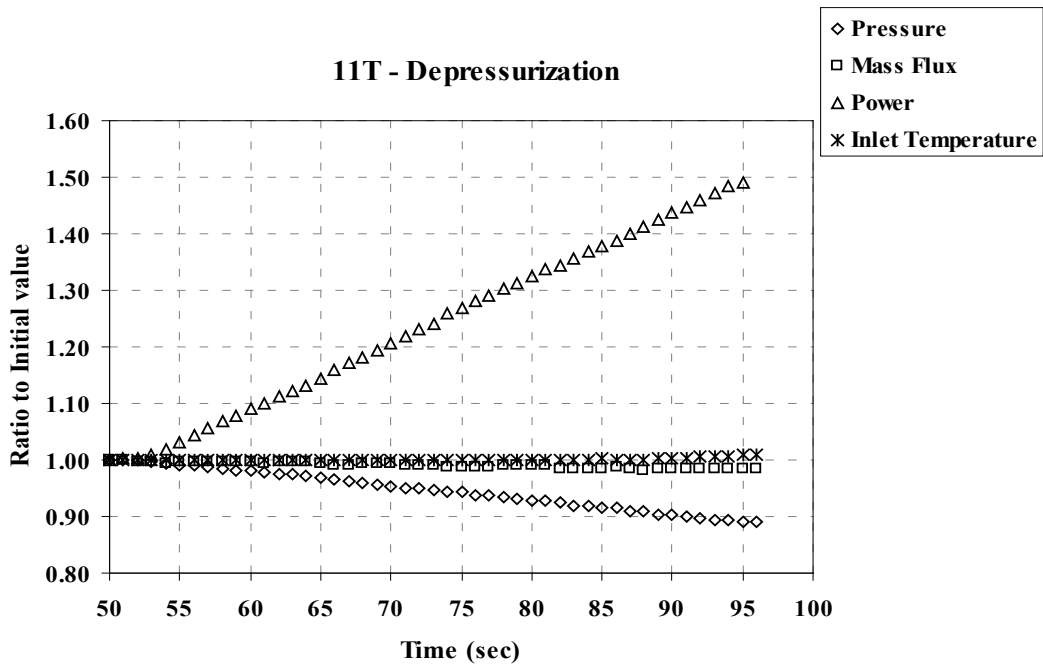
Figure 3.4.1-4 Variation of Properties for Test Case 11T (Temperature Increase)

11T - Temperature Increase
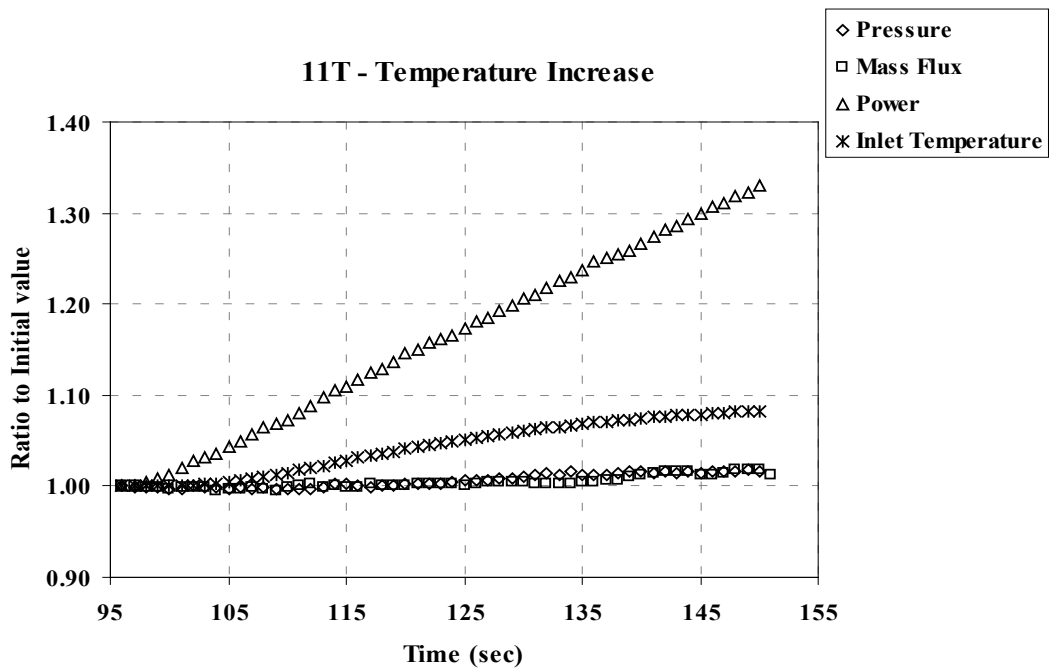
3.4.2 Participation and Submitted Results

There were a total of eight (8) participants for Exercise 3. Table 3.2.2-1 lists these participants, as well as the codes for which results were submitted.

Table 3.4.2-1 Phase II Exercise 3 Participants

Participant	Code	Code Type
EDF	THYC	Porous media
CEA-Saclay	FLICA-OVAP	Sub-channel
KAERI	MATRA	Sub-channel
KIT	SUBCHANFLOW	Sub-channel
McMaster	ASSERT-PV	Sub-channel
PSI	FLICA	Sub-channel
NRI	VIPRE	Sub-channel
KTH	TRACE	System

The questionnaires submitted for each code can be found in Appendix IV.

The DNB/CHF models used by each code were discussed in Section 3.3.2.

3.4.3 Statistical Methodology

The mean error and standard deviation were calculated for each measurement location for each test series using the equations given in Section 3.3.3.

3.4.4 Comparative Analysis of Participant Results

Appendix III contains the complete set of participant results for Exercise 3. Figure 3.4.4-1 shows the mean error of each code for detected DNB time for each test series. Figure 3.4.4-2 shows the mean error of each code for DNB power for each test series.

Figure 3.4.4-1 Mean Error of Detected Time of DNB

Mean Error - Time of Detected DNB, (sec)
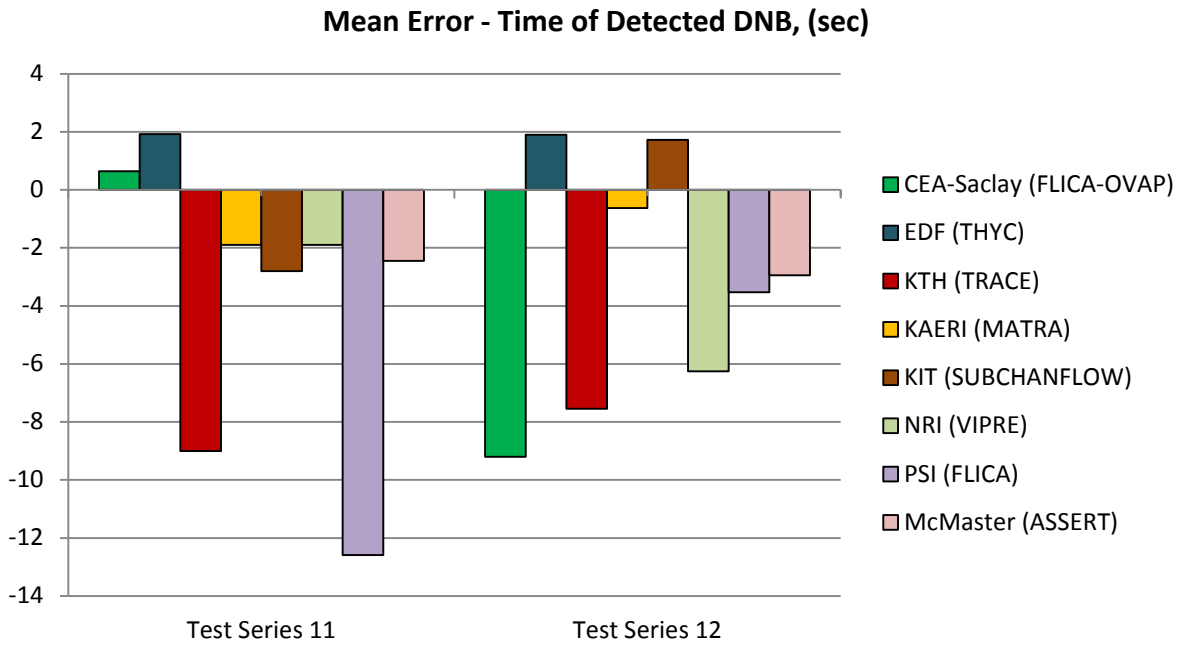
Figure 3.4.4-2 Mean Error of Predicted DNB Power

Mean Error - Predicted DNB Power, (MW)
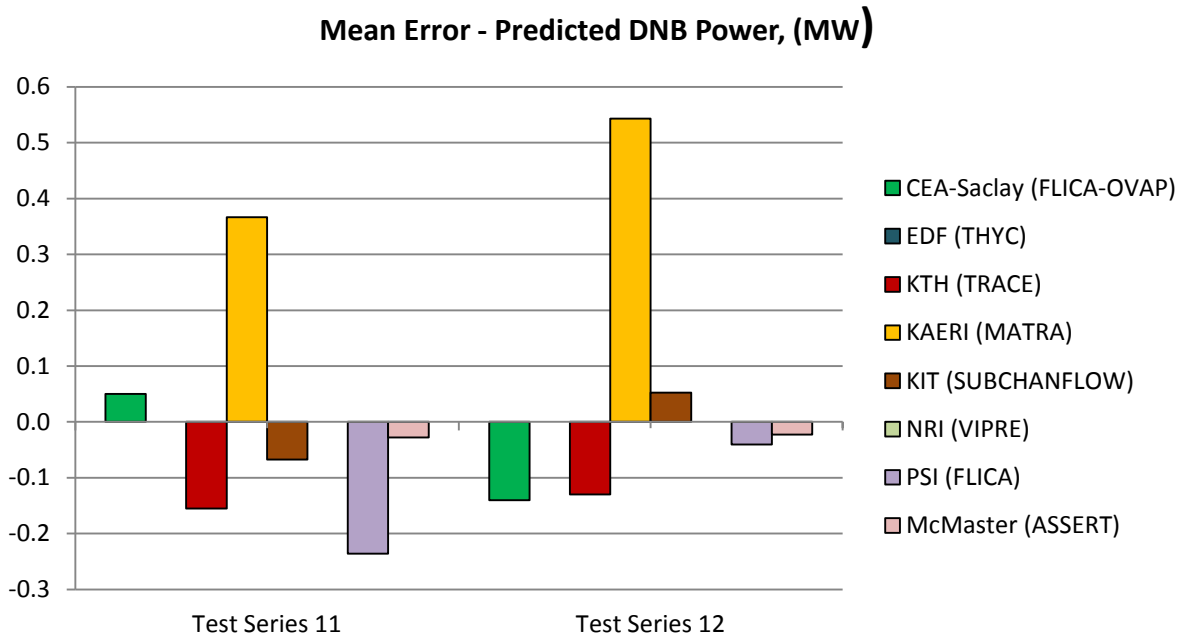
3.4.5 Discussion on the Predicted DNB Power and Time of DNB

In general, codes were not able to predict the time of DNB during the simulated transients. Most of the codes calculate earlier DNB occurrence for both bundle types (with, test series 11, and without, test series 12, thimble rod in the central region). THYC always predicts later DNB.

FLICA-OVAP and SUBCHANFLOW predictions show dependence on the radial power shape for both DNB power and DNB time.

MATRA seems to give reasonable predictions of the DNB time, but significantly overpredict the DNB power.

Chapter 4
Conclusion

The NEA/NRC PSBT Benchmark was designed to provide a set of data for the development and validation of the next generation of thermal-hydraulic codes. It consisted of two phases: a void fraction benchmark and a departure from nucleate boiling benchmark. Data regarding the test sections and conditions were provided to participants for use in calculations. The code results from all participants were then compiled and analysed.

In the development of the benchmark specification, a number of support studies were performed. Regarding Phase II, a study was undertaken to determine the effect of the downcomer region on the fluid temperature.

The results for each benchmark exercise were analysed. Based on the final results for the second phase, several conclusions were drawn. The codes were generally able to replicate the results of the mixing test, staying within 5% of the experimental fluid exit temperature. THYC showed the largest errors, while all codes had difficulty with the Test Case 01-1237. The uncertainty related to the spacer grid orientation in the mixing tests may explain the asymmetries seen in the experimental data, but no sensitivity study was performed to determine the exact effect on the flow, thus this uncertainty cannot be quantified. The improvement between FLICA-OVAP and FLICA was noticeable, with the main difference between the two being that FLICA-OVAP implicitly assigned flow regime based on drift flux, while FLICA assumed single phase flows. In Exercises 2 and 3, the codes were generally able to predict the DNB power as well as the axial location of the onset of DNB (for the steady-state cases) and the time of DNB (for the transient cases). It was noted that the codes that used the EPRI CHF correlation (such as MATRA and SUBCHANFLOW) had the lowest mean error in Exercise 2 for predicted DNB power.

The EPRI CHF correlation [8] was used by a number of benchmark participants and is applicable to a wide range of typical BWR and PWR conditions. Reddy and Fighetti state that the basic correlation covers pressure from 200 to 2450 psia, mass flux from 0.2 to 4.1 M.lbs/hr-ft^2, and quality from 0.25 to 0.75.

The basic correlation is expressed as:
$$q_c'' = \frac{A - x_{in}}{C + \left[\dfrac{x_l - x_{in}}{q_l''} \right]}$$

Where q_c'' is the critical heat flux, q_l'' is the local heat flux, x_{in} and x_l are the inlet and local qualities, and $A = P_1 P_r^{P_2} G^{(P_5 + P_7 P_r)}$ and $C = P_3 P_r^{P_4} G^{(P_6 + P_8 P_r)}$.

P_r is the reduced pressure ($P/P_{critical}$). P_1 though P_8 were optimised using non-linear regression analysis, and the values were determined to be 0.5328, 0.1212, 1.6151, 1.4066, -0.3040, 0.4843, -0.3285, and –2.0749. G is the mass flux in units of [M.lbs/hr-ft^2]. Other participants used slightly different formulations of these correlations [9].

Bibliography

[1] A. Rubin, A. Schoedel, M. Avramova, H. Utsuno, S. Bajorek, A. Velazquez-Lozada (2009), "OECD/NEA/NRC Benchmark Based on NUPEC PWR Sub-channel and Bundle Tests (PSBT), Volume I: Experimental Database and Final Problem Specifications".

[2] "OECD/NEA Benchmark Based on NUPEC PWR Sub-channel and Bundle Tests (PSBT)" (2009), Japan Nuclear Energy Safety Organization, JNES/SAE-TH08-0019.

[3] Nuclear Power Engineering Test Center (1989), "Proving Test on the Reliability for Nuclear Fuel Assemblies", Summary Report of Proving Tests on the Reliability for Nuclear Power Plant.

[4] K. Hori et al. (1993), "In-Bundle Void Fraction Measurement of PWR Fuel Assembly", ICONE-2, Vol.1, pp.69-76, San Francisco, California, US.

[5] NUPEC, "Pamphlet of Takasago Engineering Laboratory".

[6] A. Rubin, M. Avramova, H. Utsuno (2010), "OECD/NRC Benchmark Based on NUPEC PWR Subchannel and Bundle Tests (PSBT)", *Proceedings: PHYSOR-2010*, Pittsburgh, PA, US.

[7] A. Rubin, M. Avramova (2015) "OECD/NEA/NRC Benchmark Based on NUPEC PWR Sub-channel and Bundle Tests (PSBT), Volume II: Final Participant Results – Phase I", NEA/NRC Report NEA/NSC/R(2015)4.

[8] D.G. Reddy, C.F. Fighetti (1983), "Parametric study of CHF sata volume 2. A generalized sub-channel CHF correlation for PWR and BWR fuel assemblies", EPRI-NP-2609.

[9] D.H. Hwang, S.J. Kim, K.W. Seo, H. Kwon (2012), "Accuracy and Uncertainty Analysis of PSBT Benchmark Exercises Using a Sub-channel Code MATRA", Science and Technology of Nuclear Installations, Volume 2012, Article ID 603752.

Appendix I Exercise II-1 Results

Figure AI-1 Test Case 01-5343 CATHARE 3 – Error of Calculated Fluid Temperature

Test Case 01-5343 - CEA-Grenoble (CATHARE 3)
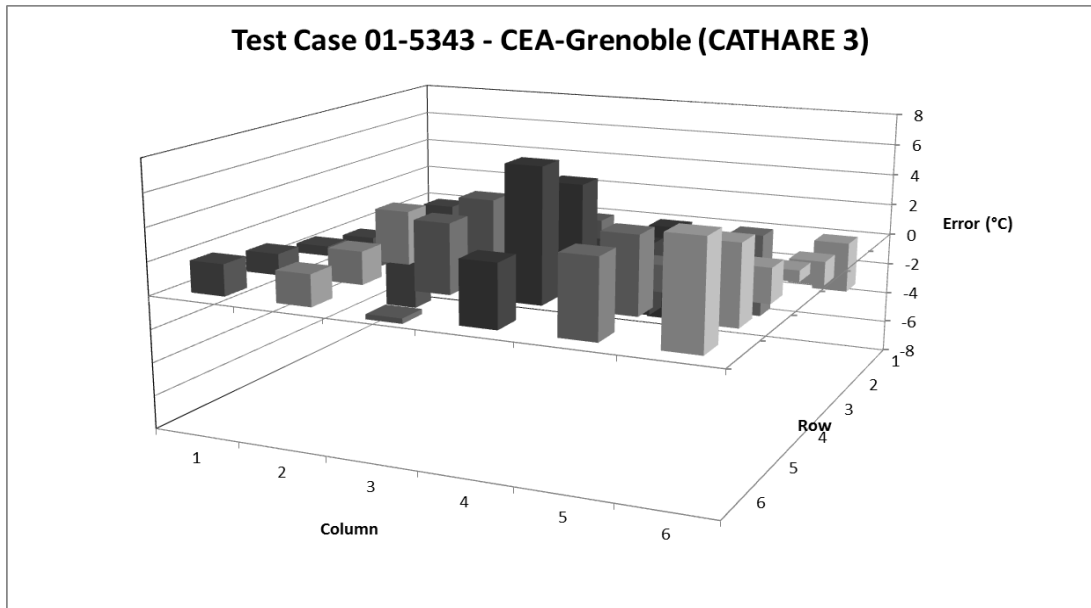
Figure AI-2 Test Case 01-5343 FLICA-OVAP – Error of Calculated Fluid Temperature

Test Case 01-5343 - CEA-Saclay (FLICA-OVAP)
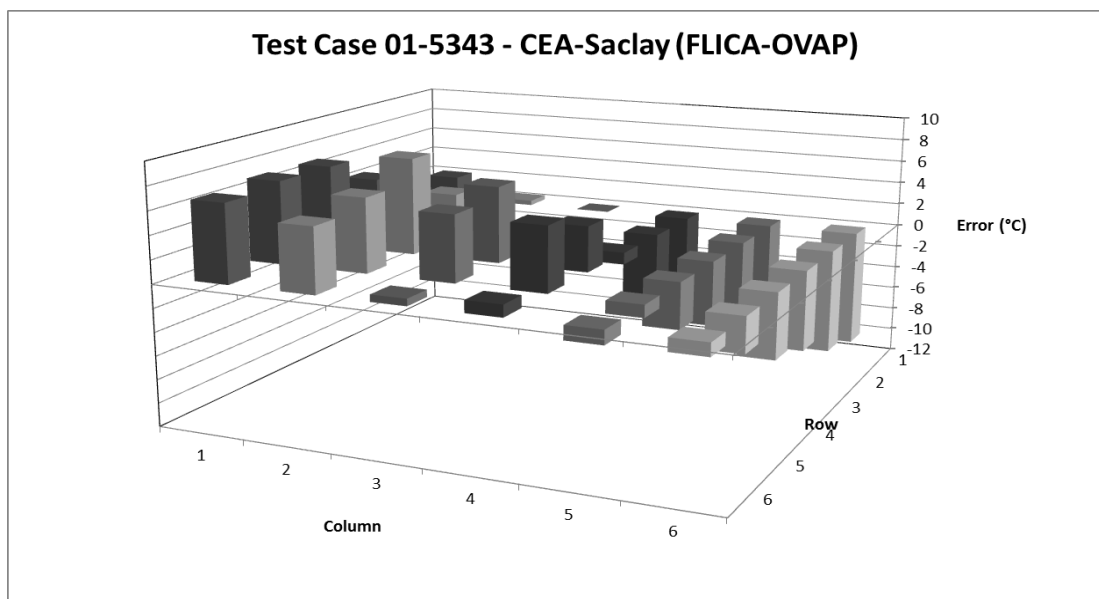
Figure AI-3 Test Case 01-5343 THYC – Error of Calculated Fluid Temperature

Test Case 01-5343 - EDF(THYC)
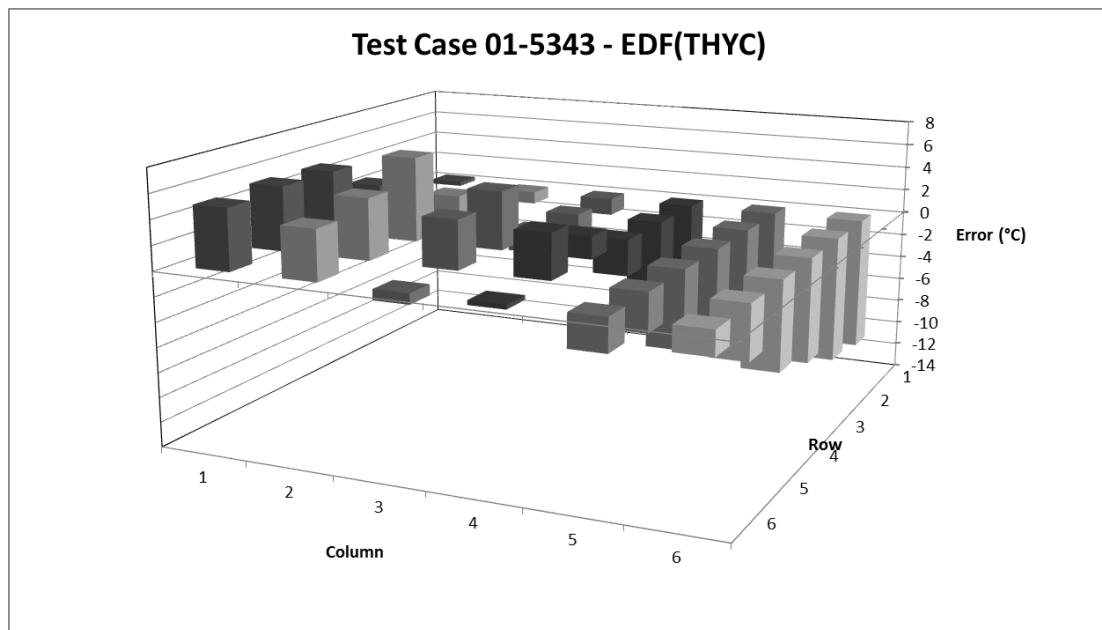
Figure AI-4 Test Case 01-5343 MATRA – Error of Calculated Fluid Temperature Figure

Test Case 01-5343 - KAERI (MATRA)

Figure AI-5 Test Case 01-5343 SUBCHANFLOW – Error of Calculated Fluid Temperature

Test Case 01-5343 - KIT (SUBCHANFLOW)
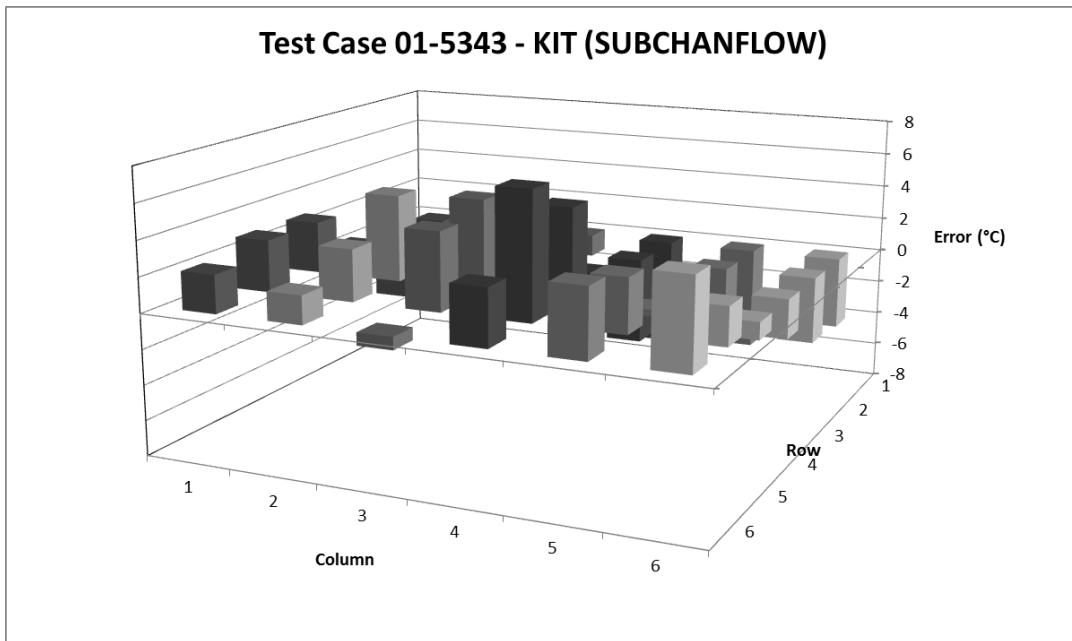
Figure AI-6 Test Case 01-5343 VIPRE – Error of Calculated Fluid Temperature

Test Case 01-5343 - NRI (VIPRE)
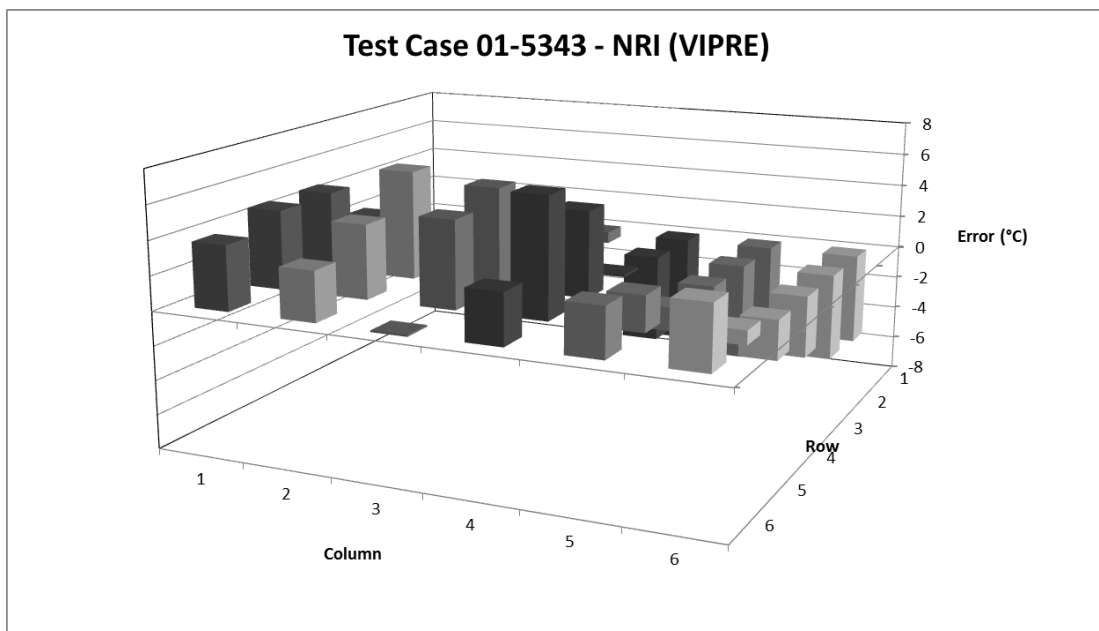
Figure AI-7 Test Case 01-5343 FLICA – Error of Calculated Fluid Temperature

Test Case 01-5343 - PSI (FLICA)
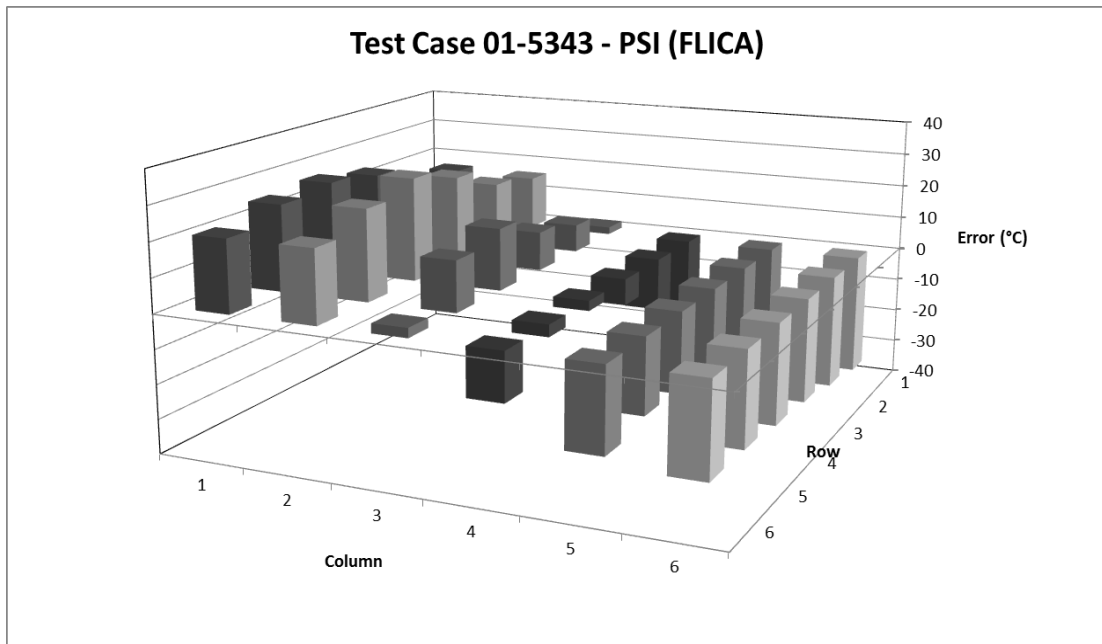
Figure AI-8 Test Case 01-5343 ASSERT – Error of Calculated Fluid Temperature

Test Case 01-5343 - McMaster (ASSERT)

Figure AI-9 Test Case 01-5342 CATHARE 3 – Error of Calculated Fluid Temperature

Figure AI-10 Test Case 01-5342 FLICA-OVAP – Error of Calculated Fluid Temperature

Figure AI-11 Test Case 01-5342 THYC – Error of Calculated Fluid Temperature

Test Case 01-5342 - EDF(THYC)

Figure AI-12 Test Case 01-5342 MATRA – Error of Calculated Fluid Temperature

Test Case 01-5342 - KAERI (MATRA)

Figure AI-13 Test Case 01-5342 SUBCHANFLOW – Error of Calculated Fluid Temperature

Figure AI-14 Test Case 01-5342 VIPRE – Error of Calculated Fluid Temperature

Figure AI-15 Test Case 01-5342 FLICA – Error of Calculated Fluid Temperature

Figure AI-16 Test Case 01-5342 ASSERT – Error of Calculated Fluid Temperature

Figure AI-17 Test Case 01-5215 CATHARE 3 – Error of Calculated Fluid Temperature

Test Case 01-5215 - CEA-Grenoble (CATHARE 3)

Figure AI-18 Test Case 01-5215 FLICA-OVAP – Error of Calculated Fluid Temperature

Test Case 01-5215 - CEA-Saclay (FLICA-OVAP)

Figure AI-19 Test Case 01-5215 THYC – Error of Calculated Fluid Temperature

Figure AI-20 Test Case 01-5215 MATRA – Error of Calculated Fluid Temperature

Figure AI-21 Test Case 01-5215 SUBCHANFLOW – Error of Calculated Fluid Temperature

Figure AI-22 Test Case 01-5215 VIPRE – Error of Calculated Fluid Temperature

Figure AI-23 Test Case 01-5215 FLICA – Error of Calculated Fluid Temperature

Test Case 01-5215 - PSI (FLICA)

Figure AI-24 Test Case 01-5215 ASSERT – Error of Calculated Fluid Temperature

Test Case 01-5215 - McMaster (ASSERT)

Figure AI-25 Test Case 01-5125 CATHARE 3 – Error of Calculated Fluid Temperature


Test Case 01-5125 - CEA-Grenoble (CATHARE 3)

Figure AI-26 Test Case 01-5125 FLICA-OVAP – Error of Calculated Fluid Temperature

Test Case 01-5125 - CEA-Saclay (FLICA-OVAP)

Figure AI-27 Test Case 01-5125 THYC – Error of Calculated Fluid Temperature

Test Case 01-5125 - EDF(THYC)

Figure AI-28 Test Case 01-5125 MATRA – Error of Calculated Fluid Temperature

Test Case 01-5125 - KAERI (MATRA)

Figure AI-29 Test Case 01-5125 SUBCHANFLOW – Error of Calculated Fluid Temperature

Test Case 01-5125 - KIT (SUBCHANFLOW)
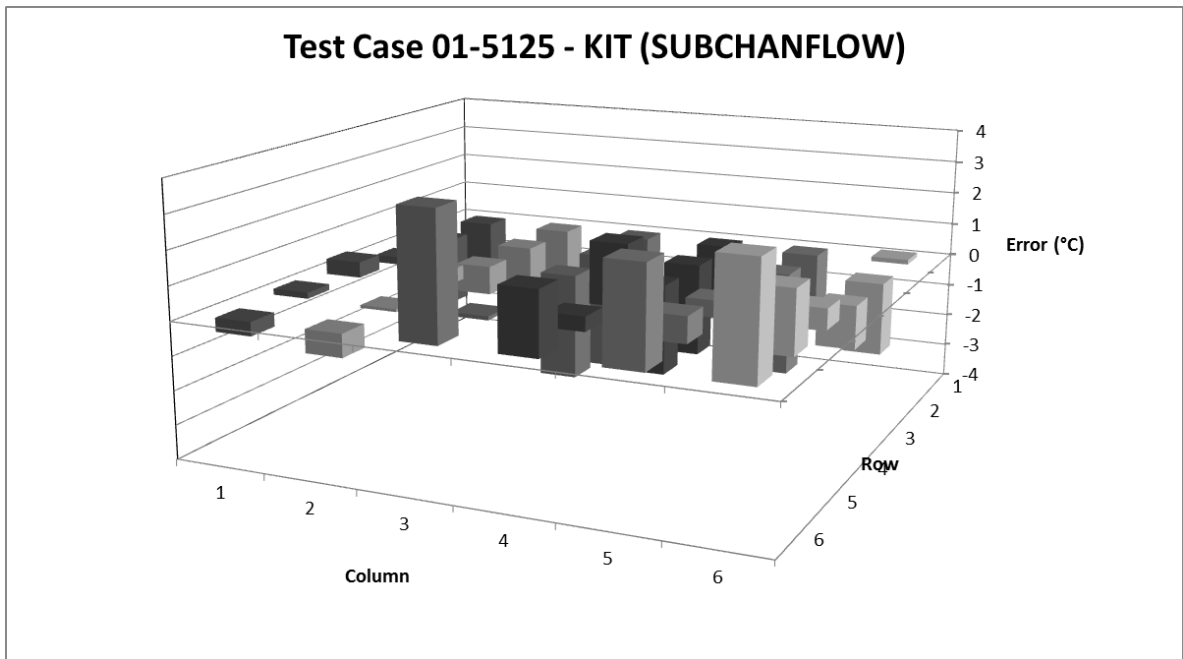
Figure AI-30 Test Case 01-5125 VIPRE – Error of Calculated Fluid Temperature

Test Case 01-5125 - NRI (VIPRE)
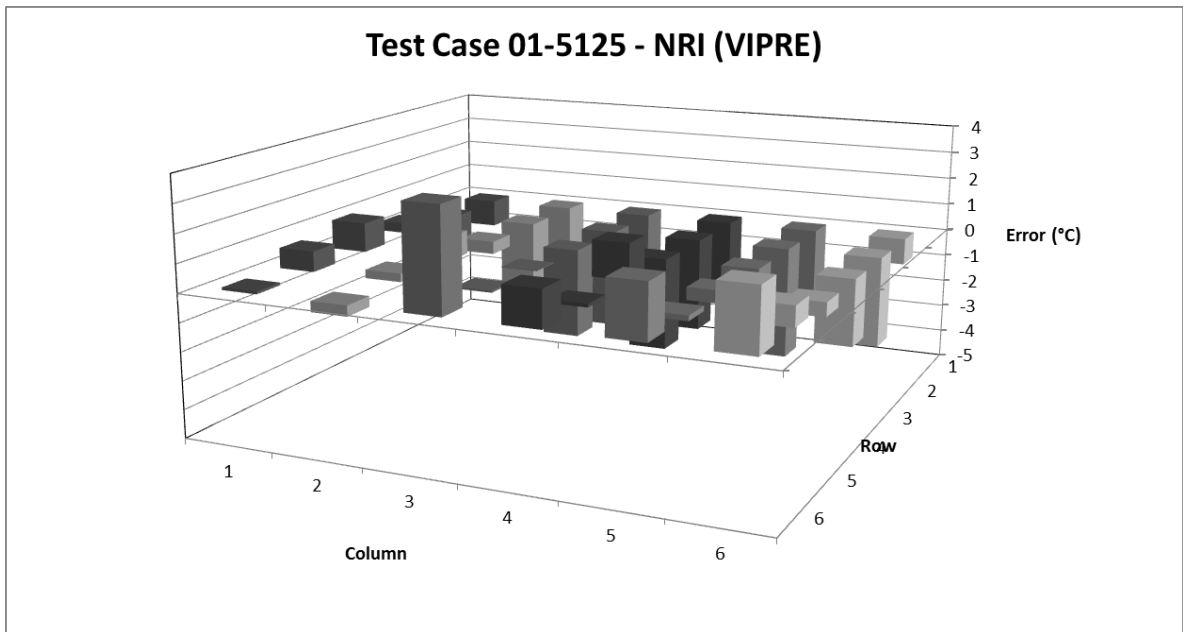
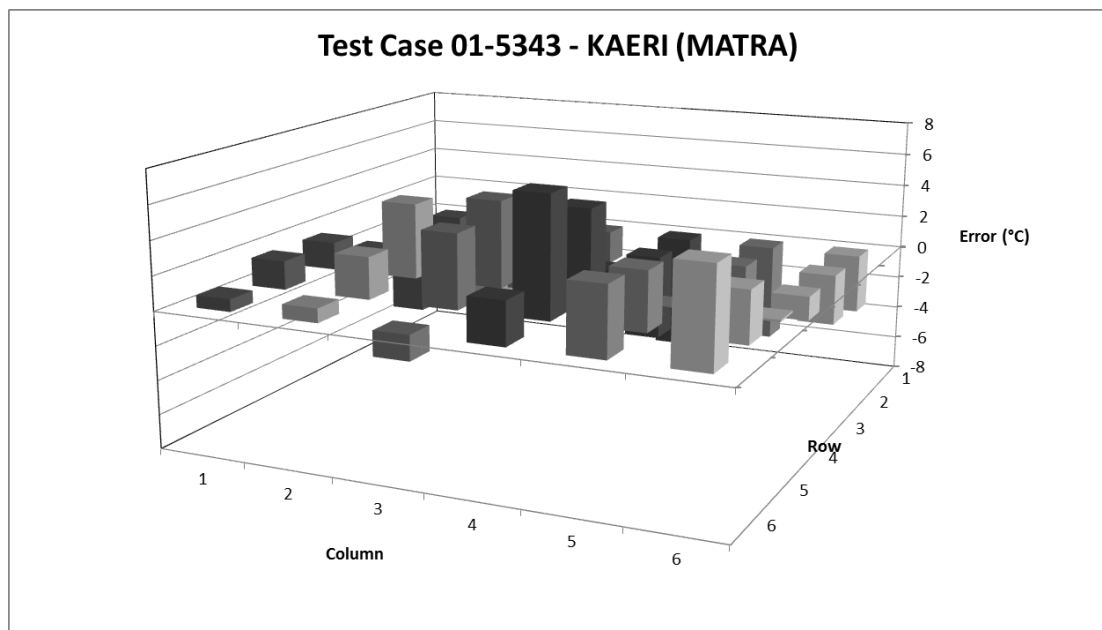**Figure AI-31 Test Case 01-5125 FLICA – Error of Calculated Fluid Temperature**

Test Case 01-5125 - PSI (FLICA)
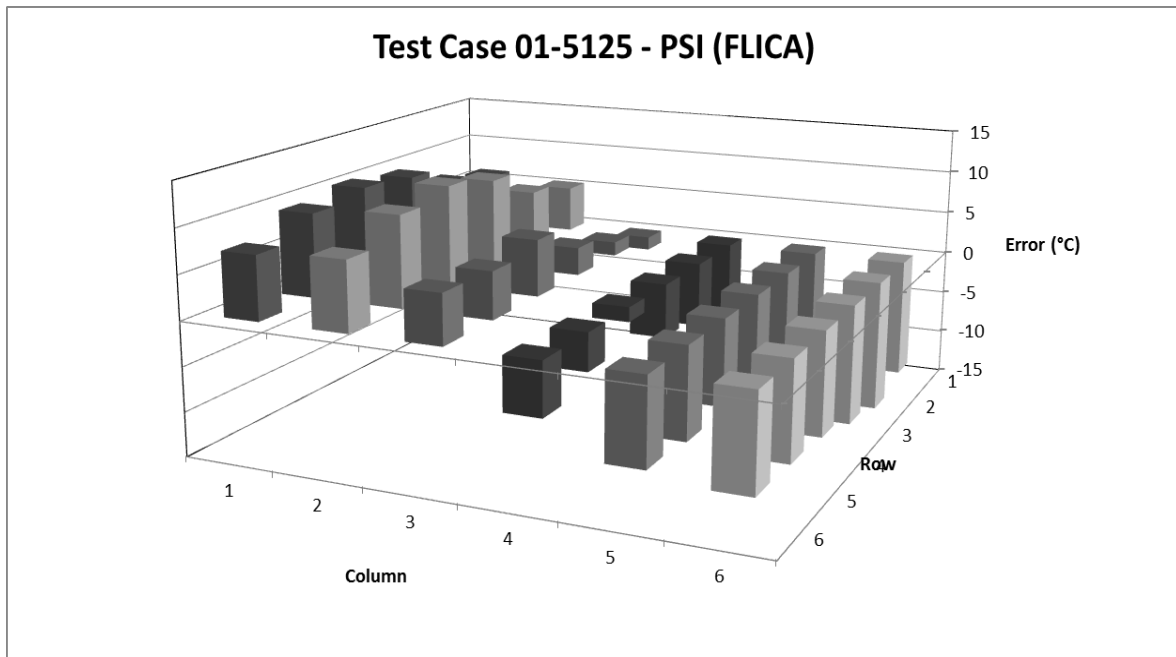
Figure AI-32 Test Case 01-5125 ASSERT – Error of Calculated Fluid Temperature

Test Case 01-5125 - McMaster (ASSERT)
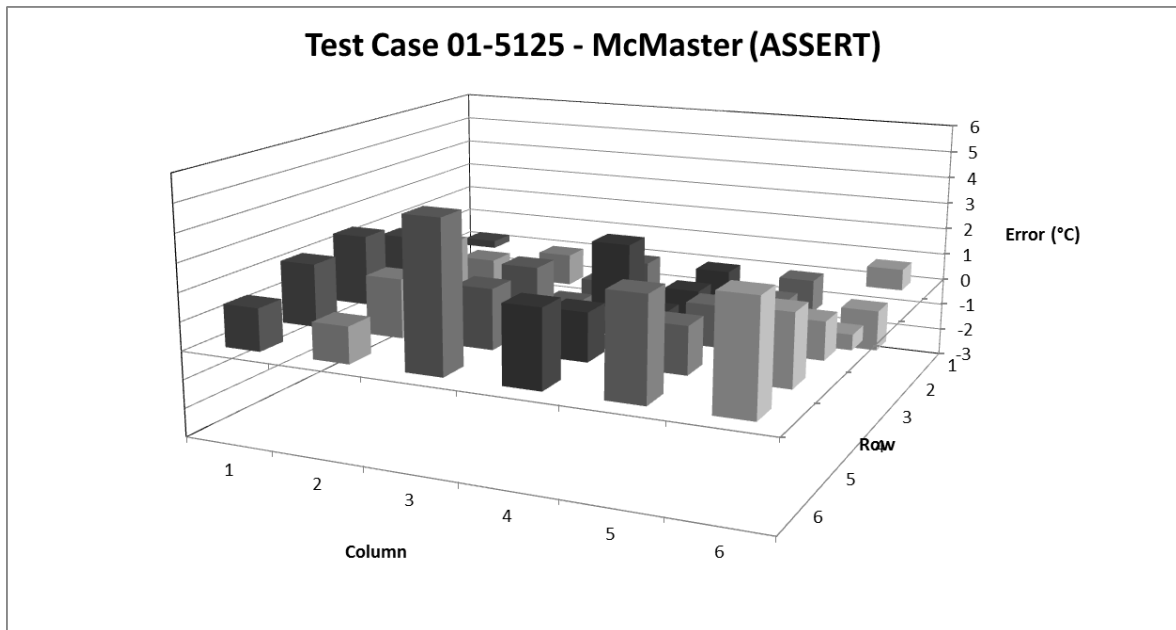
Figure AI-33 Test Case 01-5237 CATHARE 3 – Error of Calculated Fluid Temperature

Test Case 01-5237 - CEA-Grenoble (CATHARE 3)
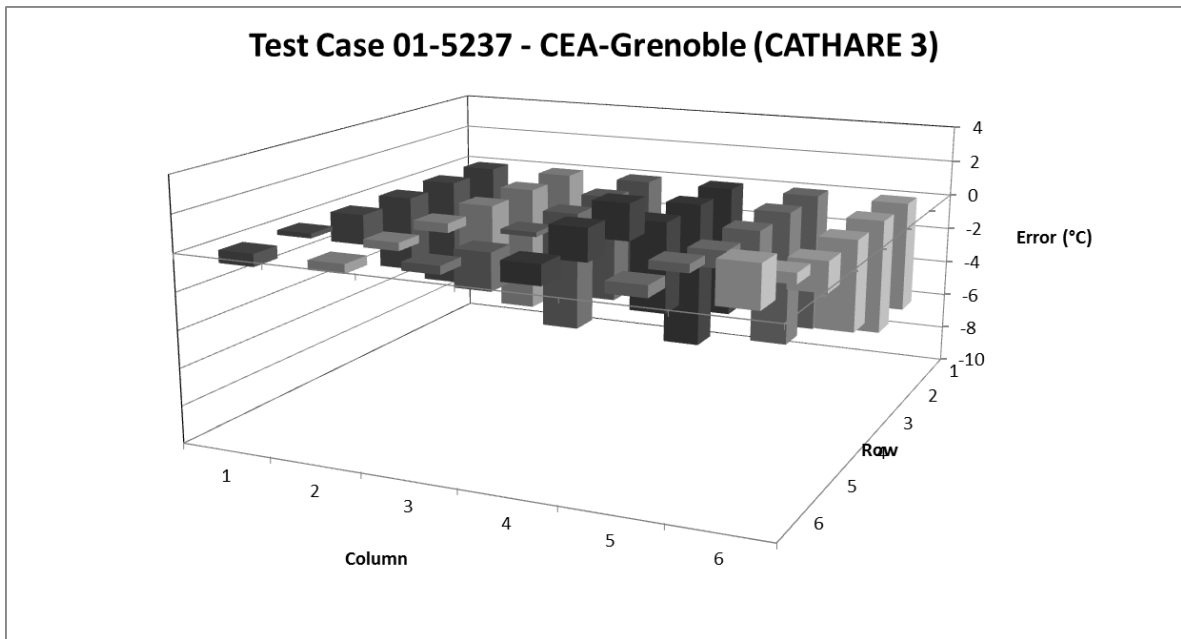
Figure AI-34 Test Case 01-5237 FLICA-OVAP – Error of Calculated Fluid Temperature

Test Case 01-5237 - CEA-Saclay (FLICA-OVAP)
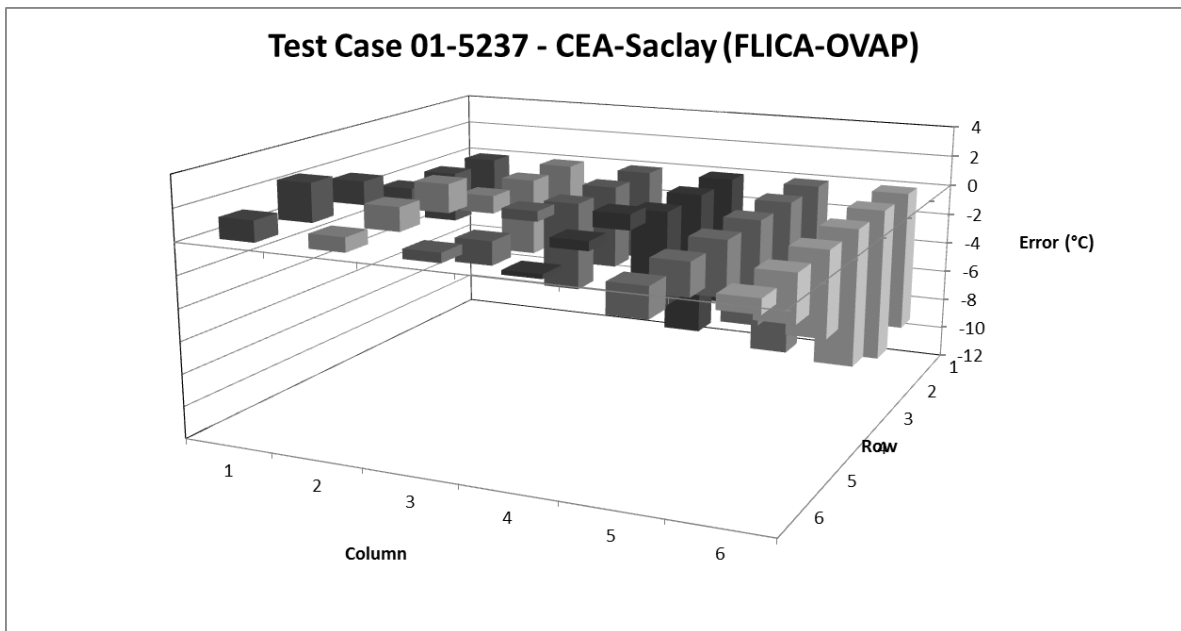
Figure AI-35 Test Case 01-5237 THYC – Error of Calculated Fluid Temperature

Test Case 01-5237 - EDF(THYC)
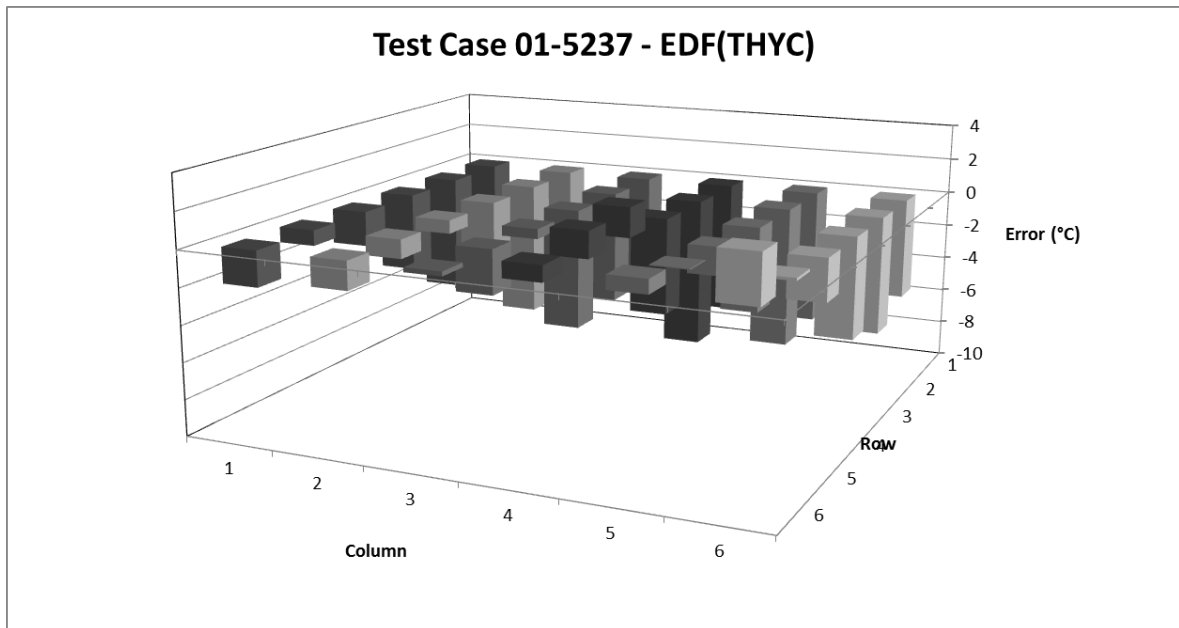
Figure AI-36 Test Case 01-5237 MATRA – Error of Calculated Fluid Temperature

Test Case 01-5237 - KAERI (MATRA)
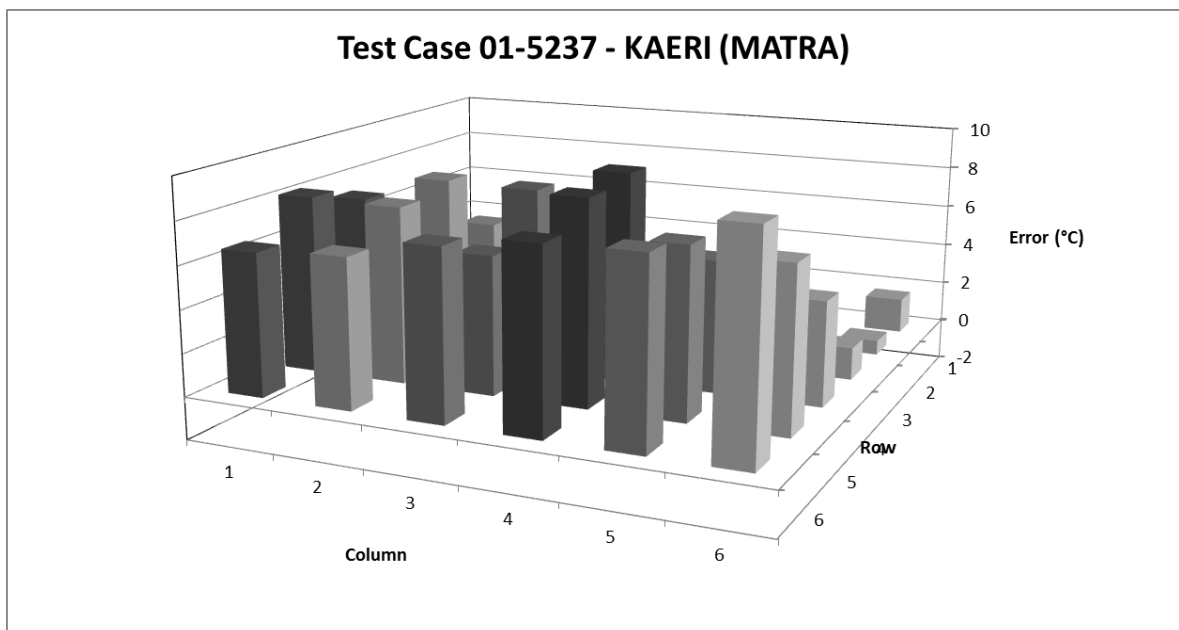
Figure AI-37 Test Case 01-5237 SUBCHANFLOW – Error of Calculated Fluid Temperature

Test Case 01-5237 - KIT (SUBCHANFLOW)
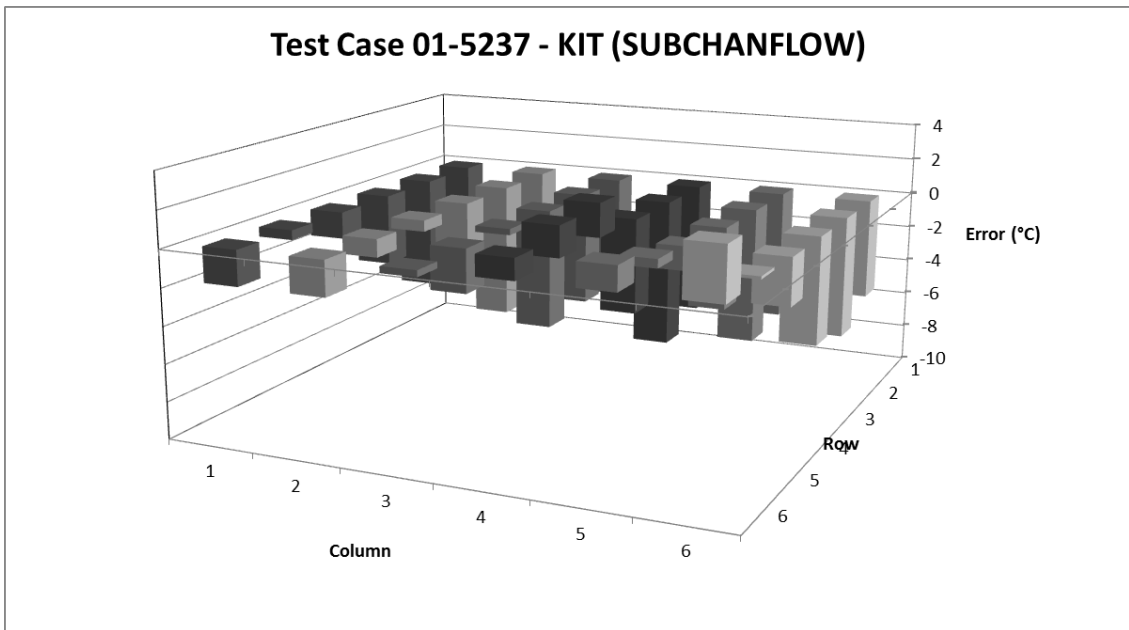
Figure AI-38 Test Case 01-5237 VIPRE – Error of Calculated Fluid Temperature

Test Case 01-5237 - NRI (VIPRE)
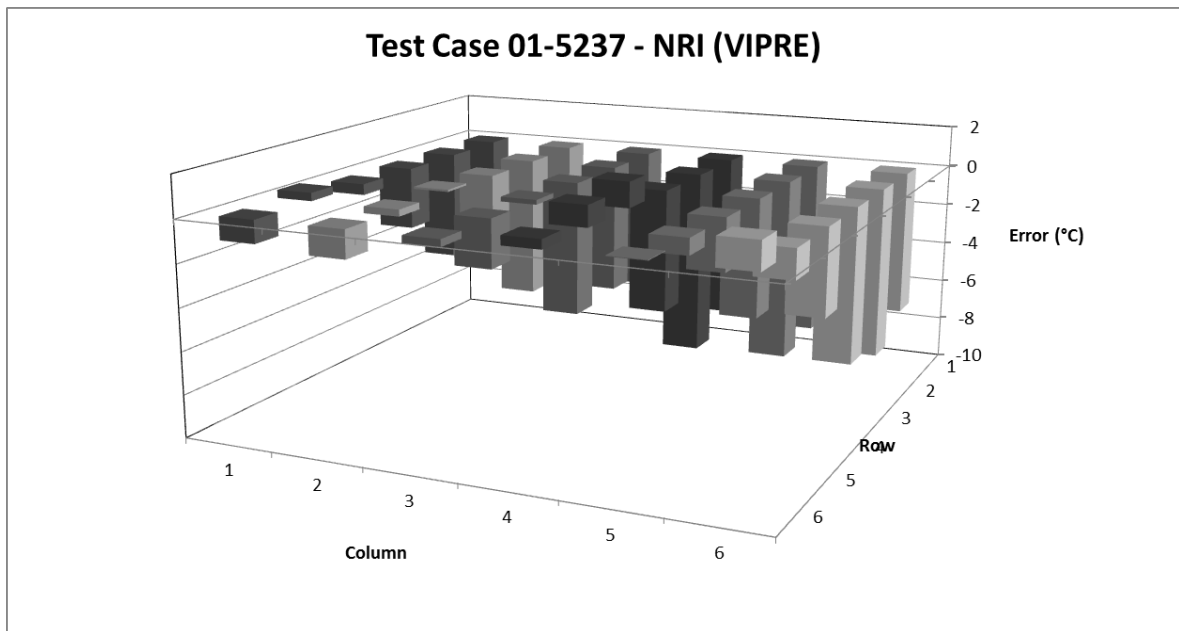
Figure AI-39 Test Case 01-5237 FLICA – Error of Calculated Fluid Temperature
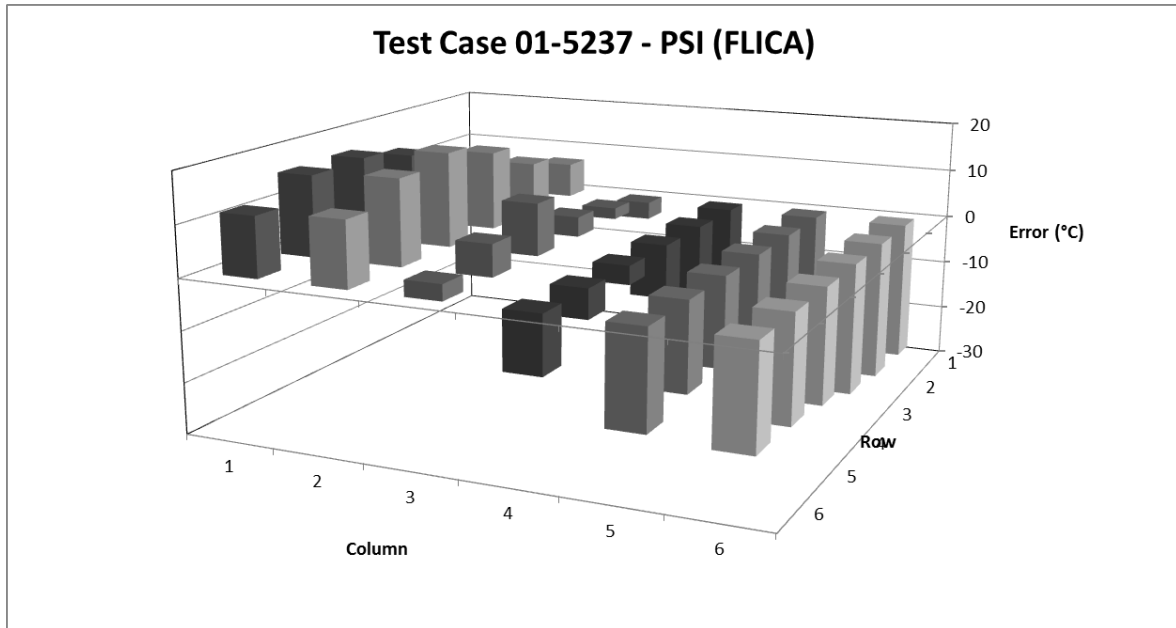
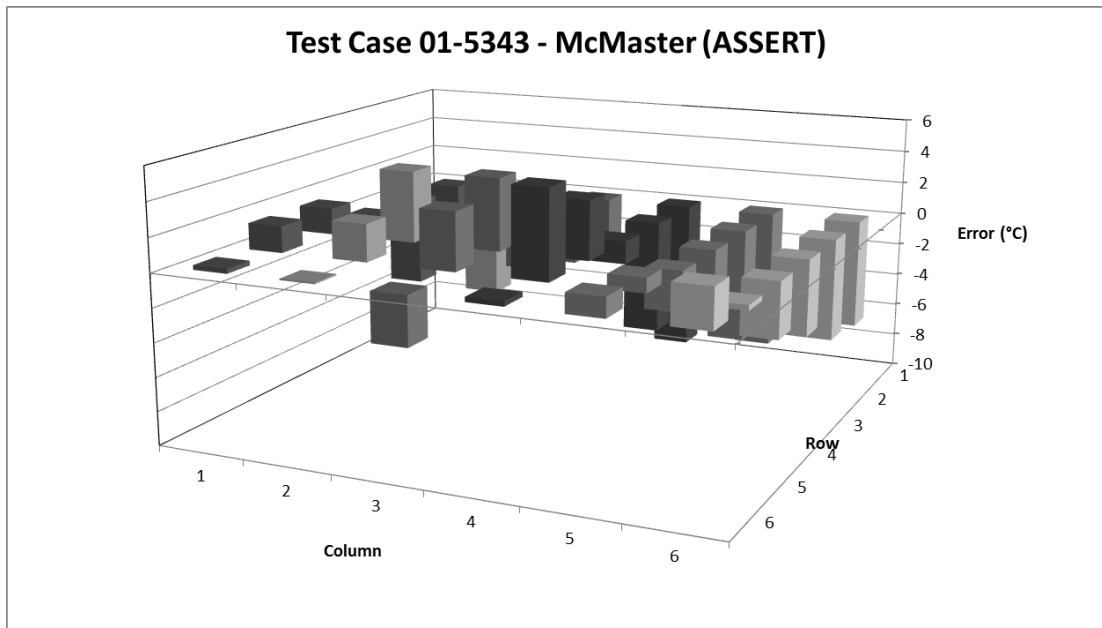**Figure AI-40 Test Case 01-5237 ASSERT – Error of Calculated Fluid Temperature**
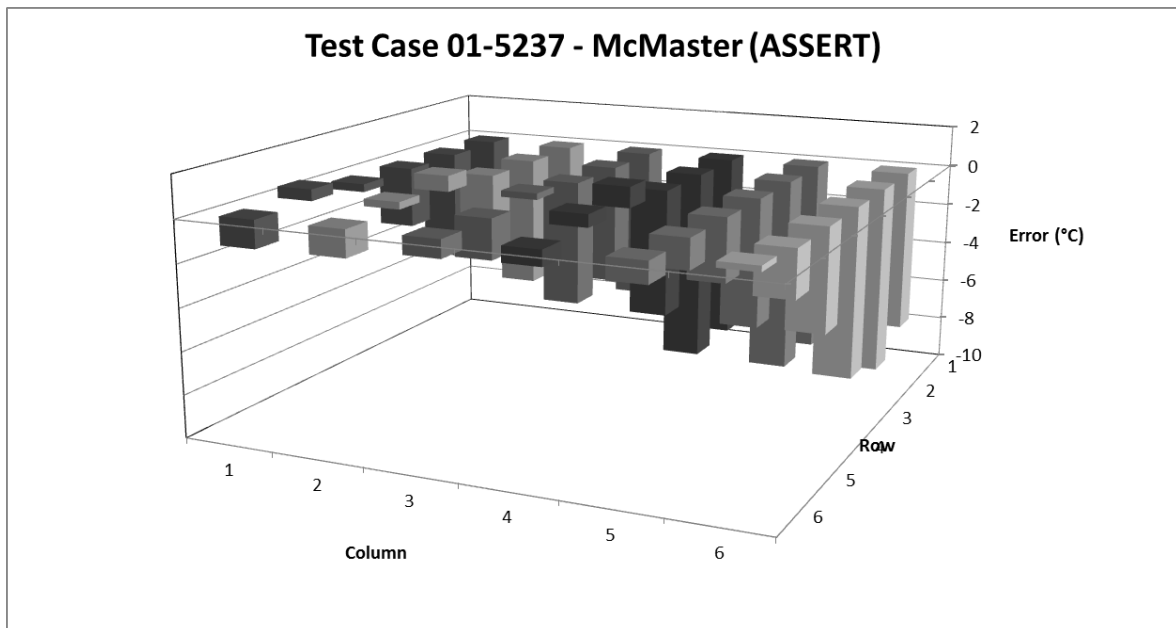
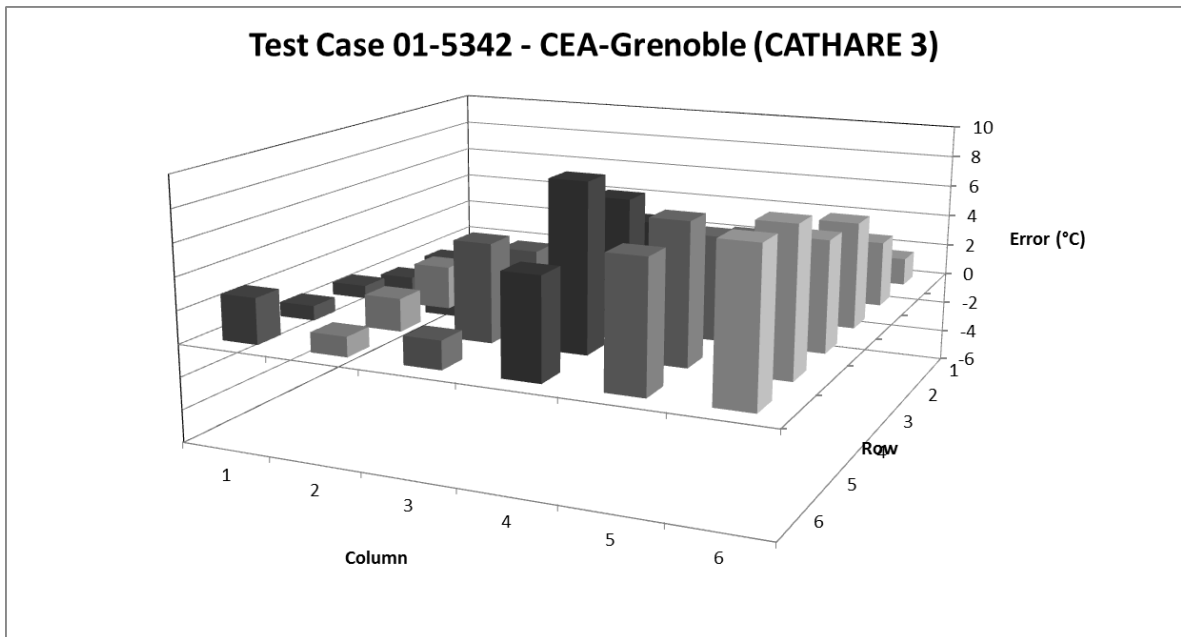**Figure AI-41 Test Case 01-6232 CATHARE 3 – Error of Calculated Fluid Temperature**
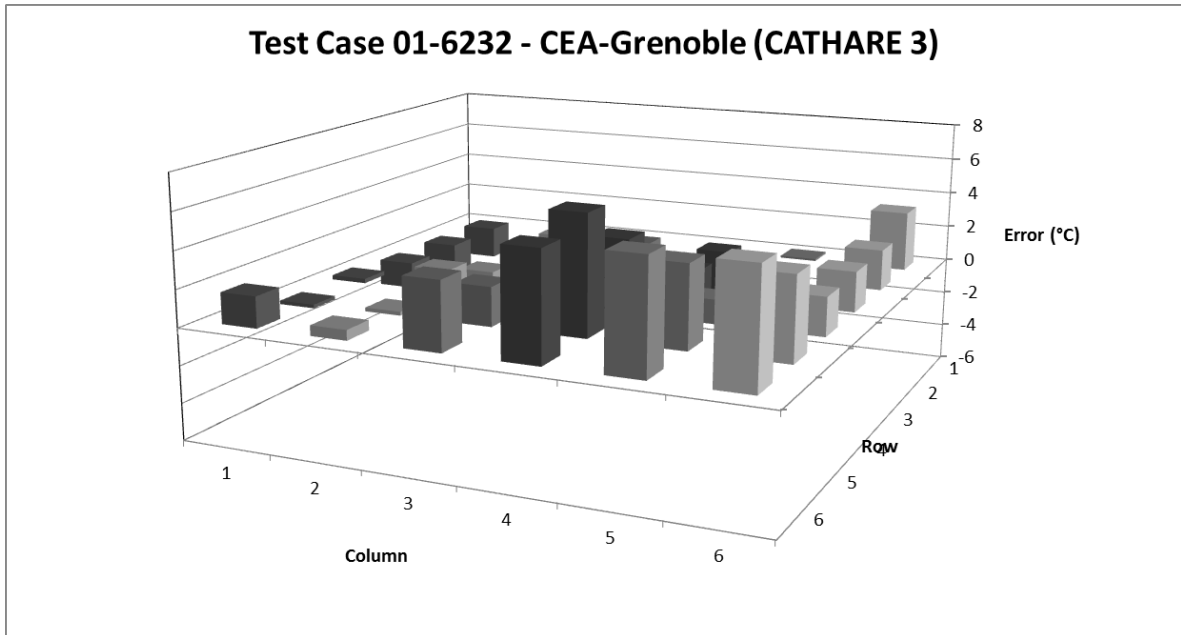
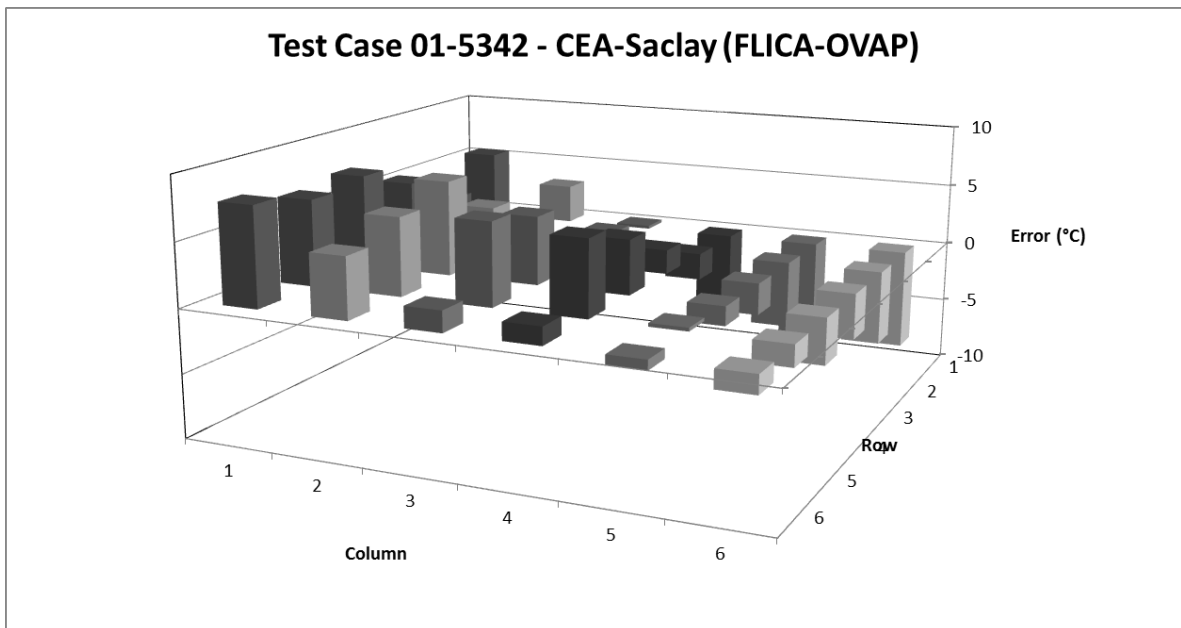**Figure AI-42 Test Case 01-6232 FLICA-OVAP – Error of Calculated Fluid Temperature**
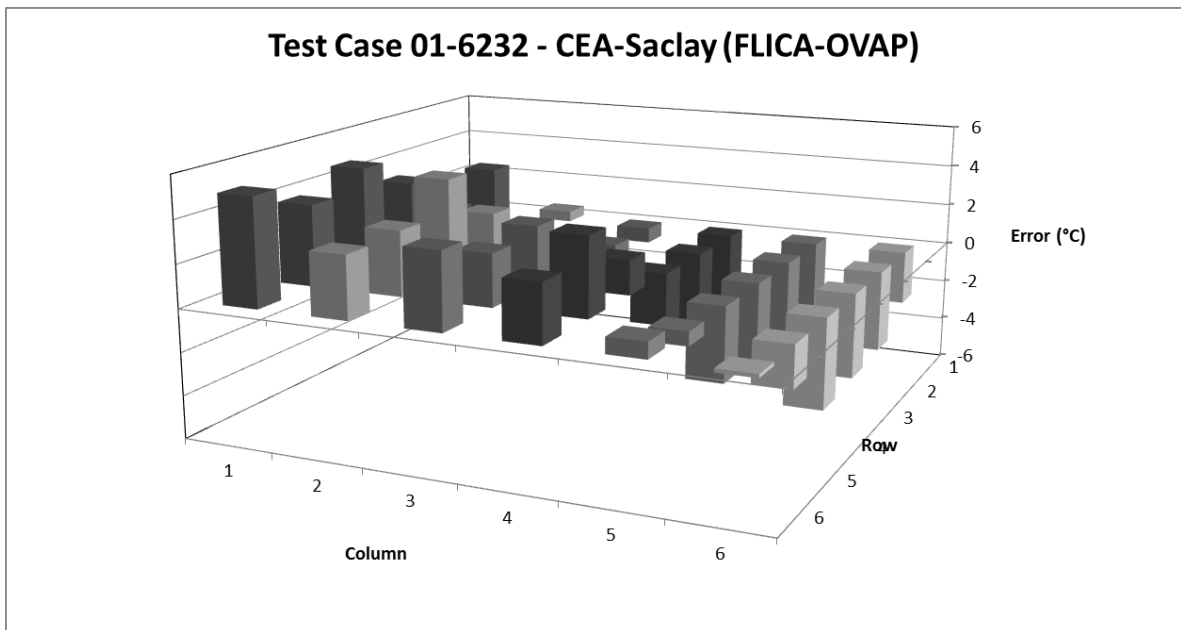
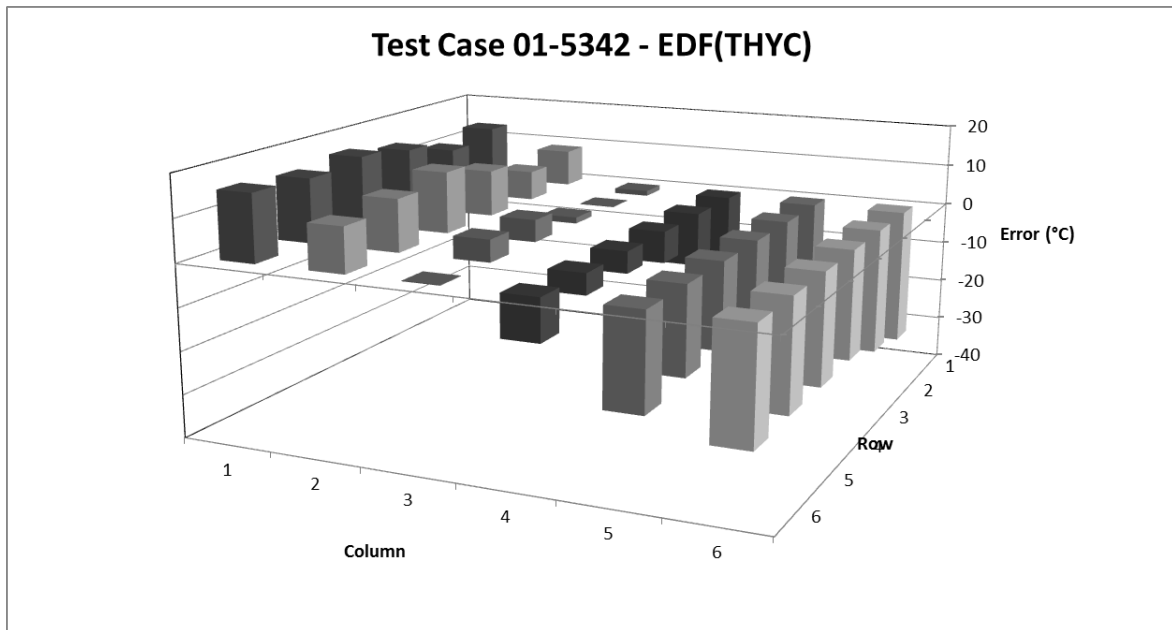**Figure AI-43 Test Case 01-6232 THYC – Error of Calculated Fluid Temperature**
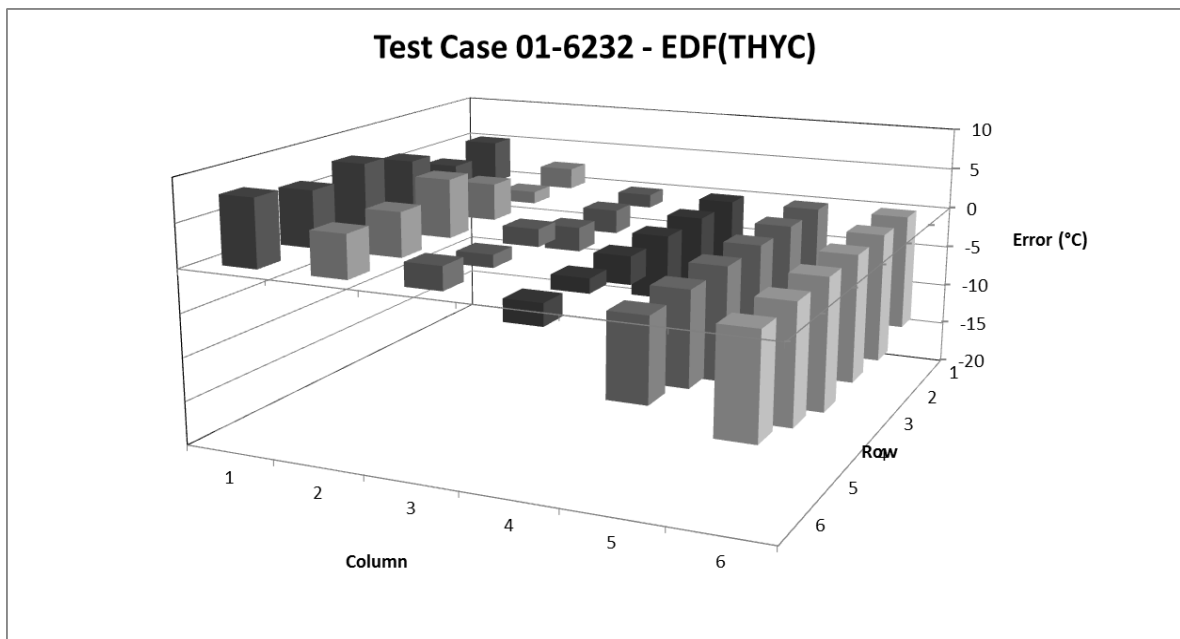
Figure AI-44 Test Case 01-6232 MATRA – Error of Calculated Fluid Temperature
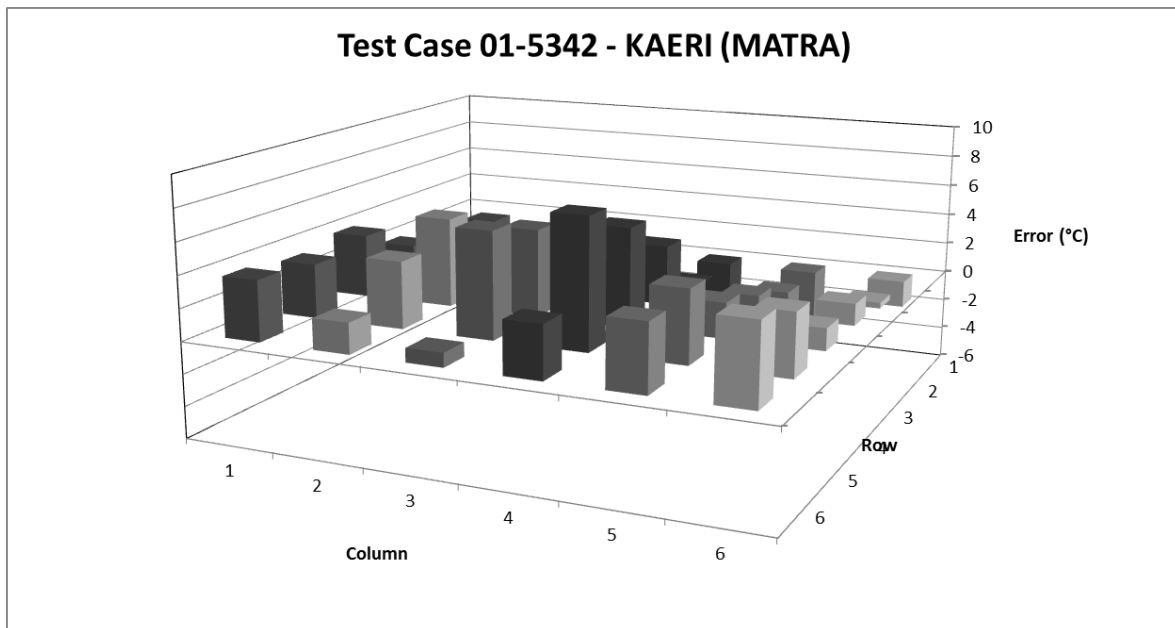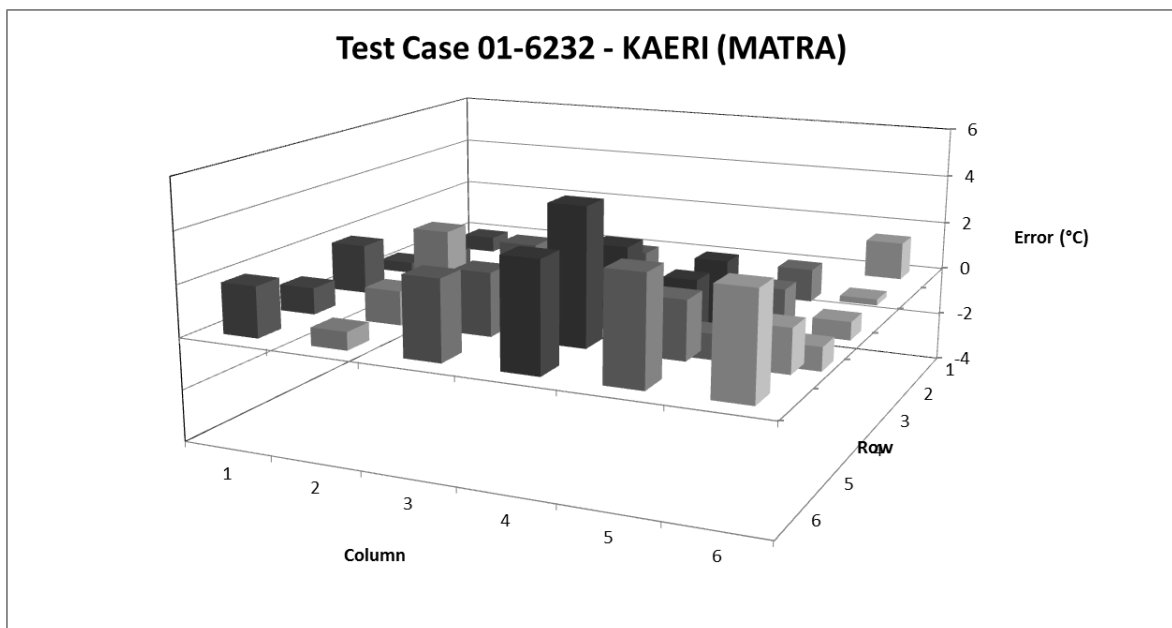
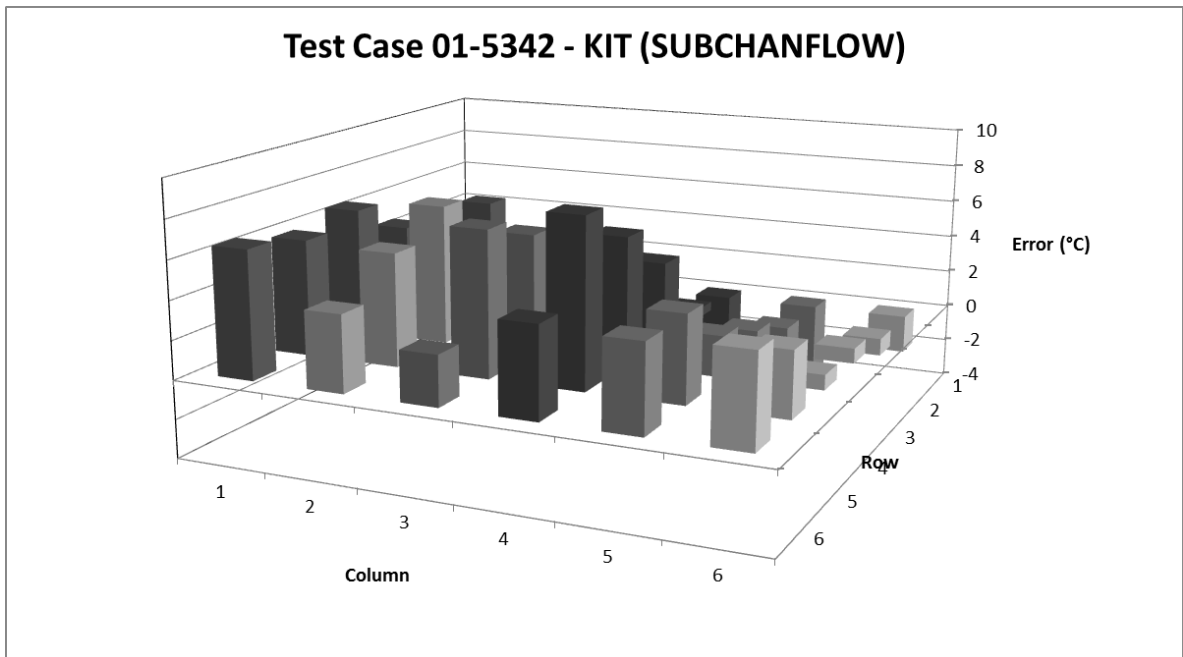**Figure AI-45 Test Case 01-6232 SUBCHANFLOW – Error of Calculated Fluid Temperature**
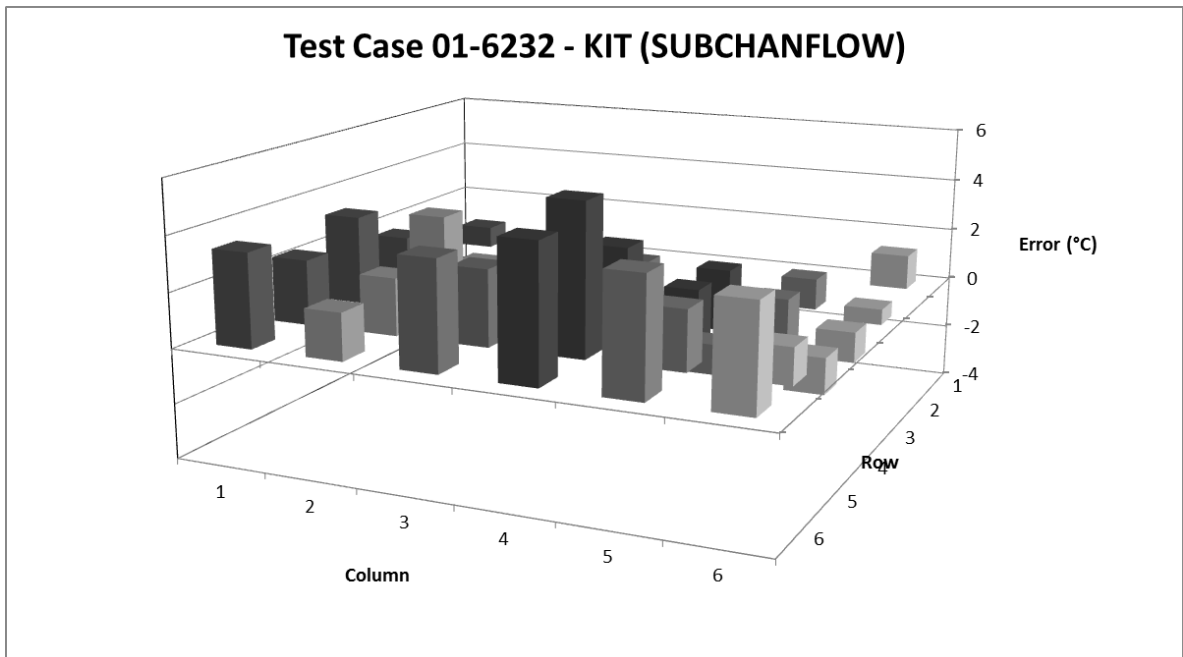
Figure AI-46 Test Case 01-6232 VIPRE – Error of Calculated Fluid Temperature
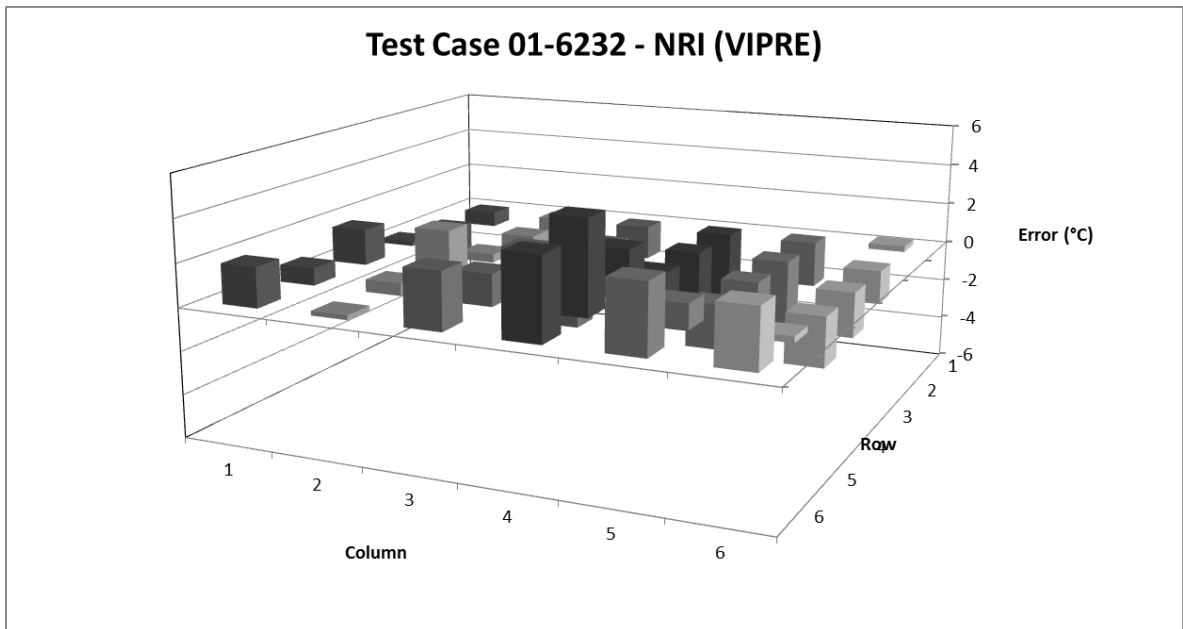
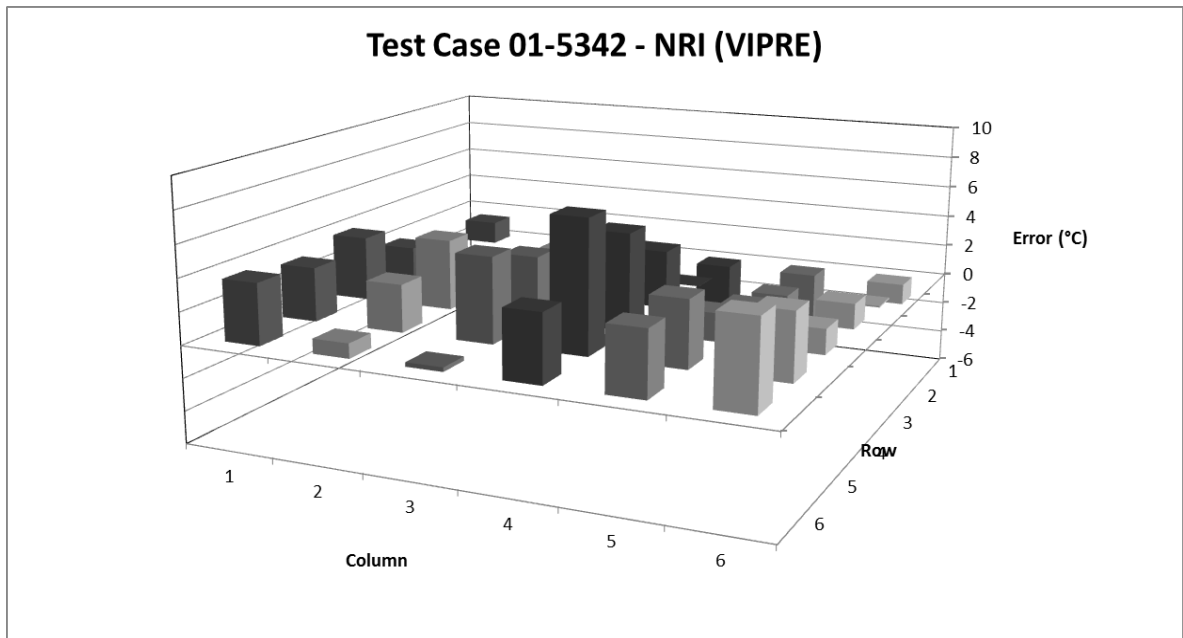**Figure AI-47 Test Case 01-6232 FLICA – Error of Calculated Fluid Temperature**

Test Case 01-6232 - PSI (FLICA)
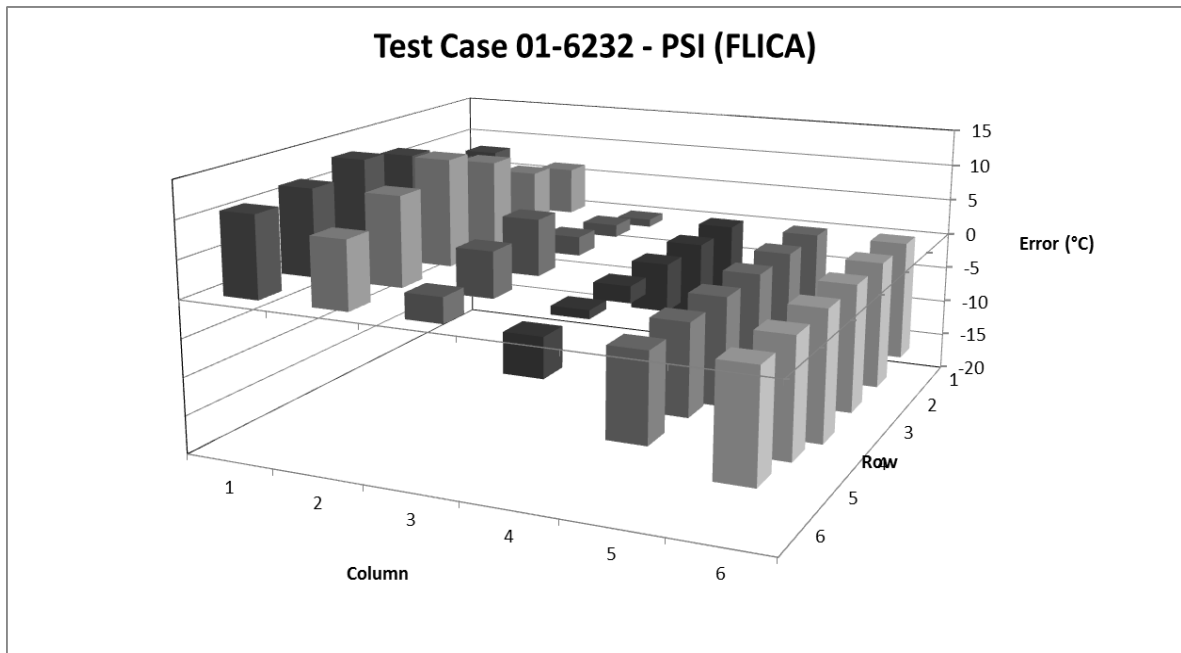
Figure AI-48 Test Case 01-6232 ASSERT – Error of Calculated Fluid Temperature

Test Case 01-6232 - McMaster (ASSERT)
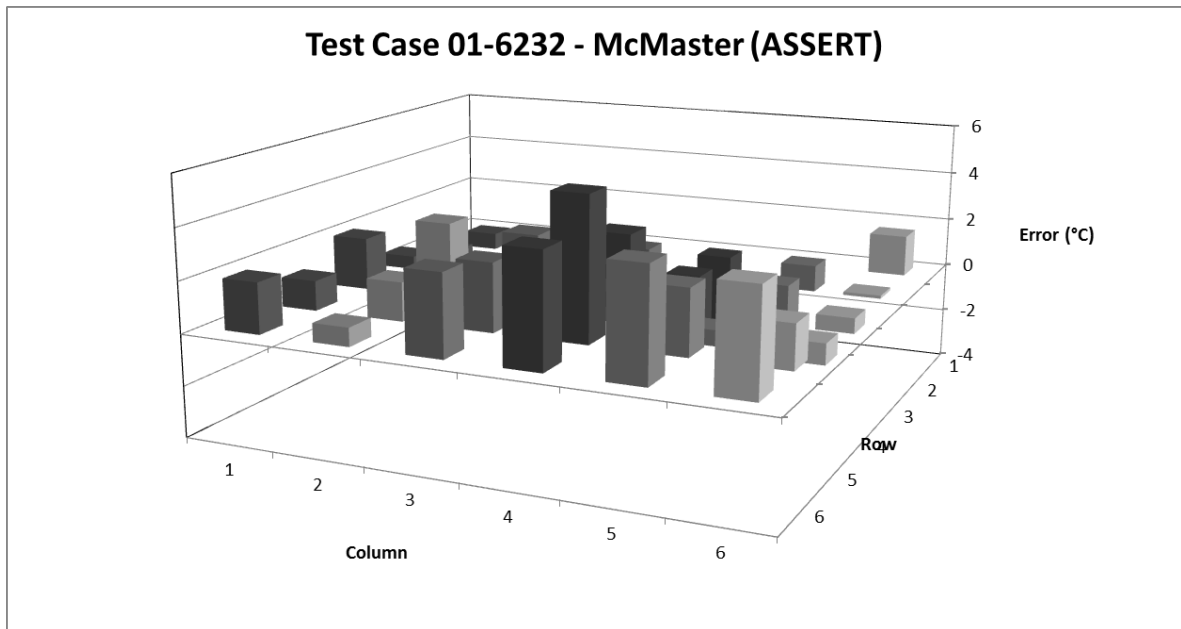
Figure AI-49 Test Case 01-6233 CATHARE 3 – Error of Calculated Fluid Temperature
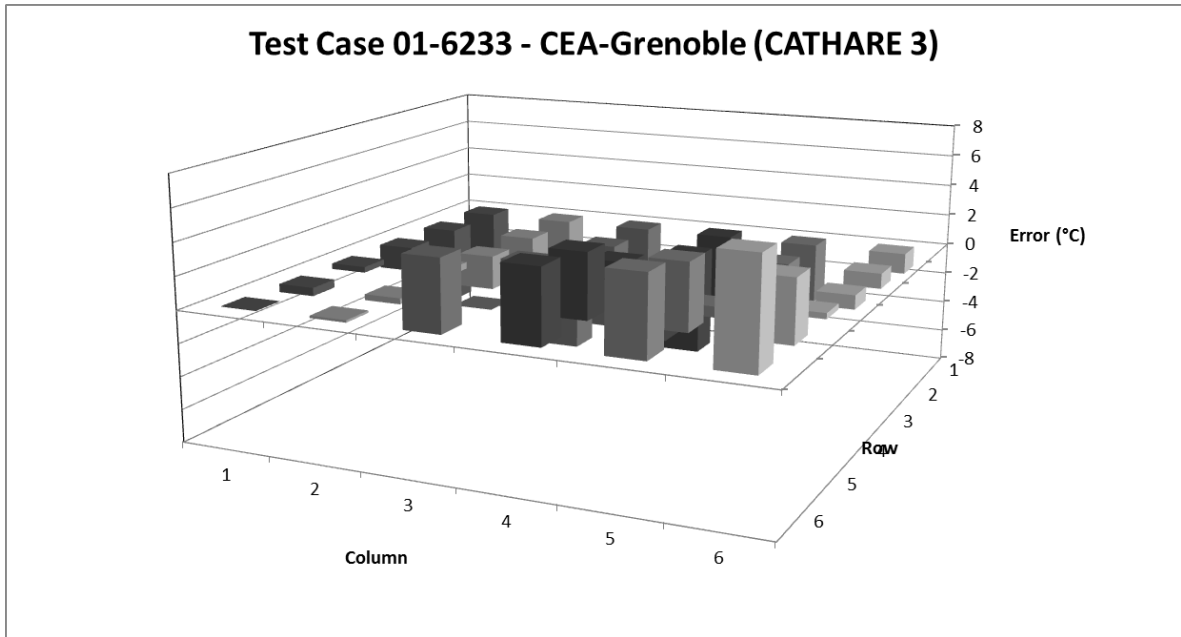
Figure AI-50 Test Case 01-6233 FLICA-OVAP – Error of Calculated Fluid Temperature

NEA/NSC/R(2015)7
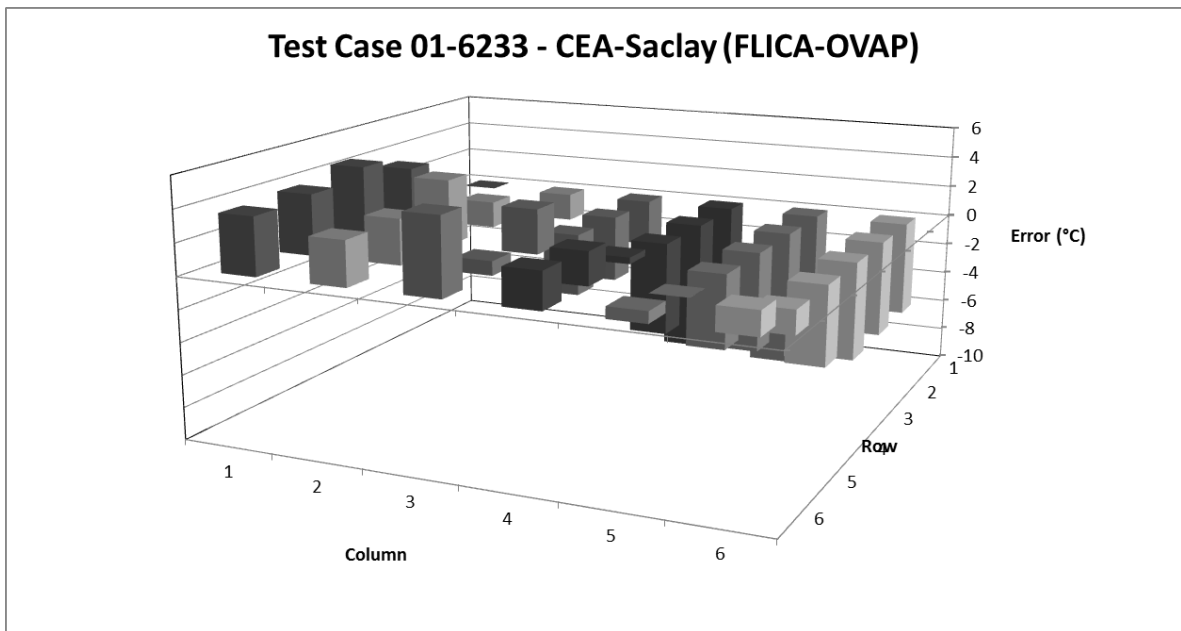
Figure AI-51 Test Case 01-6233 THYC – Error of Calculated Fluid Temperature

Test Case 01-6233 - EDF(THYC)
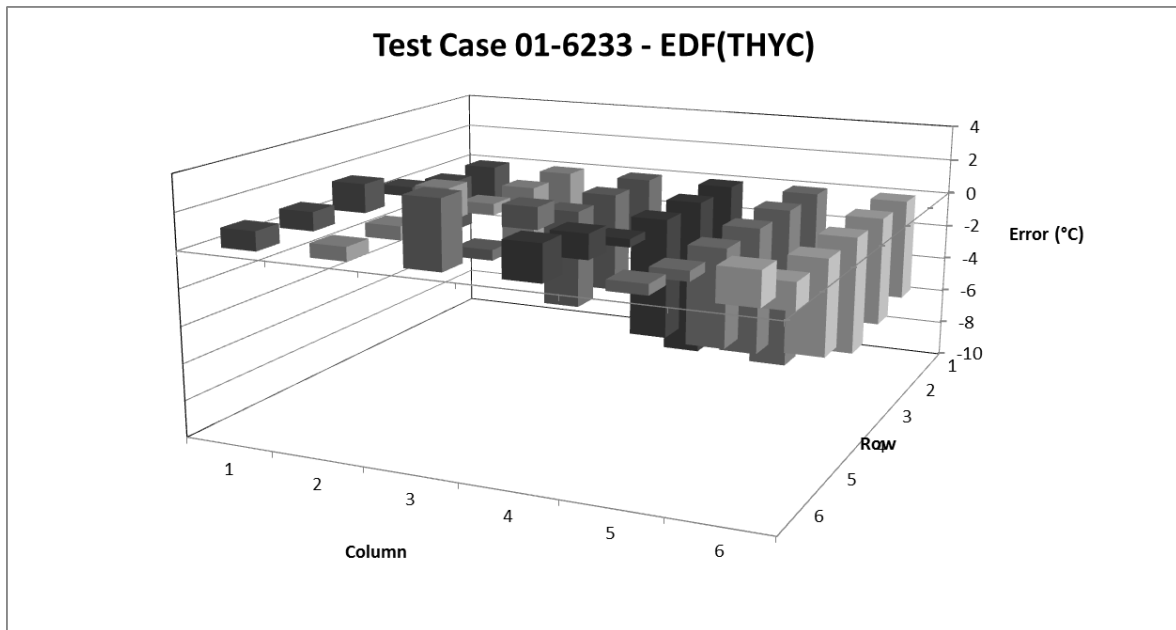
Figure AI-52 Test Case 01-6233 MATRA – Error of Calculated Fluid Temperature

Test Case 01-6233 - KAERI (MATRA)
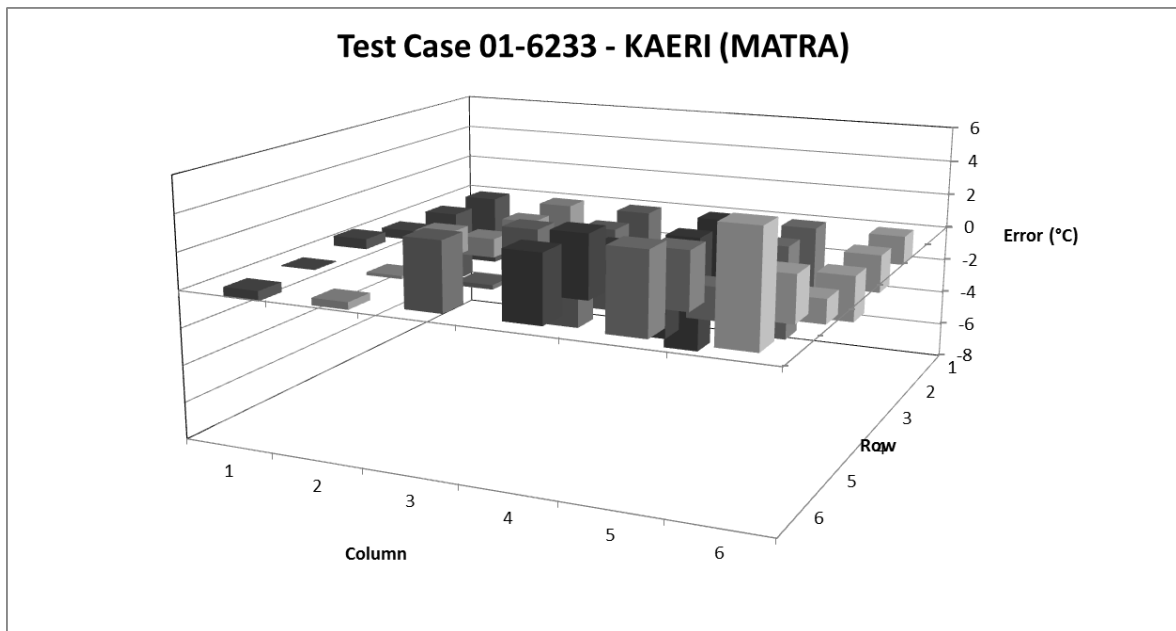
Figure AI-53 Test Case 01-6233 SUBCHANFLOW – Error of Calculated Fluid Temperature
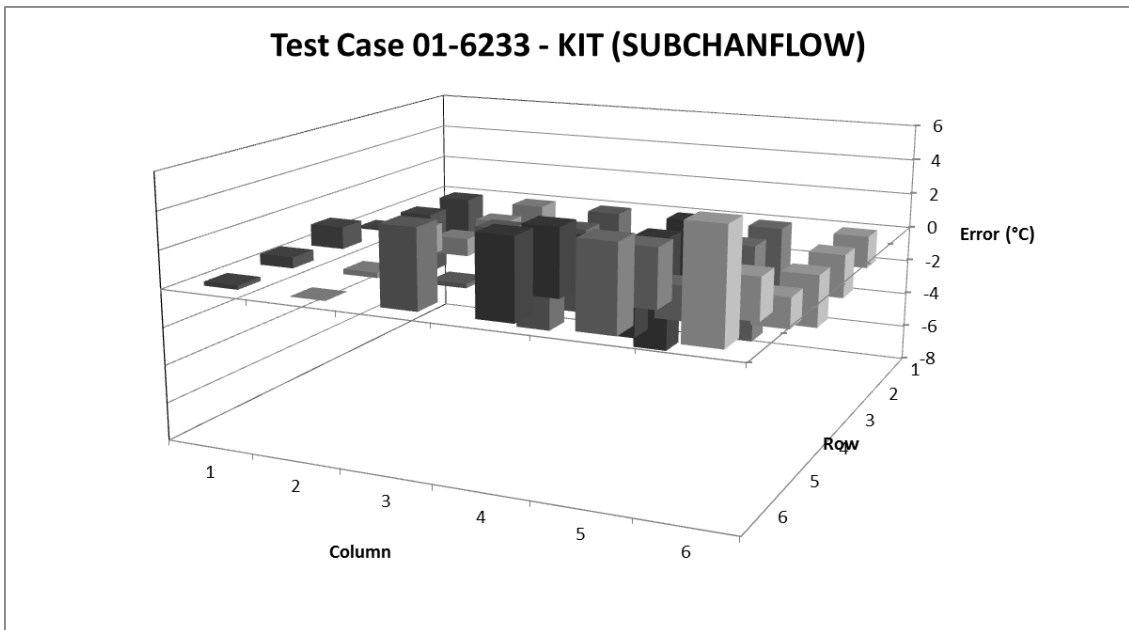
Figure AI-54 Test Case 01-6233 VIPRE – Error of Calculated Fluid Temperature
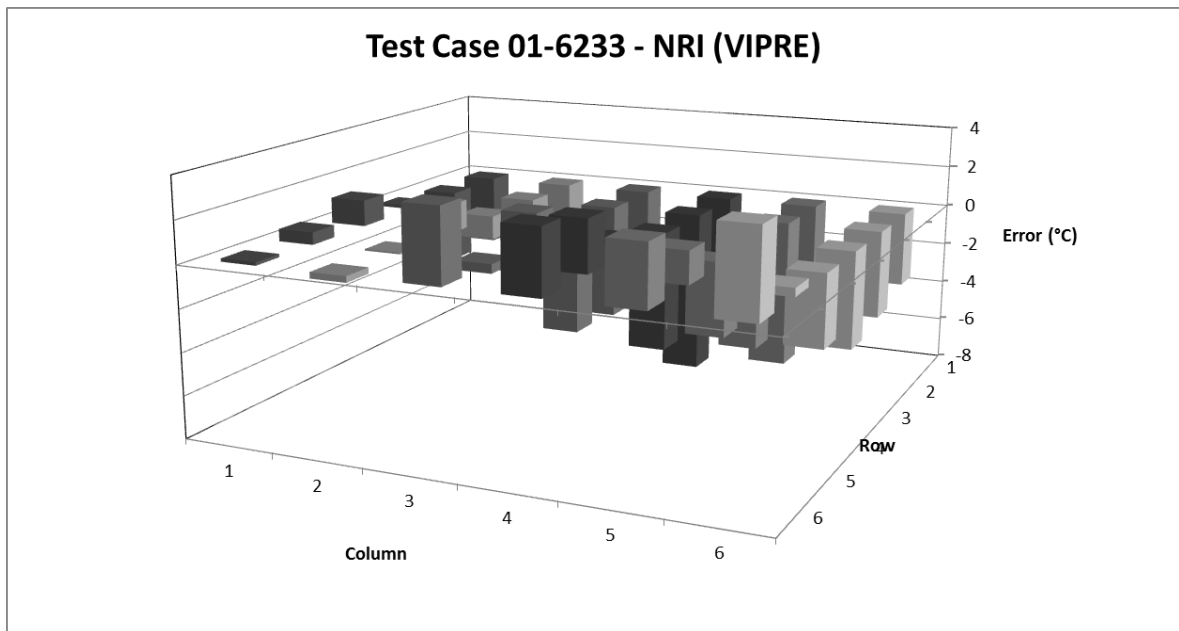
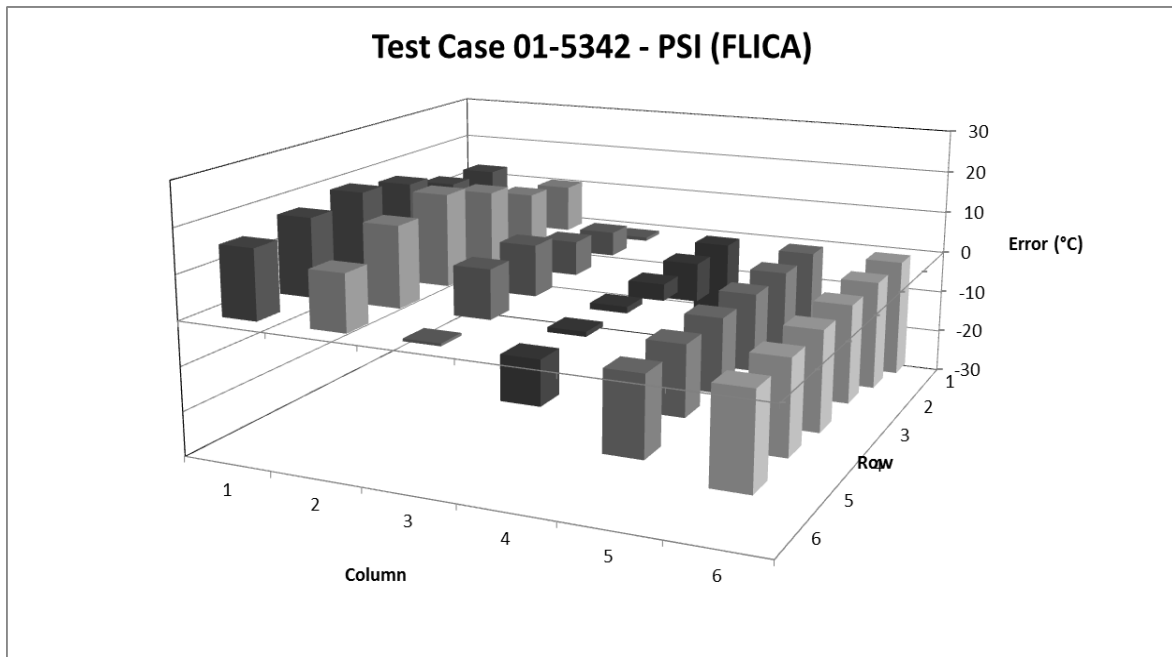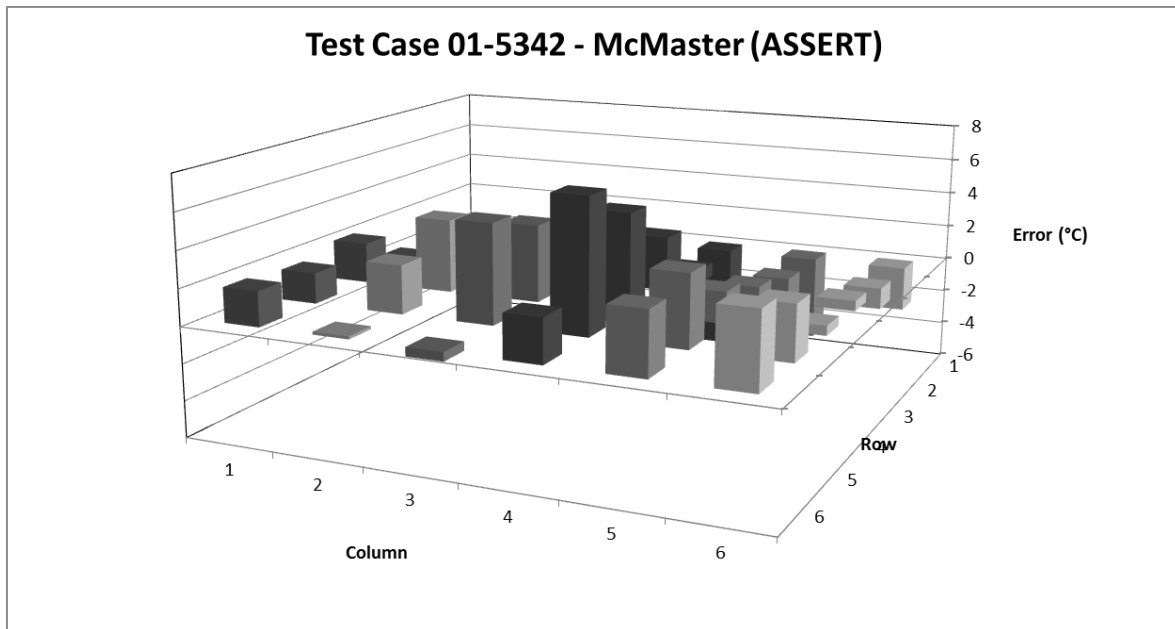**Figure AI-55 Test Case 01-6233 FLICA – Error of Calculated Fluid Temperature**

Test Case 01-6233 - PSI (FLICA)
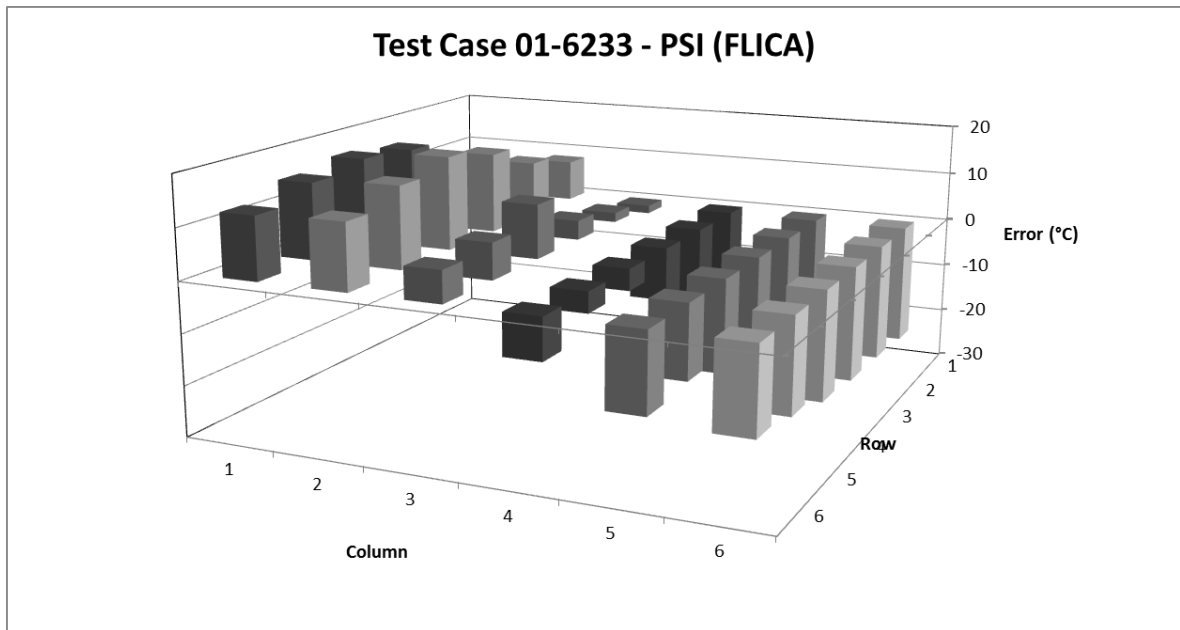
Figure AI-56 Test Case 01-6233 ASSERT – Error of Calculated Fluid Temperature

Test Case 01-6233 - McMaster (ASSERT)
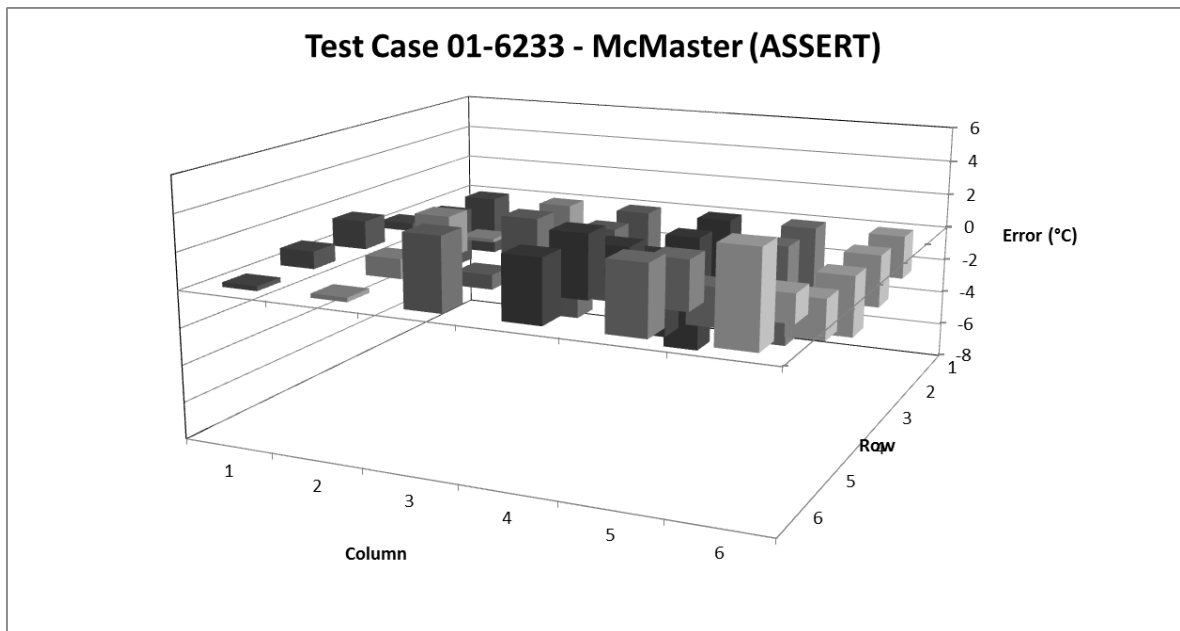
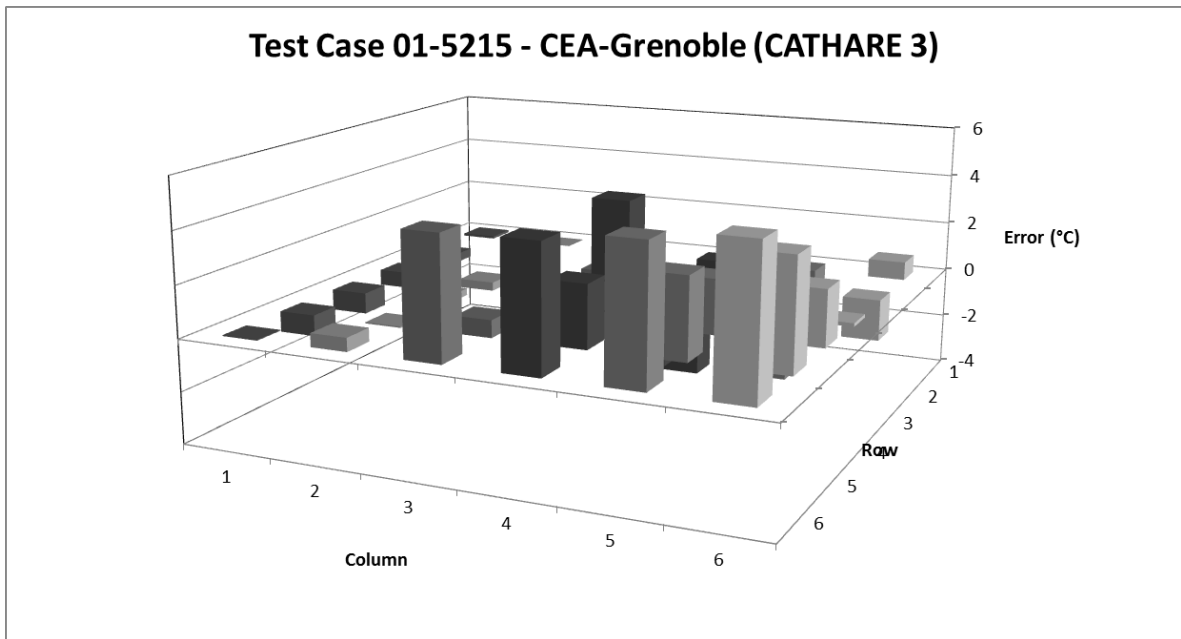**Figure AI-57 Test Case 01-1237 CATHARE 3 – Error of Calculated Fluid Temperature**
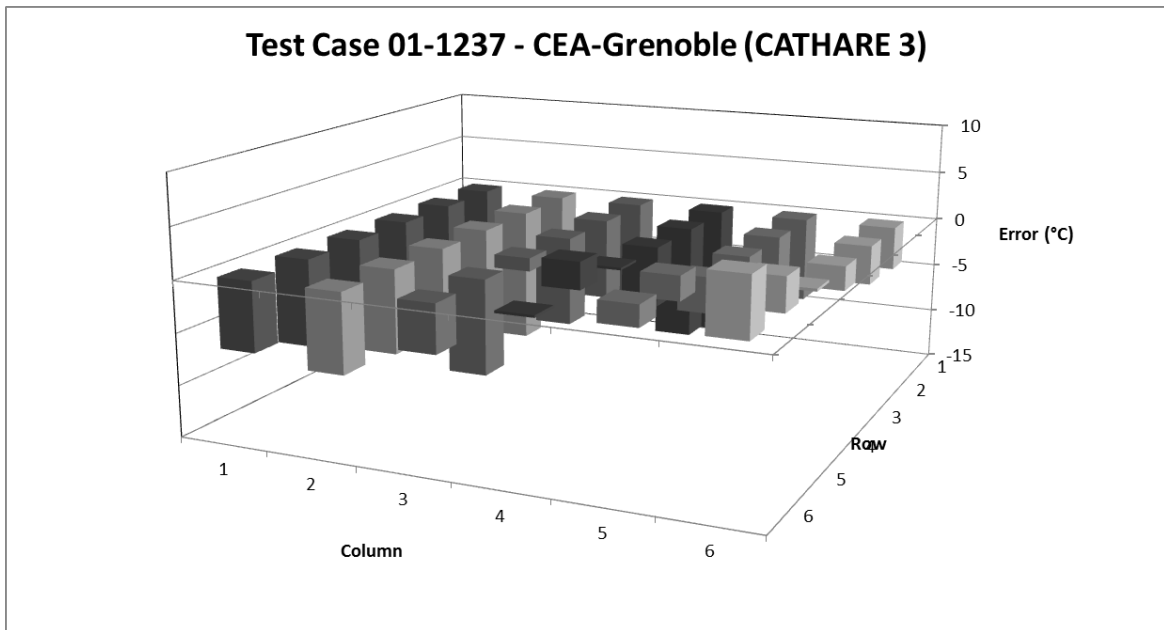
Figure AI-58 Test Case 01-1237 FLICA-OVAP – Error of Calculated Fluid Temperature
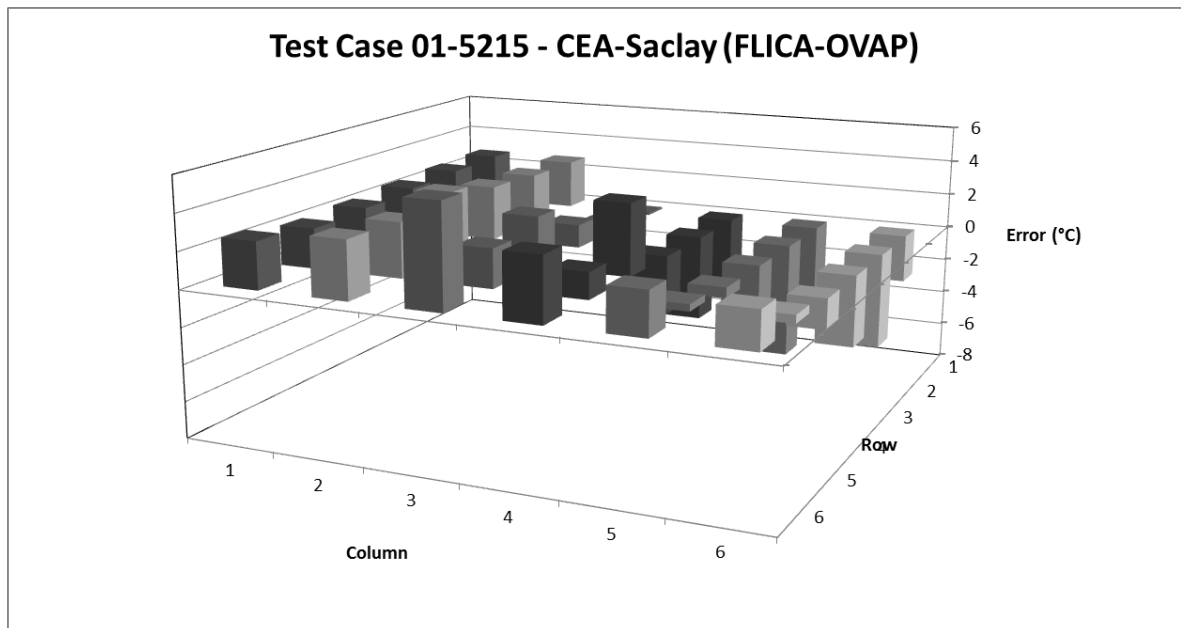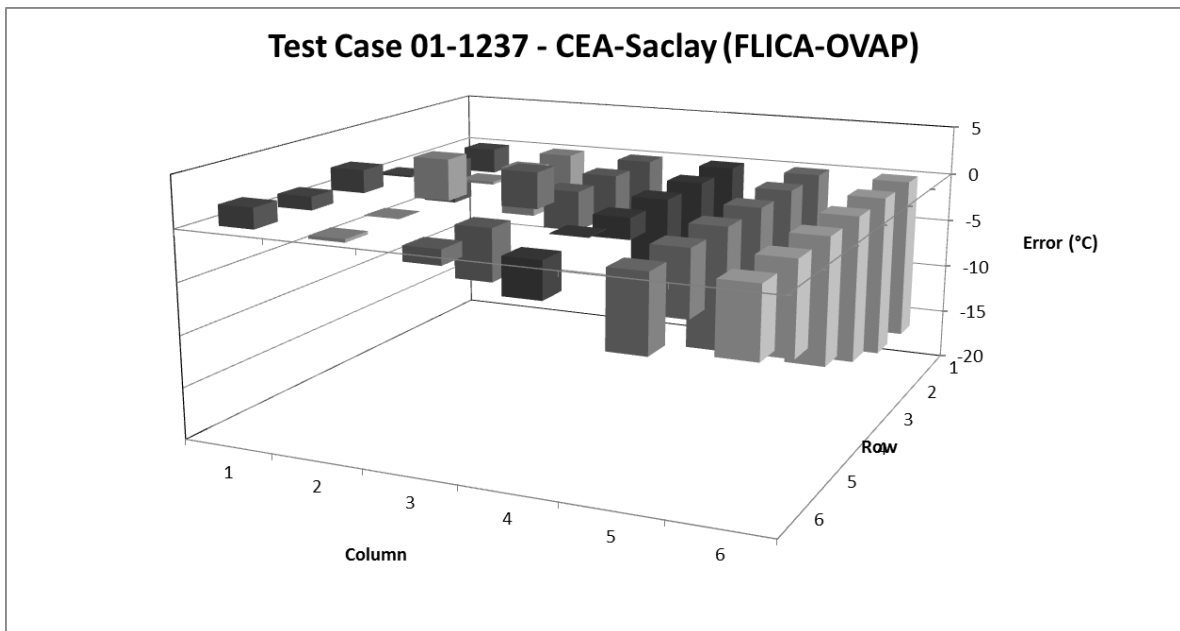
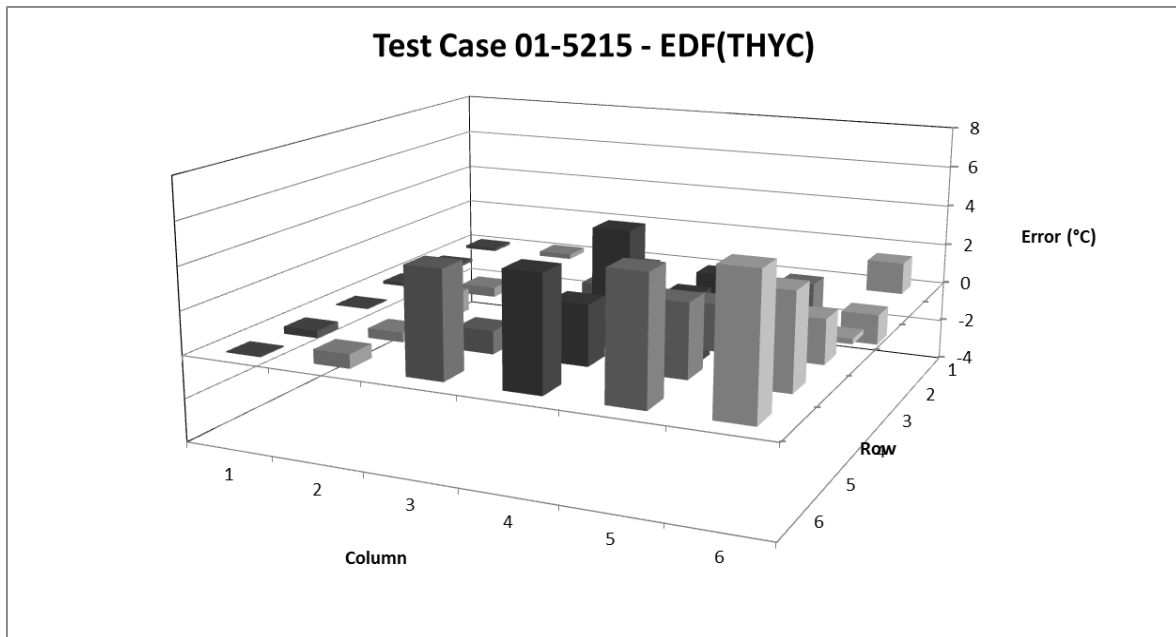**Figure AI-59 Test Case 01-1237 THYC – Error of Calculated Fluid Temperature**

Test Case 01-1237 - EDF(THYC)
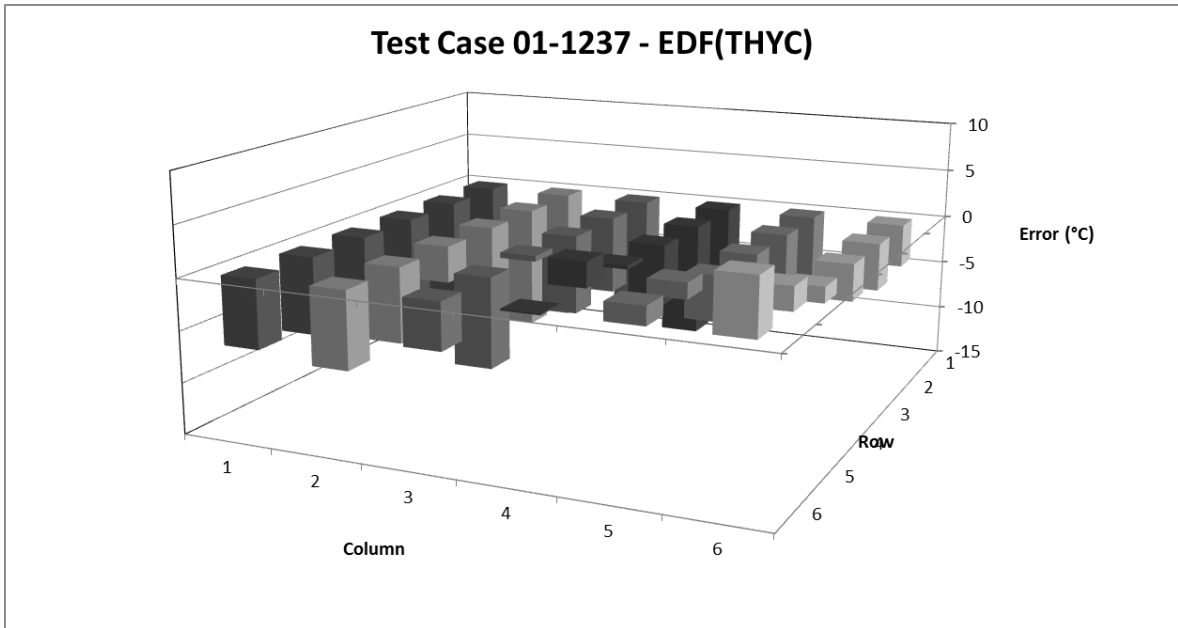
Figure AI-60 Test Case 01-1237 MATRA – Error of Calculated Fluid Temperature

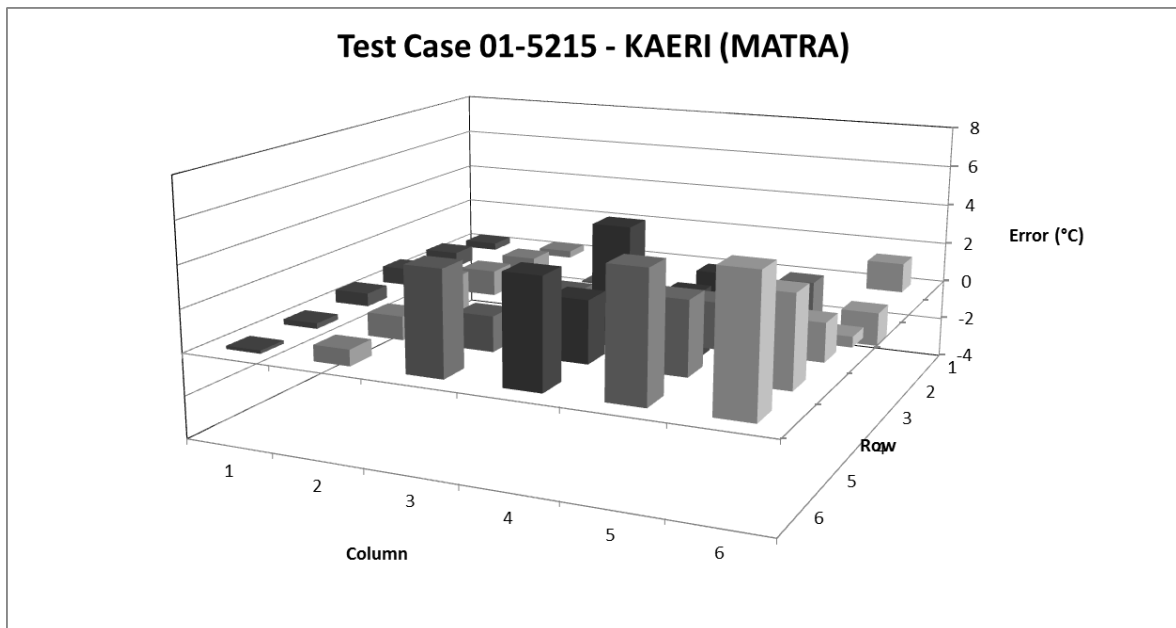
Test Case 01-1237 - KAERI (MATRA)
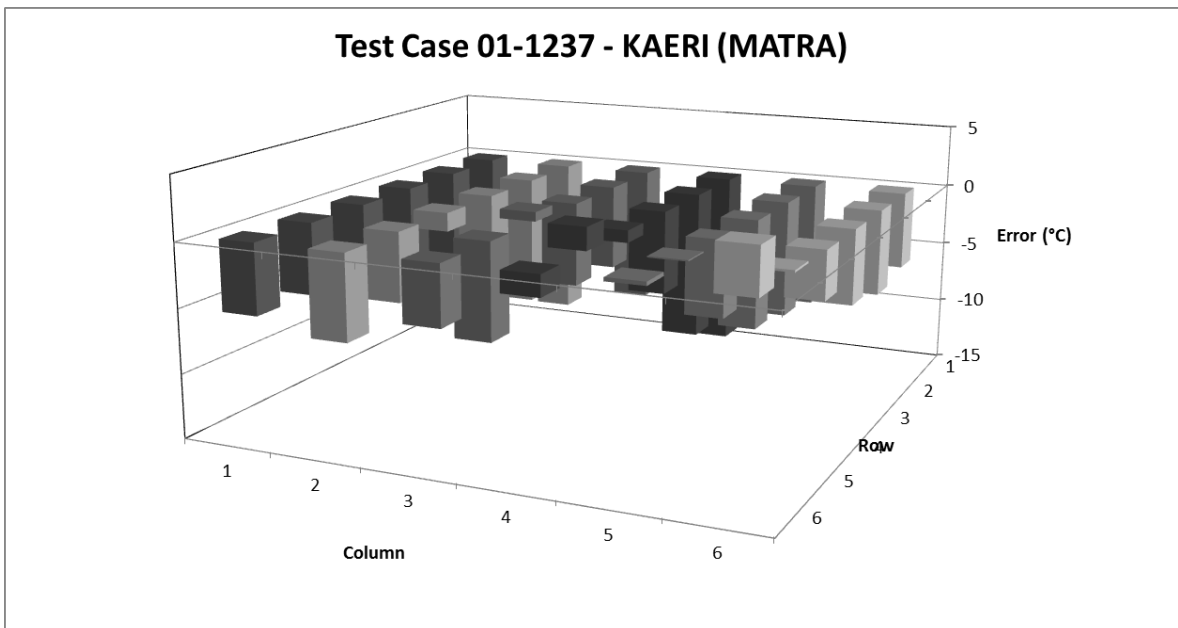
Figure AI-61 Test Case 01-1237 SUBCHANFLOW – Error of Calculated Fluid Temperature
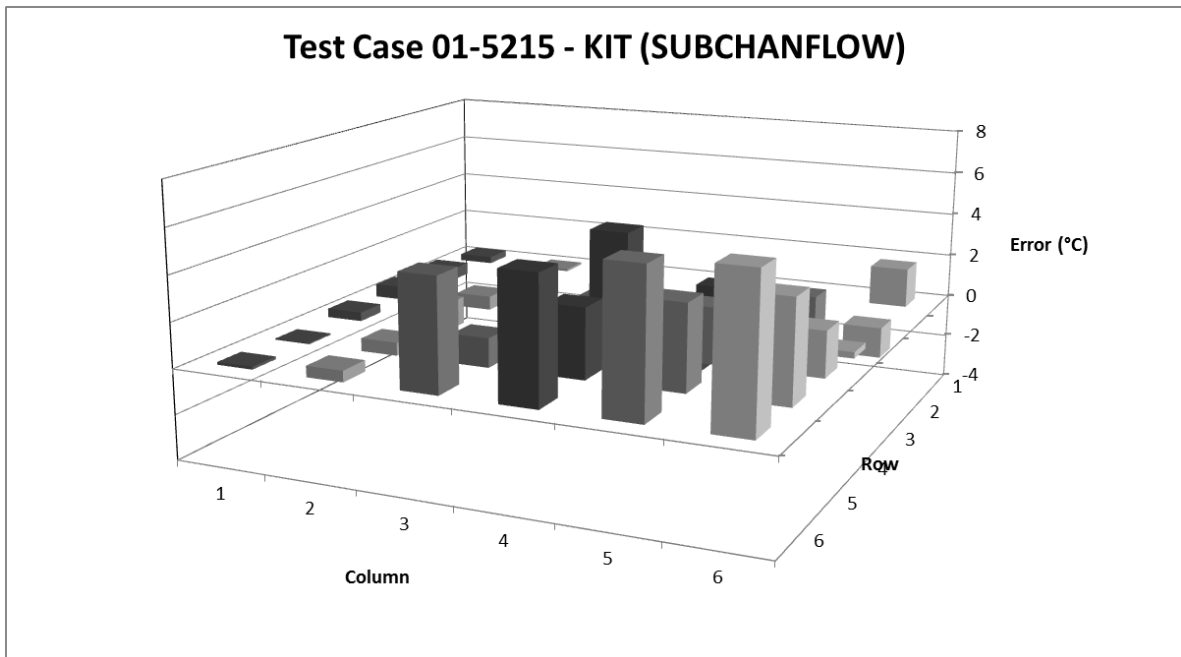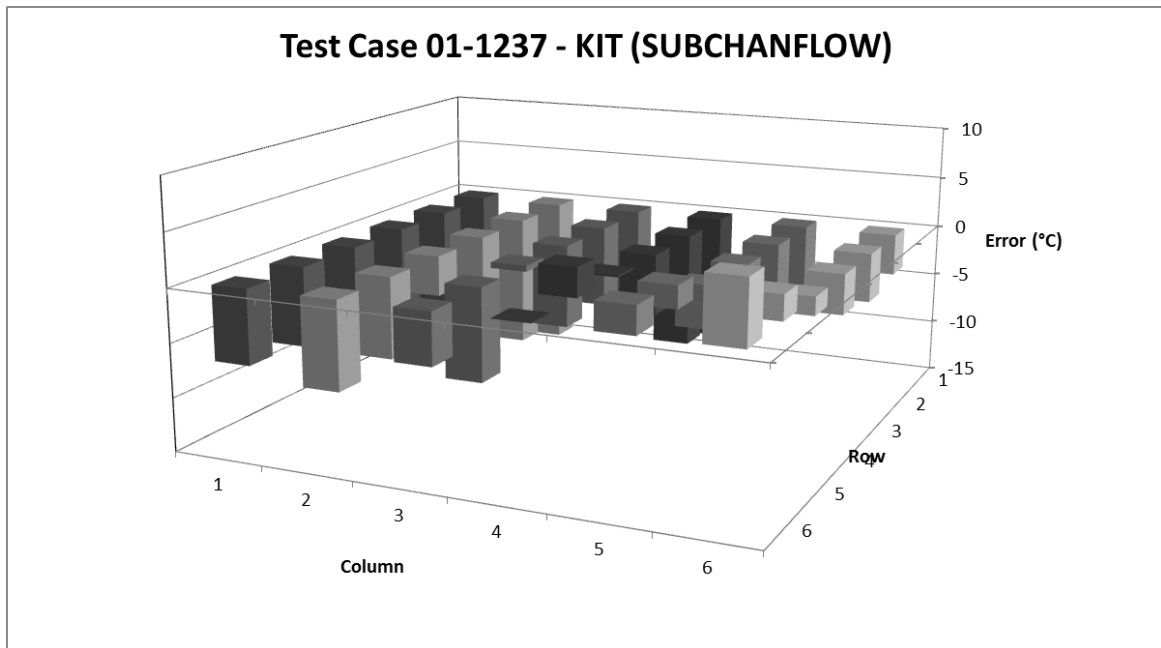

Figure AI-62 Test Case 01-1237 VIPRE – Error of Calculated Fluid Temperature
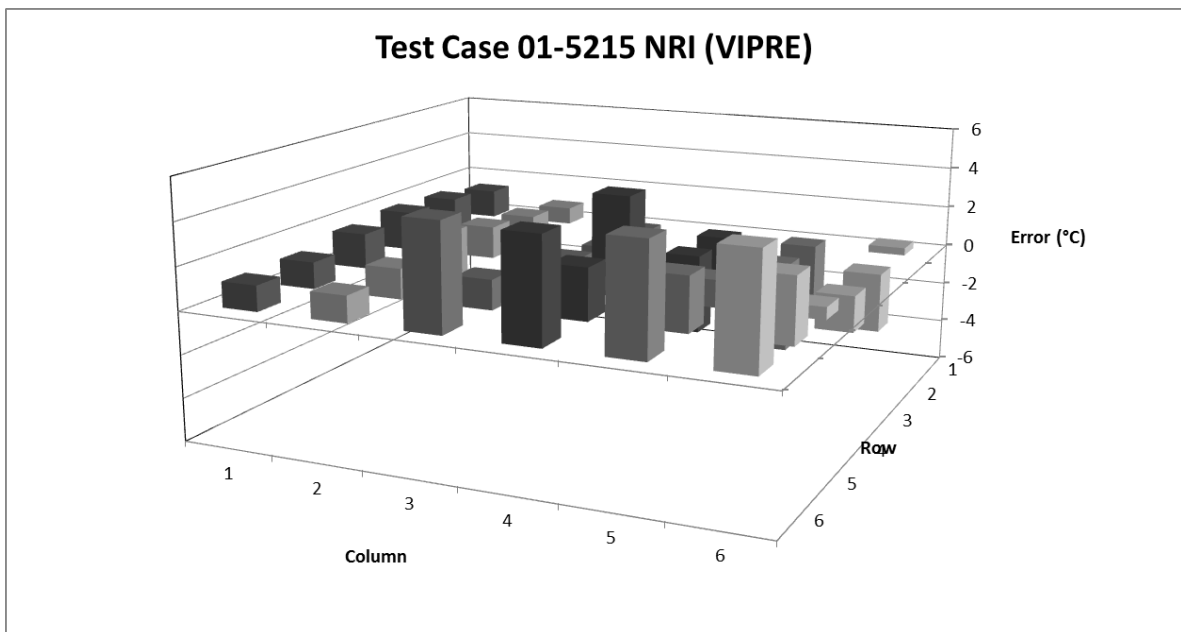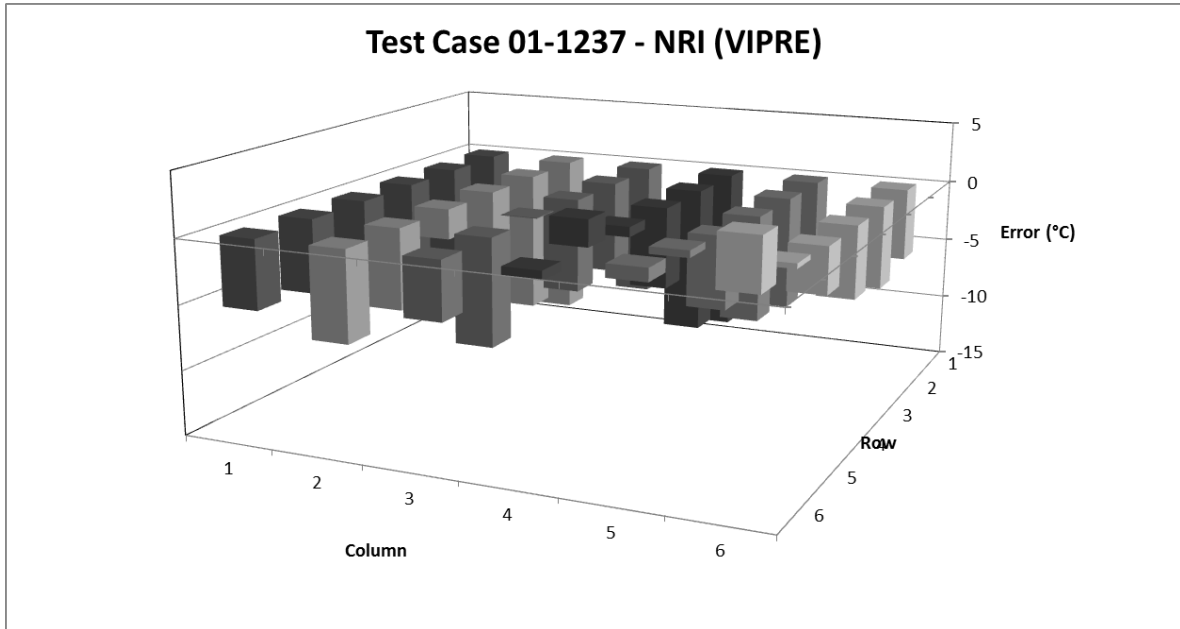
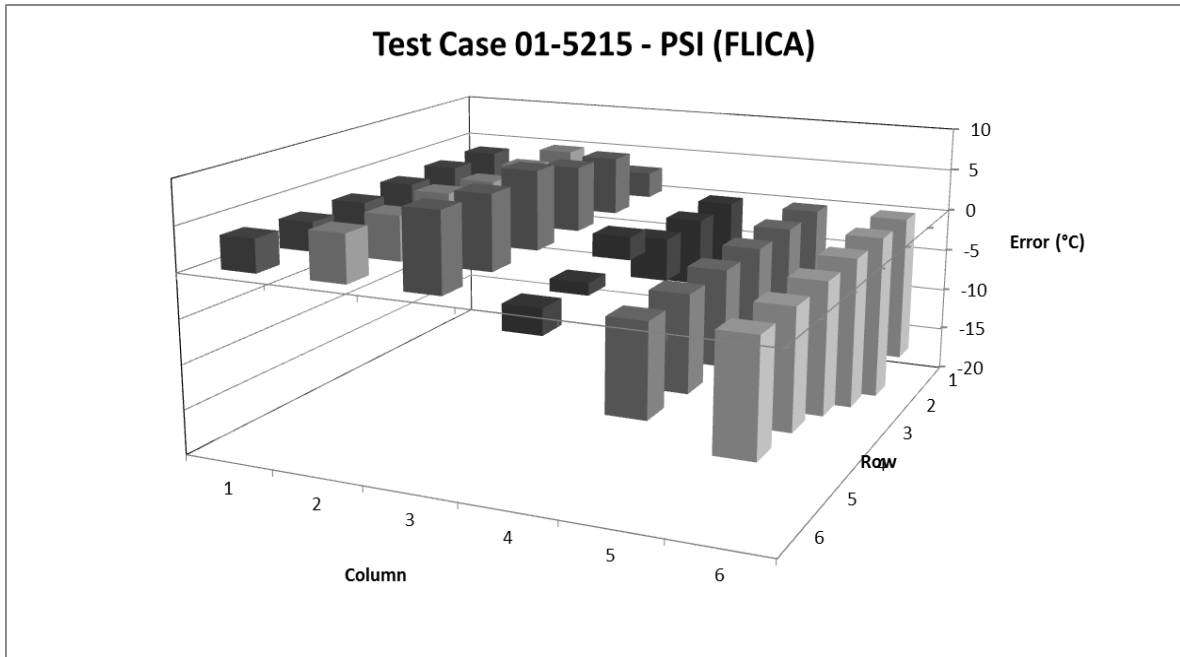**Figure AI-63 Test Case 01-1237 FLICA – Error of Calculated Fluid Temperature**

Test Case 01-1237 - PSI (FLICA)
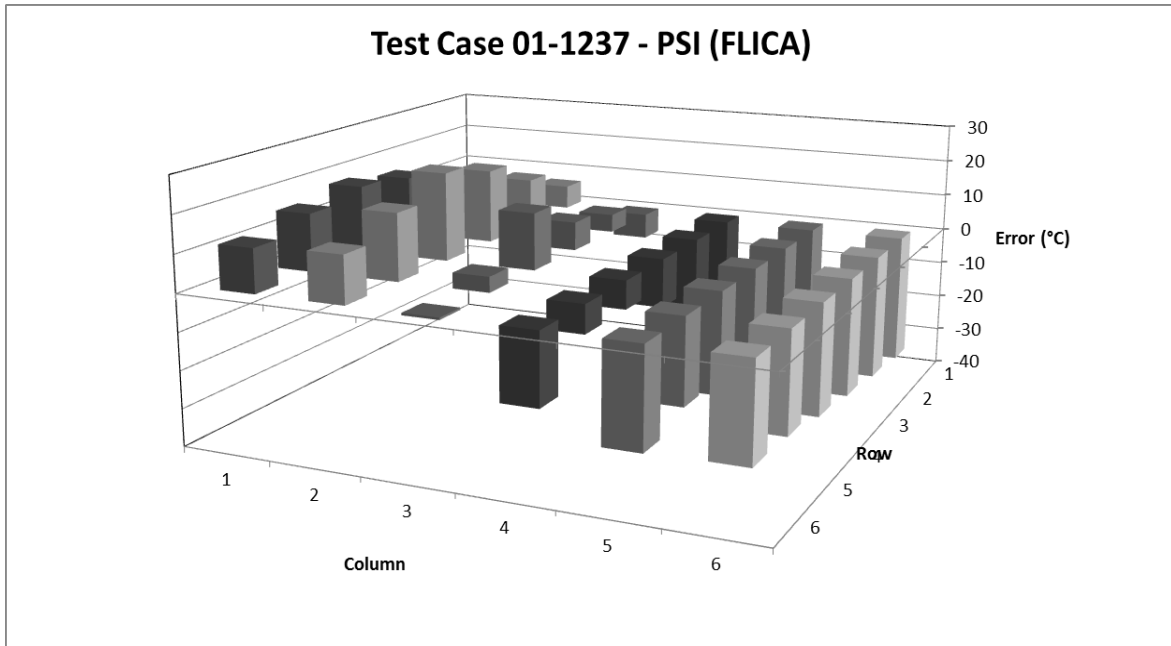
Figure AI-64 Test Case 01-1237 ASSERT – Error of Calculated Fluid Temperature

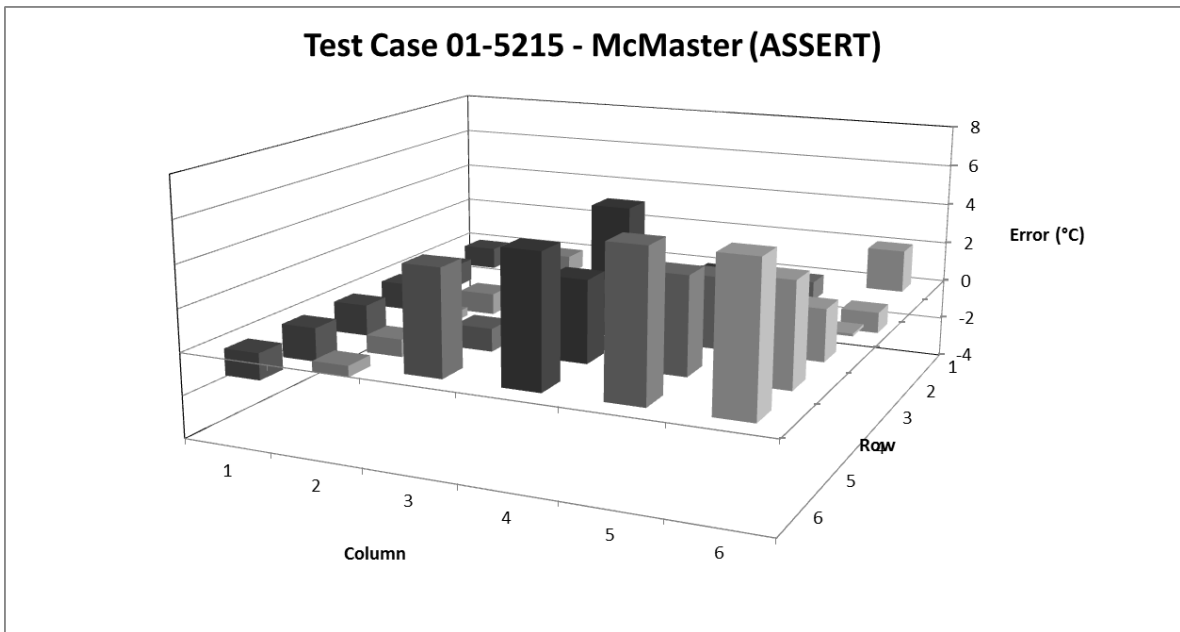
Test Case 01-1237 - McMaster (ASSERT)
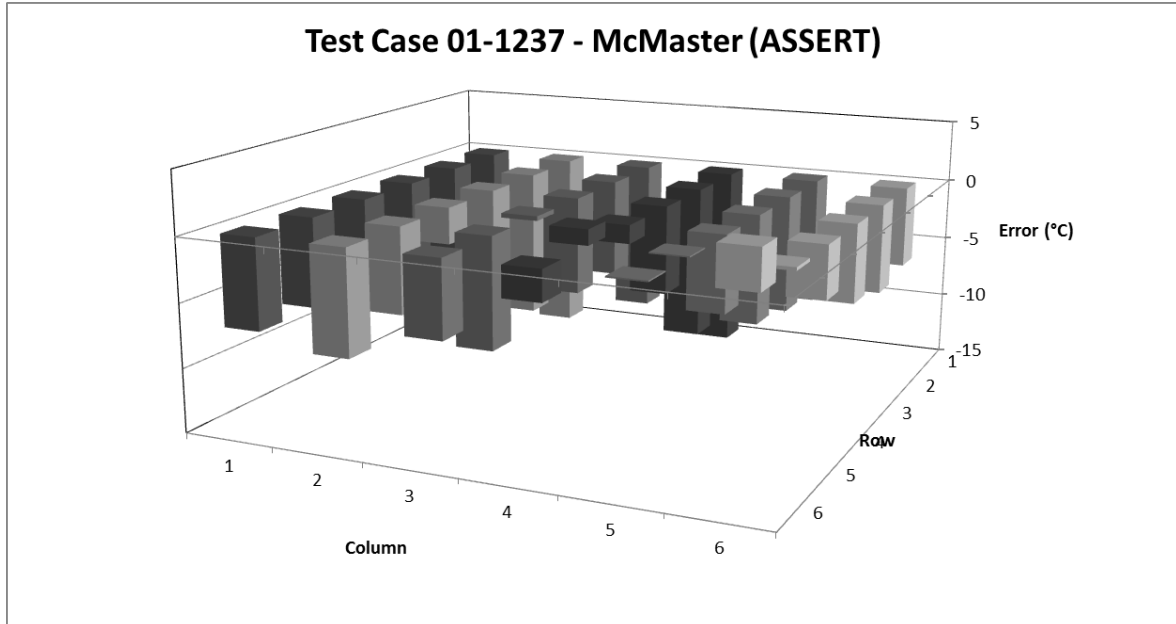
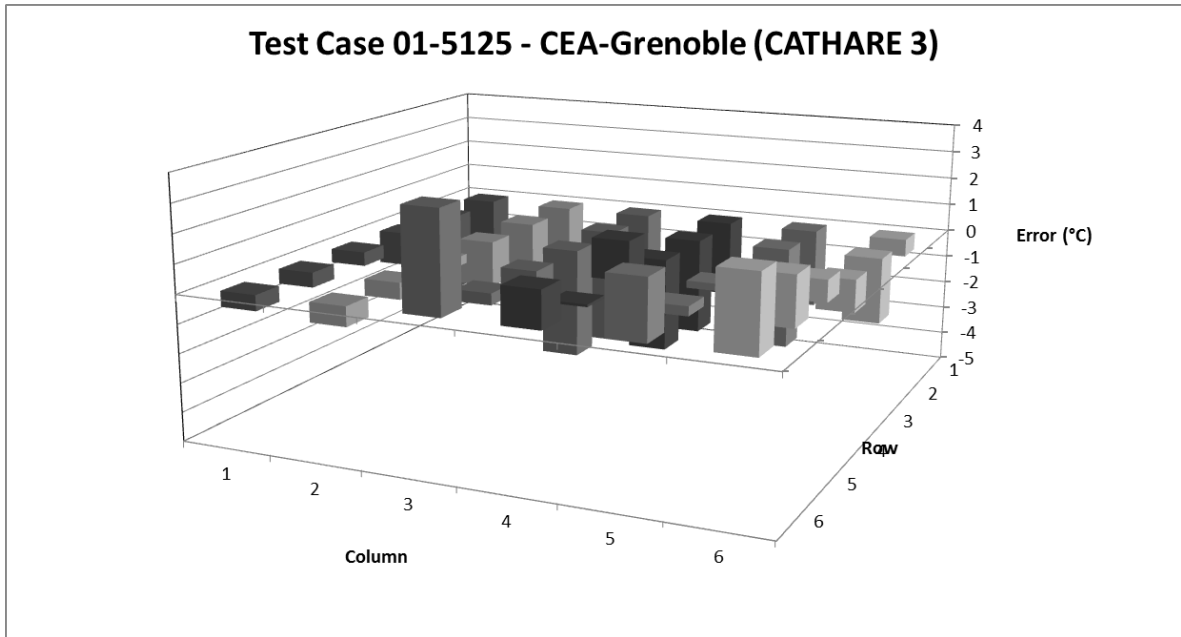**Figure AI-65 Test Case 01-5252 CATHARE 3 – Error of Calculated Fluid Temperature**
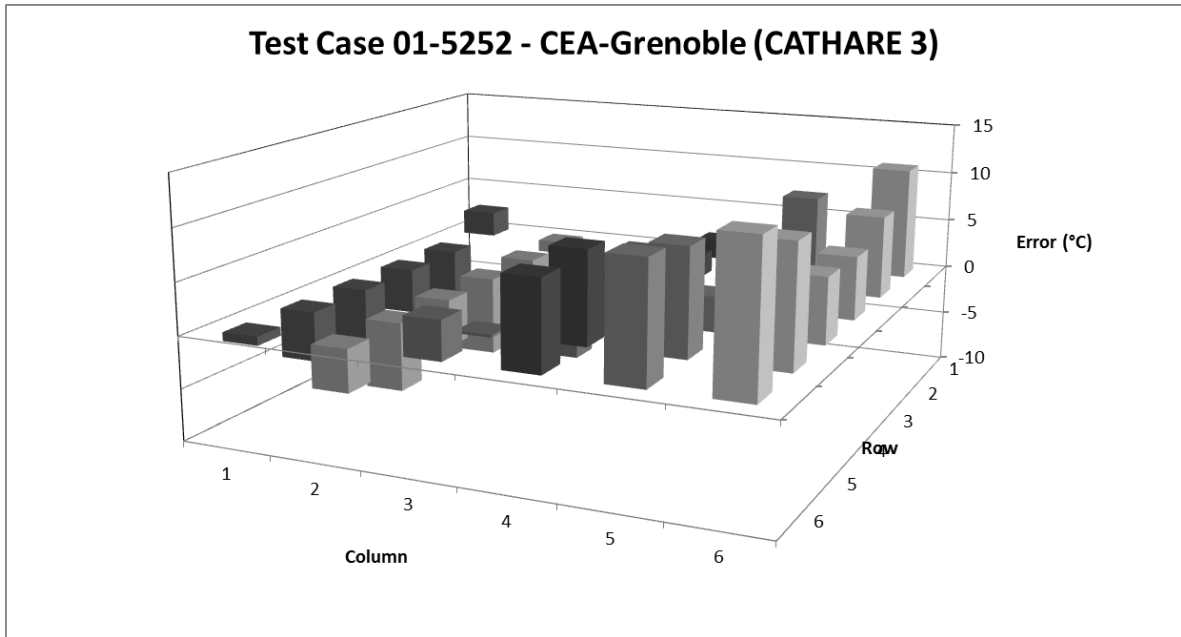
Figure AI-66 Test Case 01-5252 FLICA-OVAP – Error of Calculated Fluid Temperature
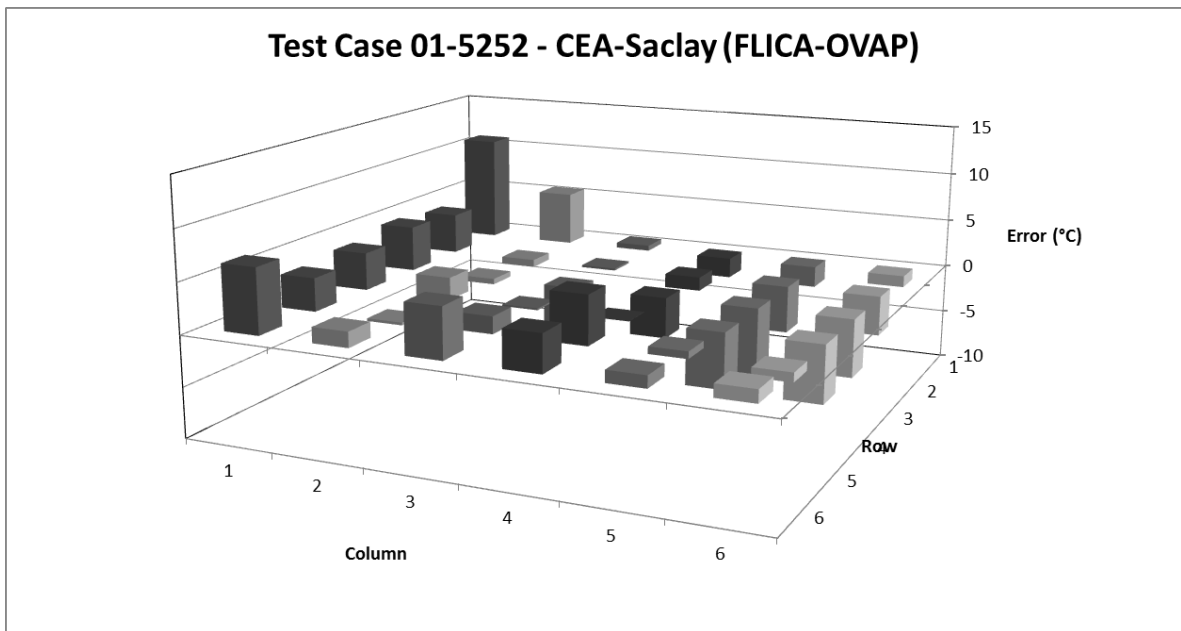
Figure AI-67 Test Case 01-5252 THYC – Error of Calculated Fluid Temperature

Test Case 01-5252 - EDF(THYC)
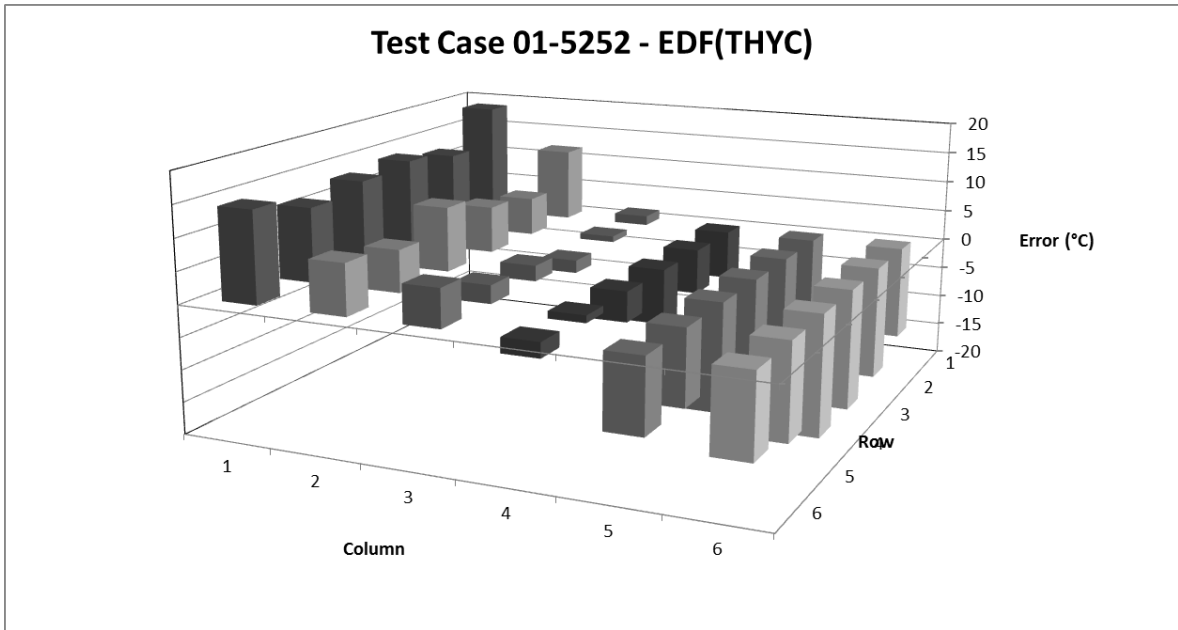
Figure AI-68 Test Case 01-5252 MATRA – Error of Calculated Fluid Temperature

Test Case 01-5252 - KAERI (MATRA)
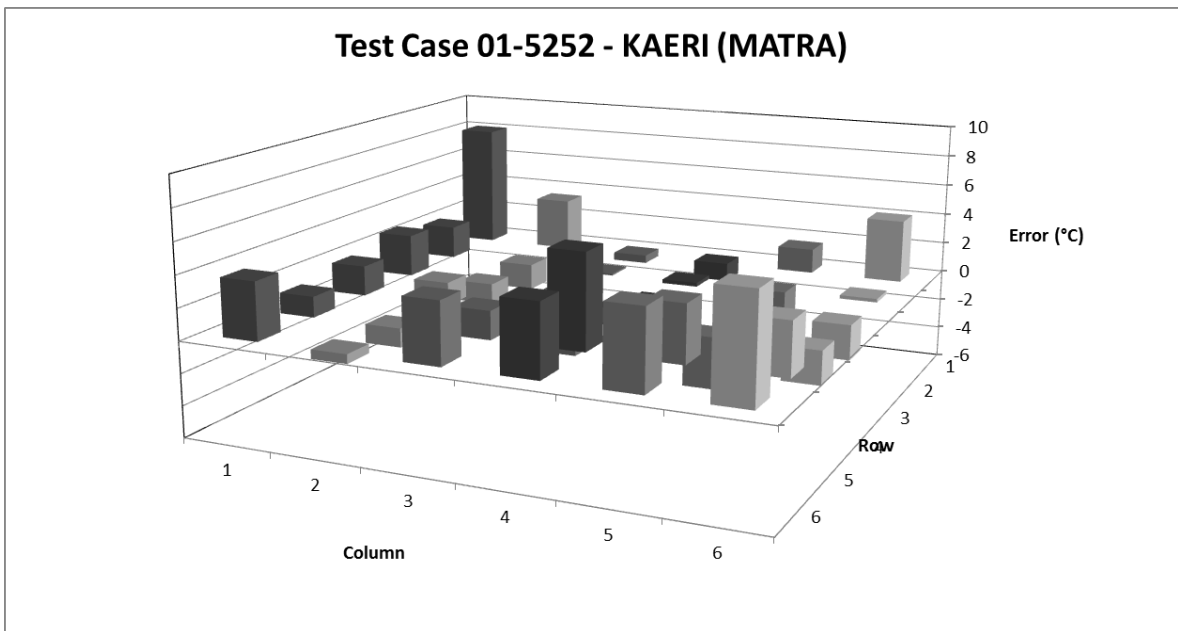
Figure AI-69 Test Case 01-5252 SUBCHANFLOW – Error of Calculated Fluid Temperature
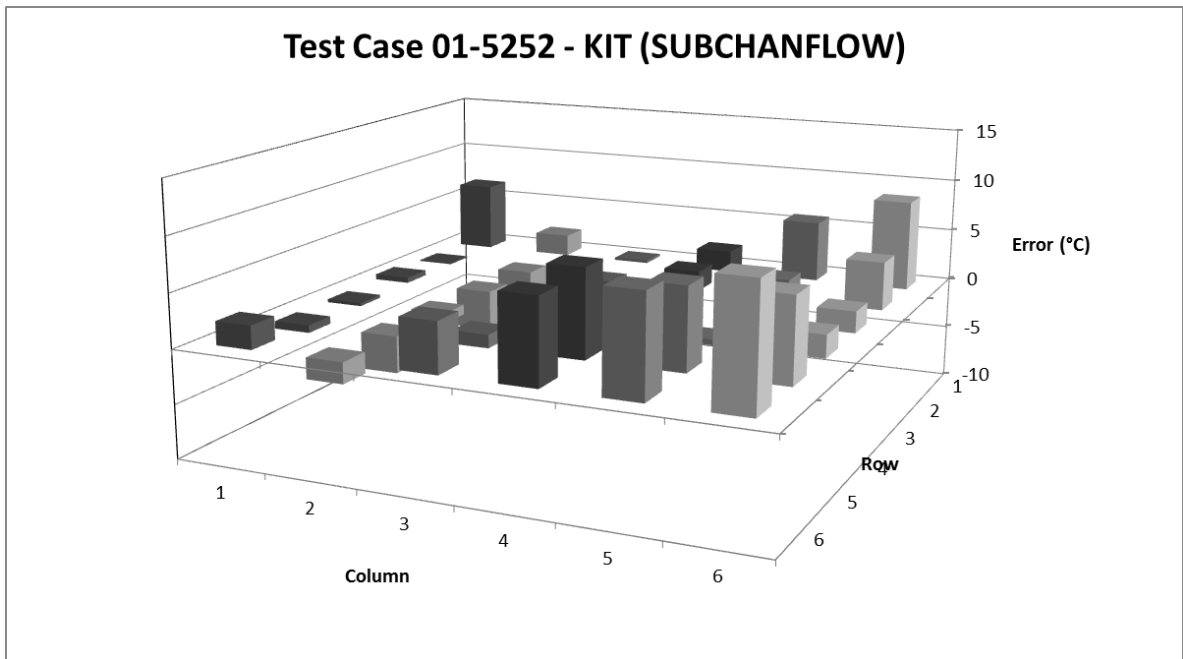
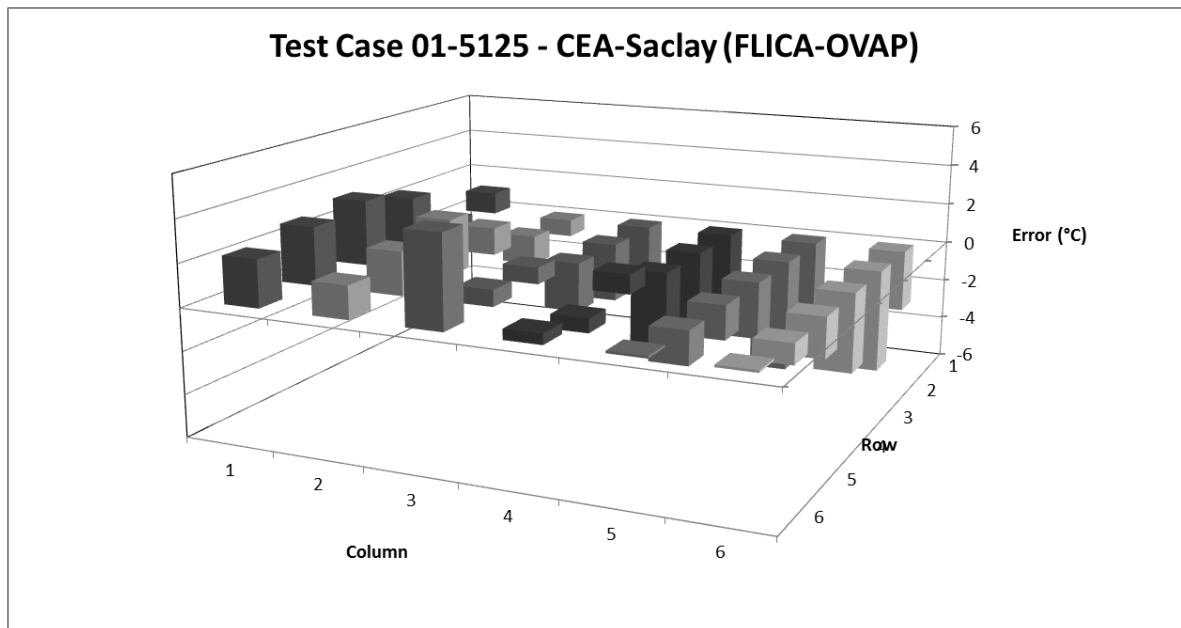**Figure AI-70 Test Case 01-5252 VIPRE – Error of Calculated Fluid Temperature**
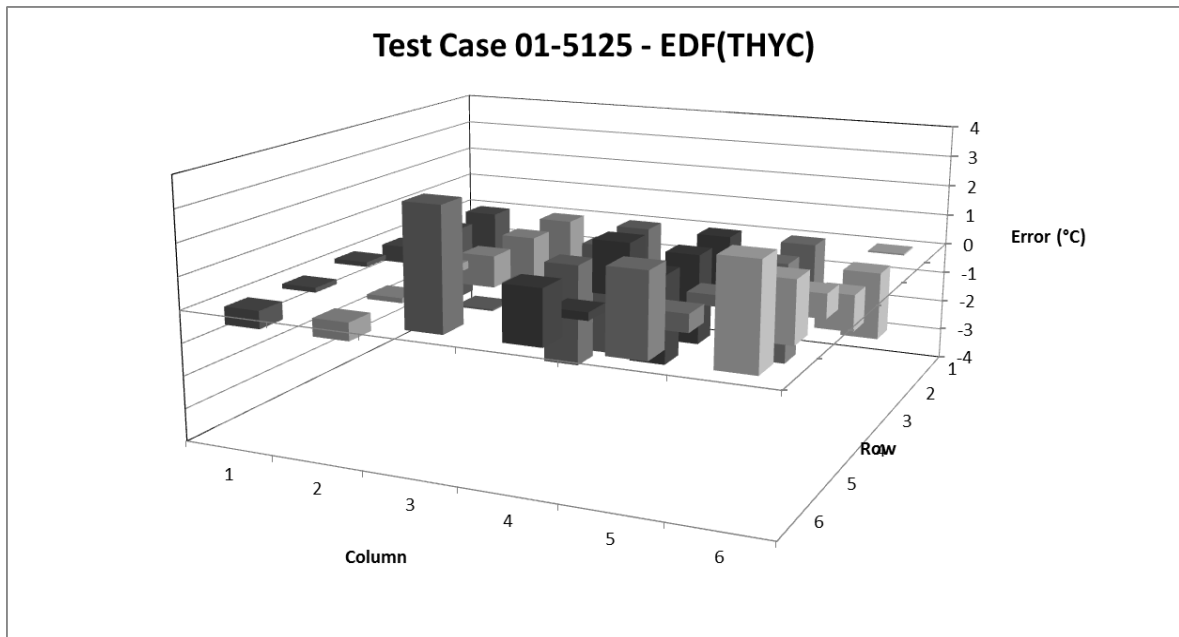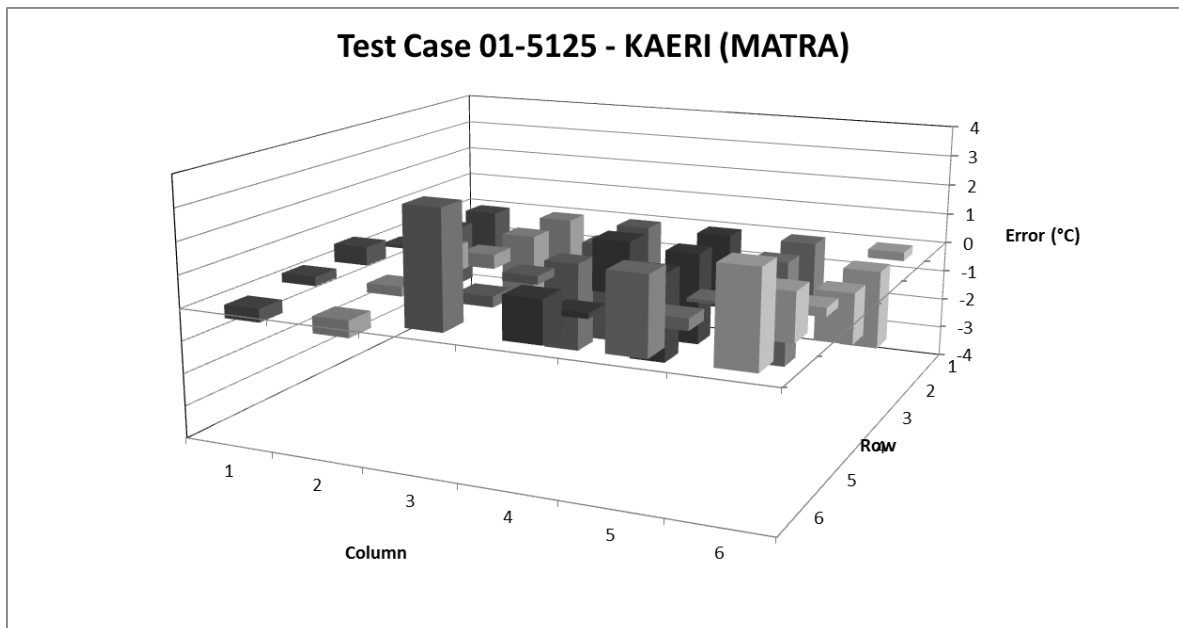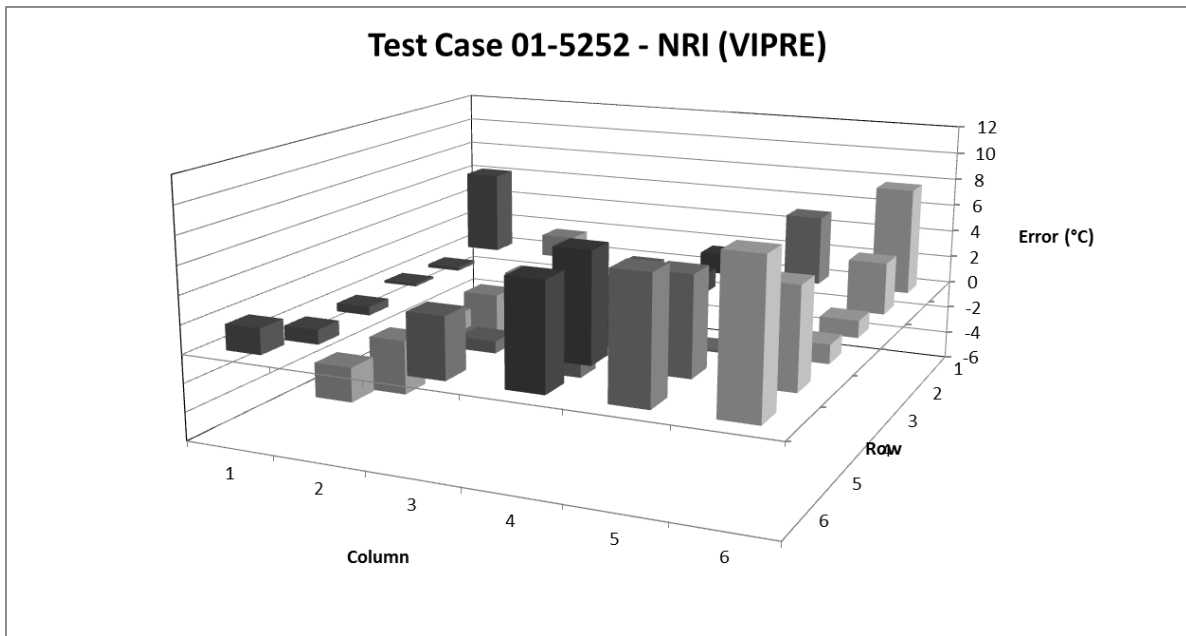
Figure AI-71 Test Case 01-5252 FLICA – Error of Calculated Fluid Temperature
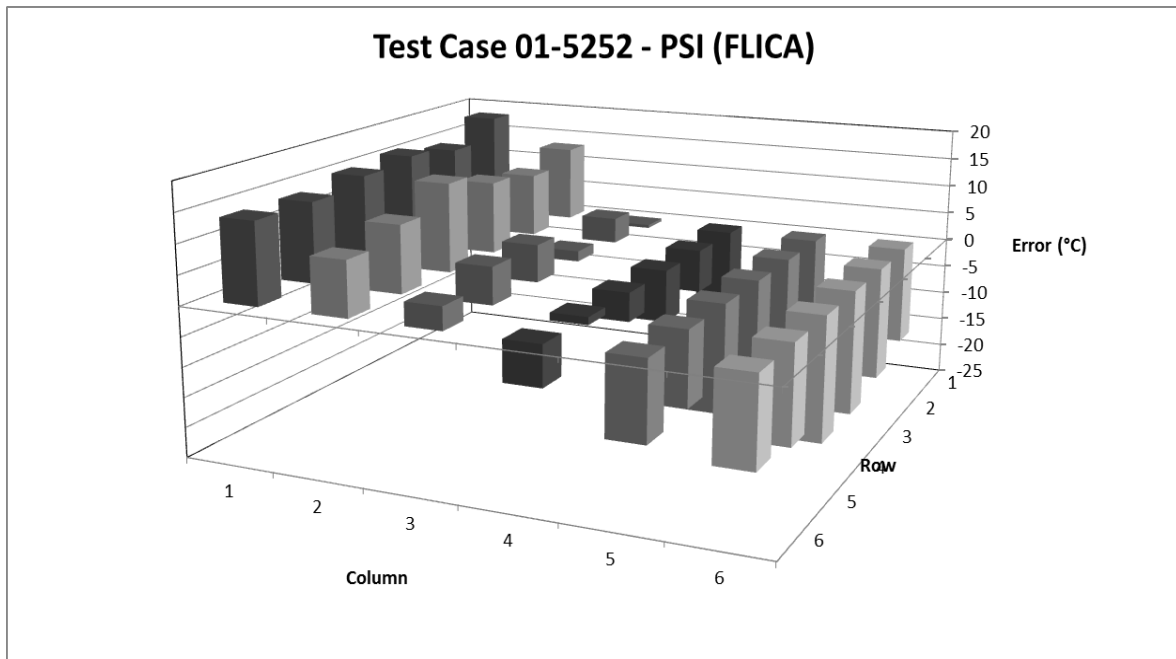
Figure AI-72 Test Case 01-5252 ASSERT – Error of Calculated Fluid Temperature
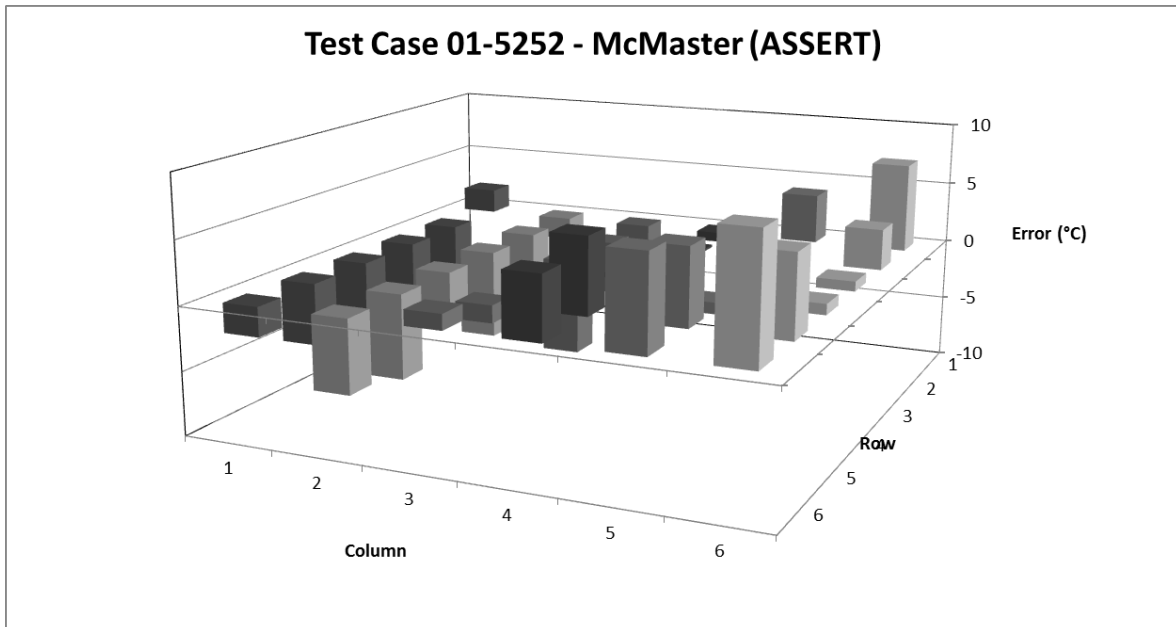
Appendix II Exercise II-2 Results

Figure AII-1 Test Series 0 DNB Power Results
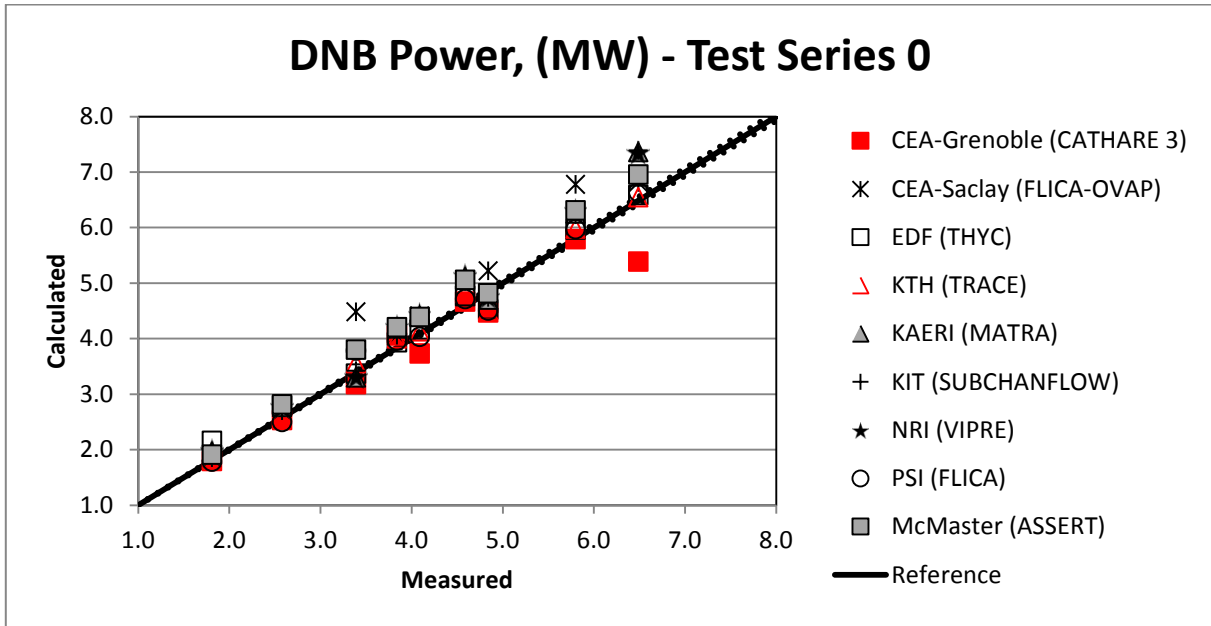
Figure AII-2 Test Series 2 DNB Power Results
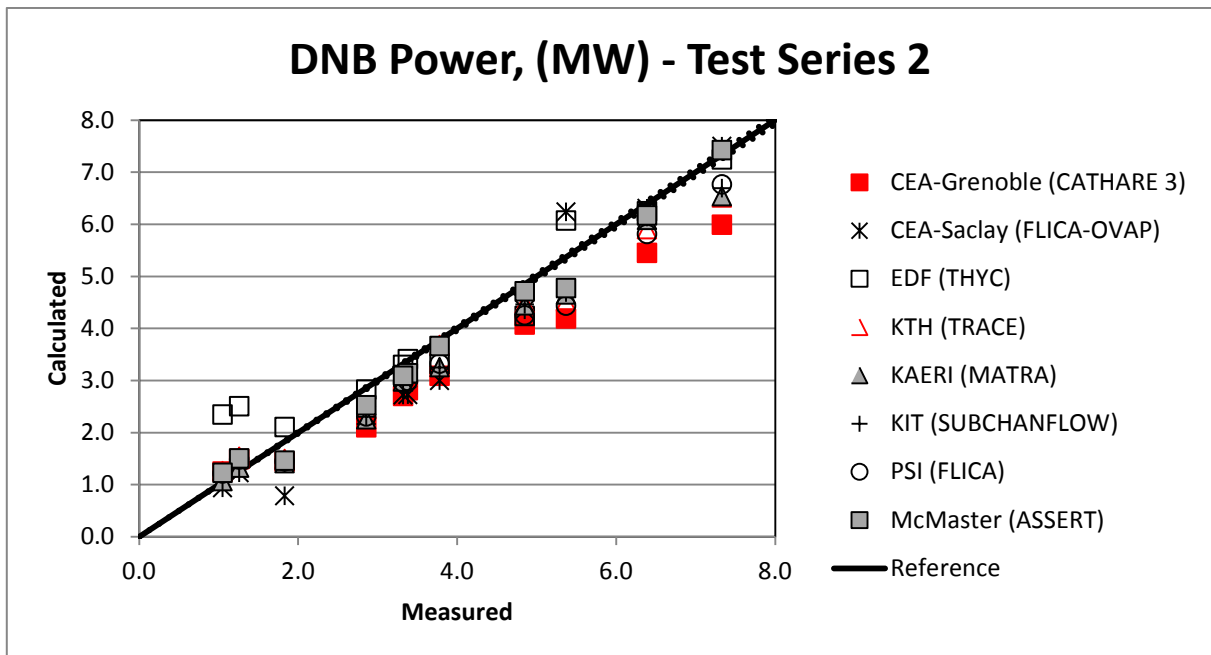
Figure AII-3 Test Series 3 DNB Power Results

DNB Power, (MW) - Test Series 3
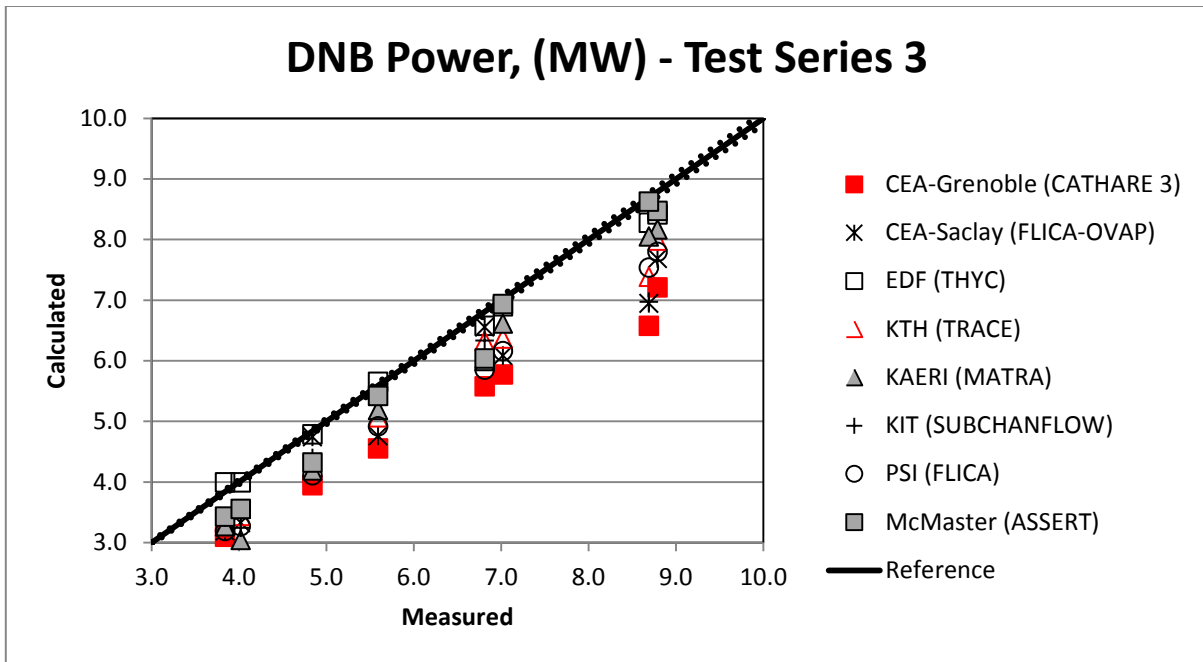
Figure AII-4 Test Series 4 DNB Power Results

DNB Power, (MW) - Test Series 4
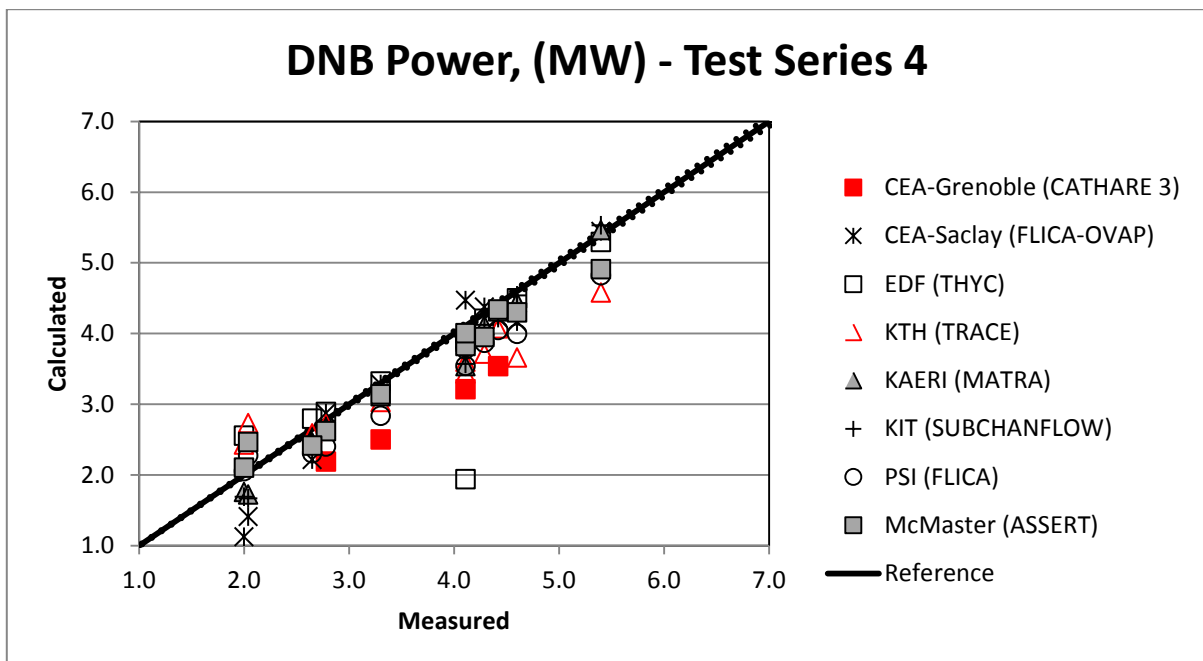
Figure AII-5 Test Series 8 DNB Power Results
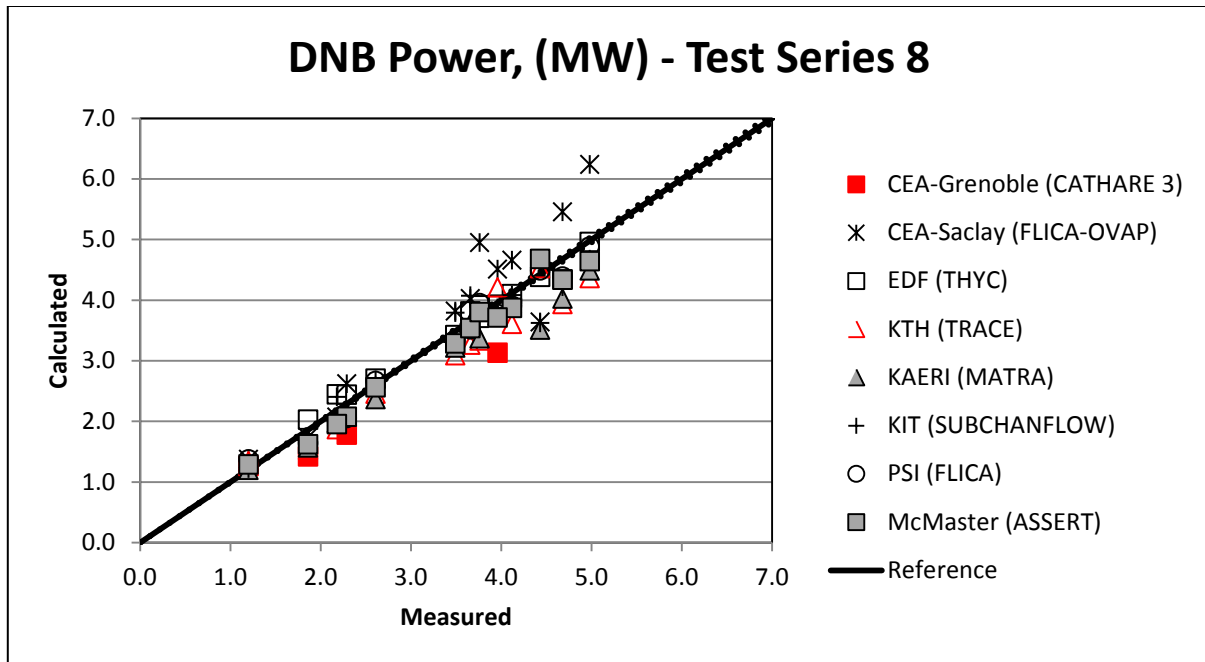
Figure AII-6 Test Series 13 DNB Power Results
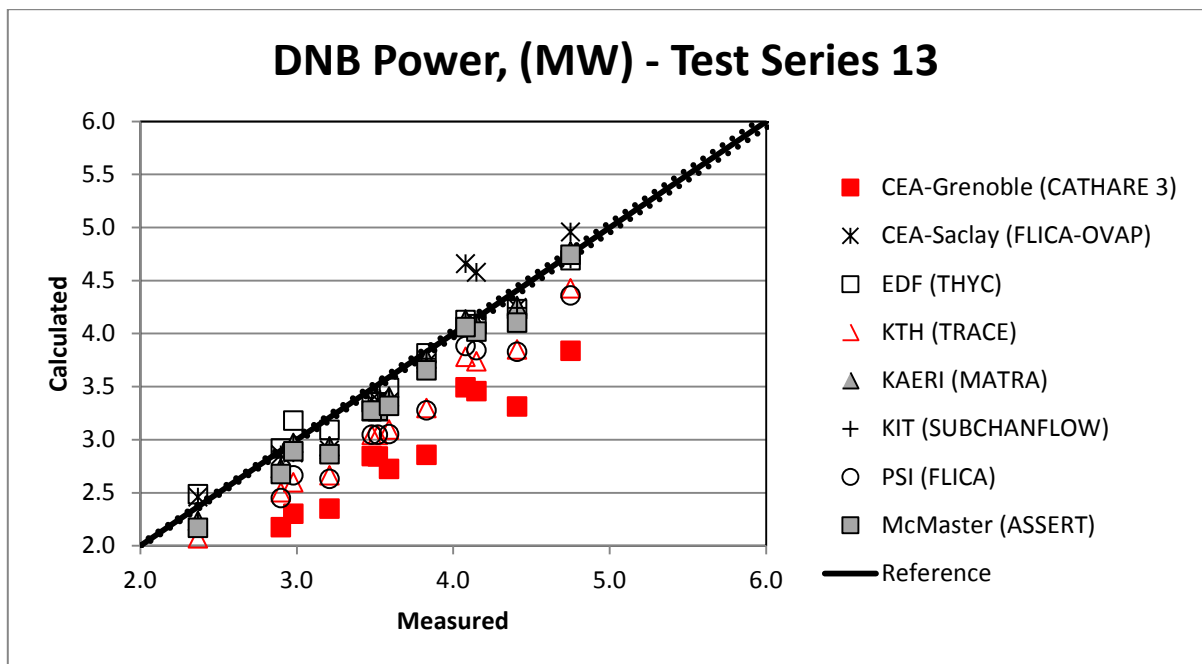
Figure AII-7 Test Series 4 Elevation of First Detected DNB Results
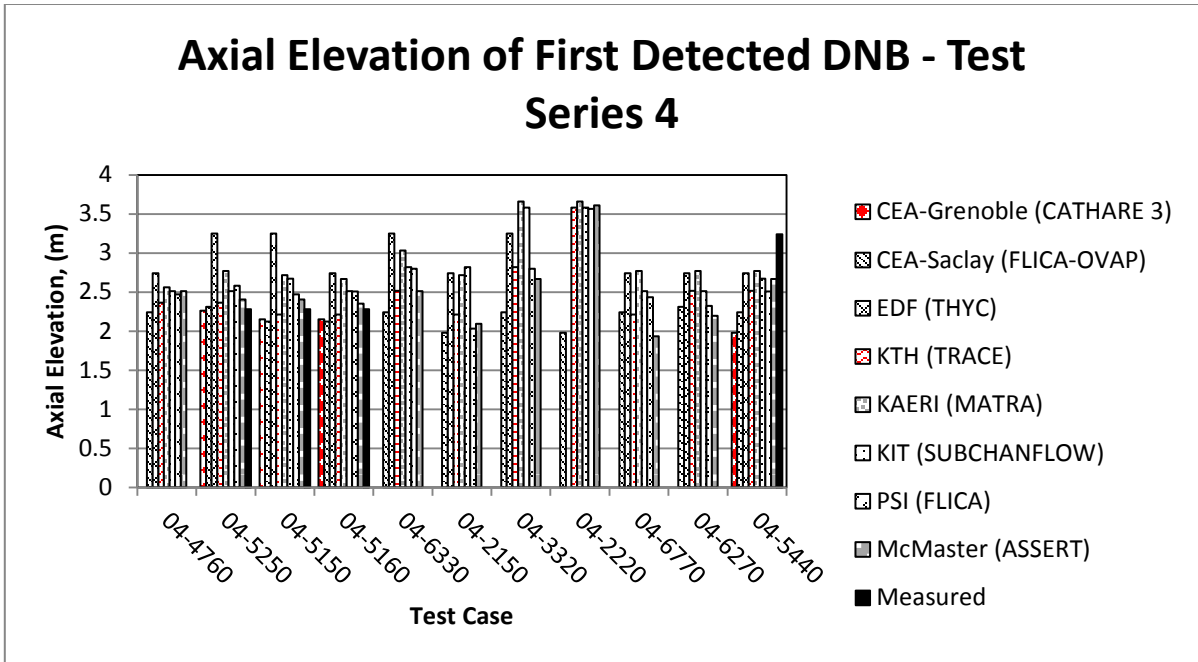
Figure AII-8 Test Series 8 Elevation of First Detected DNB Results
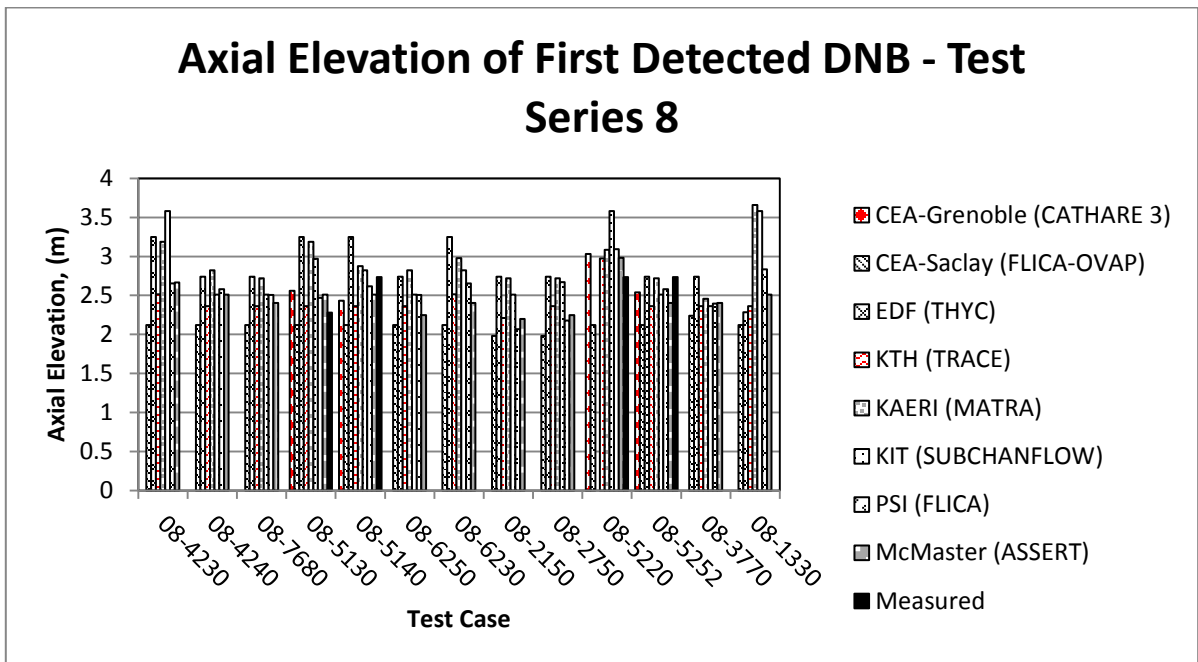
Figure AII-9 Test Series 13 Elevation of First Detected DNB Results
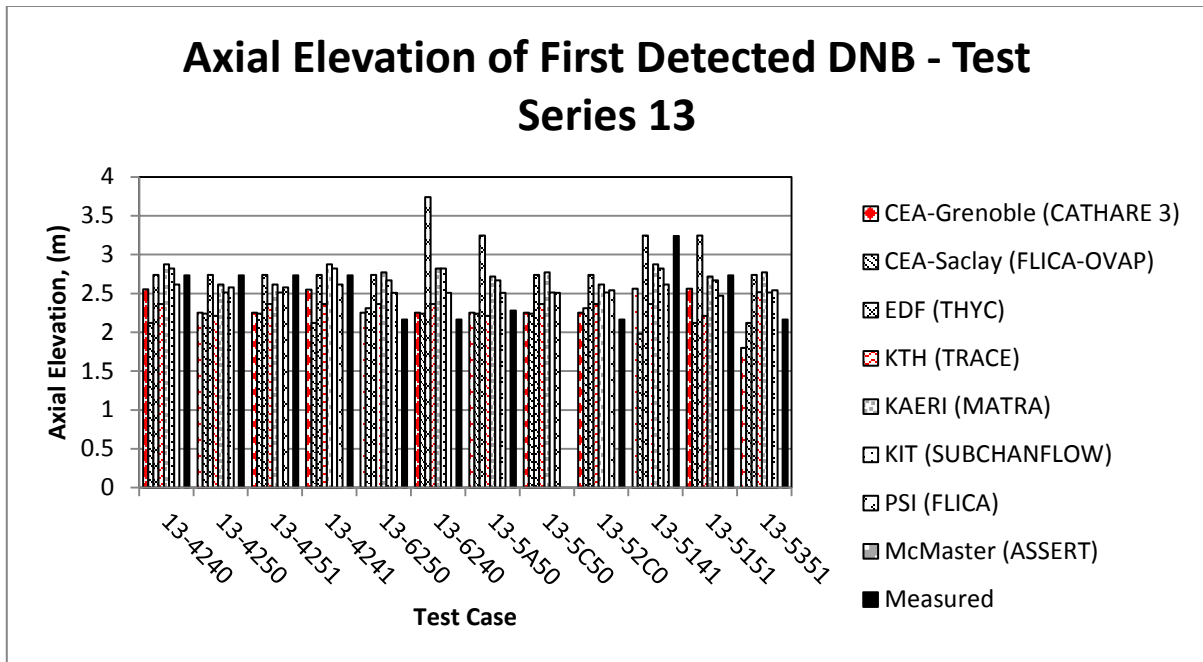
Table AII-1 Radial Position of First Predicted DNB

Run No.	Radial Position of First Predicted DNB							
	CEA-Grenoble (CATHARE 3)	CEA-Saclay (FLICA-OVAP)	EDF (THYC)	KAERI (MATRA)	KIT (SUBCHANFLOW)	PSI (FLICA)	McMaster (ASSERT)	Measured
04-4760		central	central	central	central	central	central	n/a
04-5250	central	central	central	central	central	central	central	central
04-5150	central	central	central	central	central	central	central	central
04-5160	central	central	central	central	central	central	central	central
04-6330		central	central	central	central	central	central	n/a
04-2150		central	central	central	central	central	central	n/a
04-3320		central	central	central	central	central	central	n/a
04-2220		central		central	central	central	central	n/a
04-6770		central	central	central	central	central	central	n/a
04-6270		central	central	central	central	central	central	n/a
04-5440	central	central	central	central	central	central	central	central
08-4230		central	peripheral	central	central	central	central	central
08-4240		central	peripheral	central	central	central	central	central
08-7680		central	peripheral	central	central	central	central	central
08-5130	central	central	peripheral	central	central	central	central	central
08-5140	central	central	peripheral	central	central	central	central	central
08-6250		central	peripheral	central	central	central	central	central
08-6230		central	peripheral	central	central	central	central	central
08-2150		central	peripheral	central	central	central	central	central
08-2750		central	peripheral	central	central	central	central	central
08-5220	central	central		central	central	central	central	central
08-5252	central	central	peripheral	central	central	central	central	central
08-3770		central	peripheral	central	central	central	central	central
08-1330		central	peripheral	central	central	central	central	central
13-4240	central	central	central	central	central	central	central	central
13-4250	central	central	central	central	central	central	central	central
13-4251	central	central	central	central	central	central	central	central
13-4241	central	central	central	central	central	central	central	central
13-6250	central	central	central	central	central	central	central	central
13-6240	central	central	central	central	central	central	central	central
13-5A50	central	central	central	central	central	central	central	central
13-5C50	central	central	central	central	central	central	central	n/a
13-52C0	central	central	central	central	central	central	central	central
13-5141	central	central	central	central	central	central	central	peripheral
13-5151	central	central	central	central	central	central	central	central
13-5351	central	central	central	central	central	central	central	central

Appendix III Exercise II-3 Results

Figure AIII-1 Exercise 3 Time of Detected DNB Results (Test Series 11T)
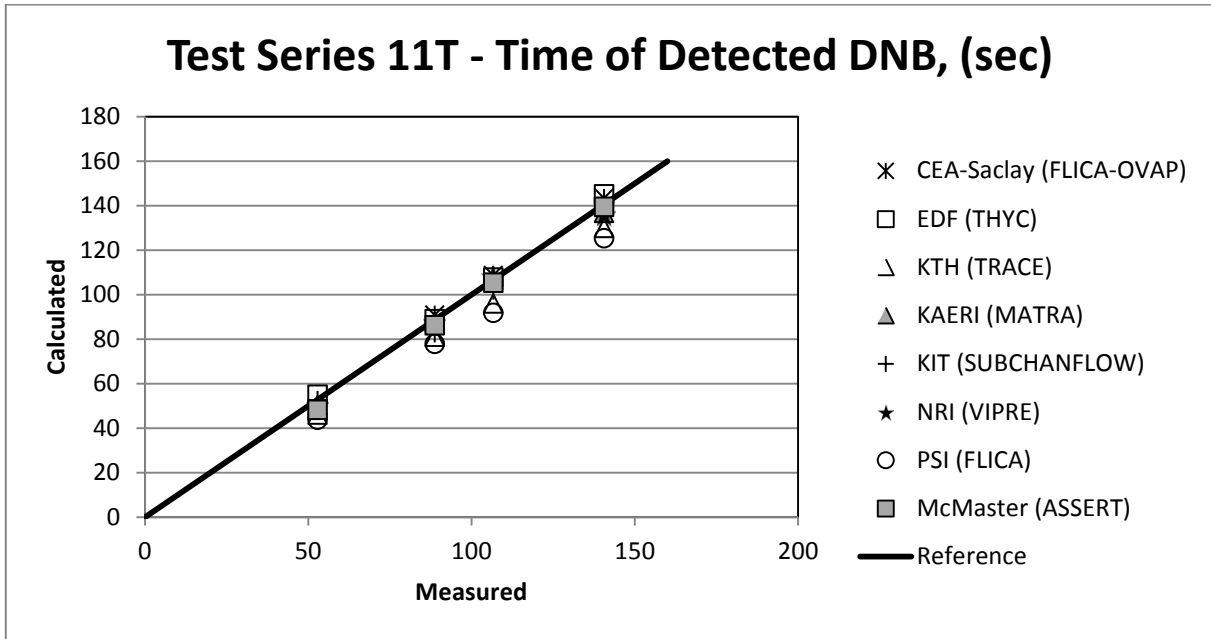
Figure AIII-2 Exercise 3 Time of Detected DNB Results (Test Series 12T)
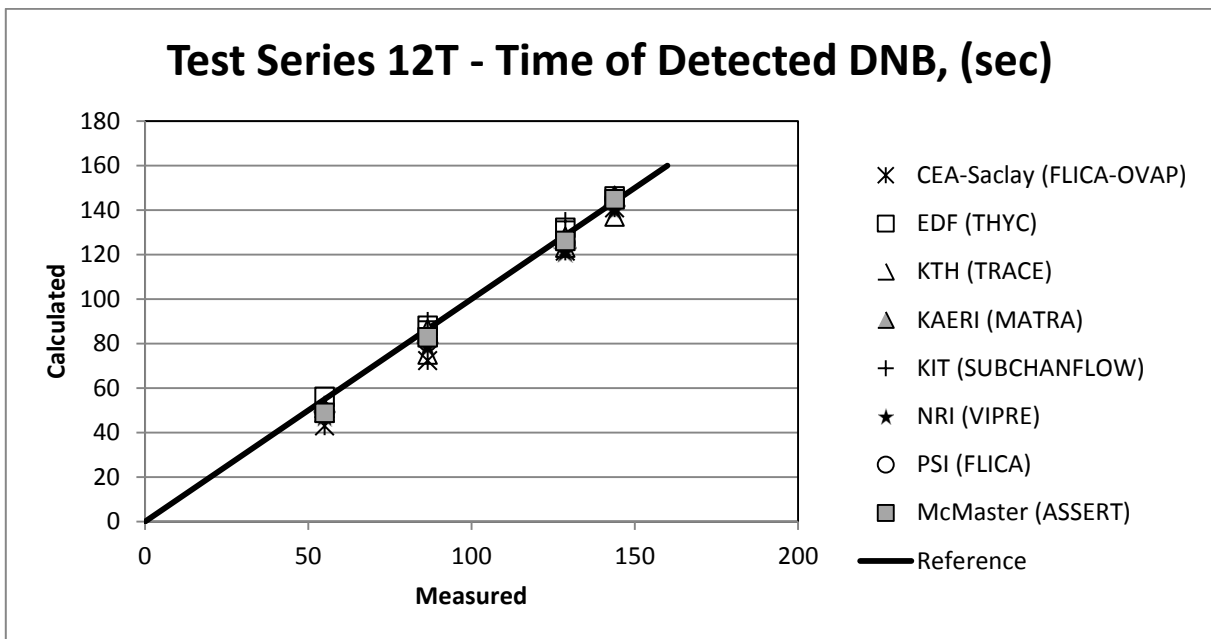
Figure AIII-3 Exercise 3 DNB Power Results (Test Series 11T)

Test Series 11T - DNB Power, (MW)

Legend:
- CEA-Saclay (FLICA-OVAP)
- KTH (TRACE)
- KAERI (MATRA)
- KIT (SUBCHANFLOW)
- PSI (FLICA)
- McMaster (ASSERT)

X-axis (Test Case): 11-0312, 11-0112, 11-0212, 11-0321
Y-axis (Calculated): 0 to 5
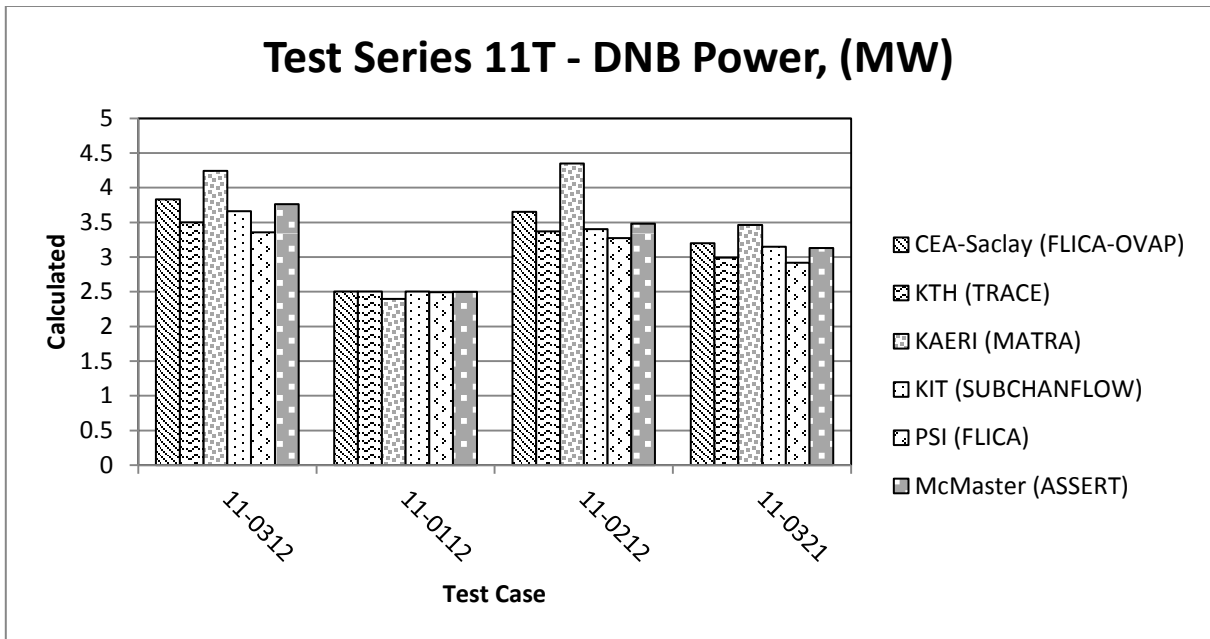
Figure AIII-4 Exercise 3 DNB Power Results (Test Series 12T)

Test Series 12T - DNB Power, (MW)

Legend:
- CEA-Saclay (FLICA-OVAP)
- KTH (TRACE)
- KAERI (MATRA)
- KIT (SUBCHANFLOW)
- PSI (FLICA)
- McMaster (ASSERT)

X-axis (Test Case): 12-0312, 12-0112, 12-0211, 12-0321
Y-axis (Calculated): 0 to 5
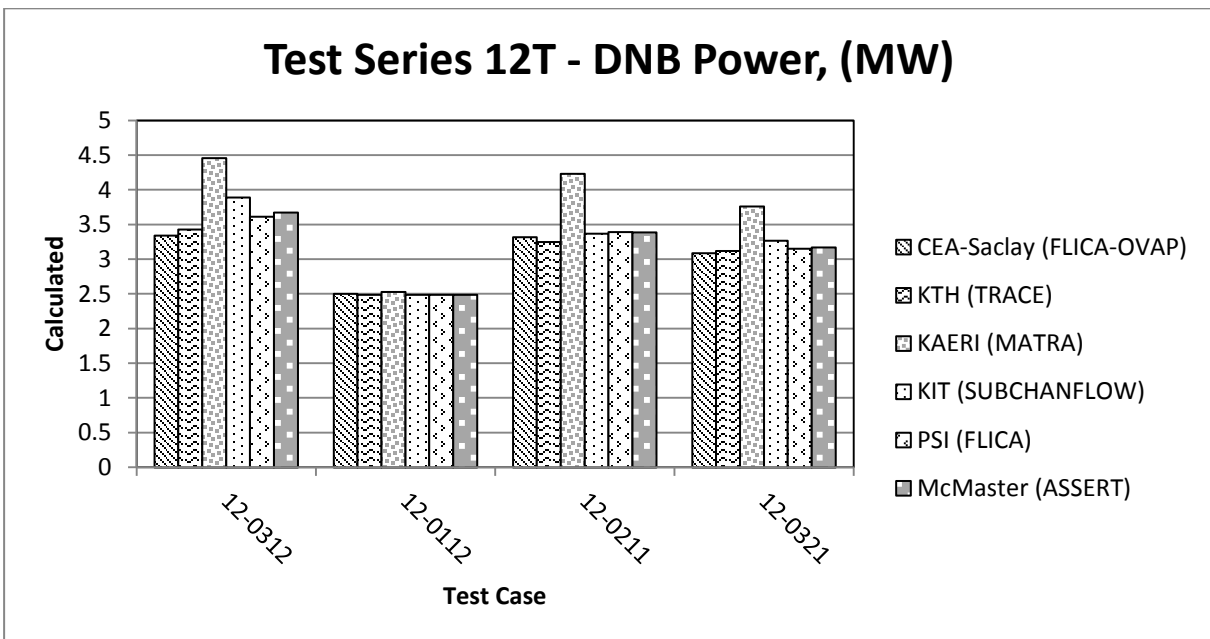
Figure AIII-5 Exercise 3 DNB Power Results (Test Series 11T)

Test Series 11T - DNB Power, (MW)

Legend:
- ✳ CEA-Saclay (FLICA-OVAP)
- ⌐ KTH (TRACE)
- ▲ KAERI (MATRA)
- + KIT (SUBCHANFLOW)
- ○ PSI (FLICA)
- ▢ McMaster (ASSERT)
- — Reference
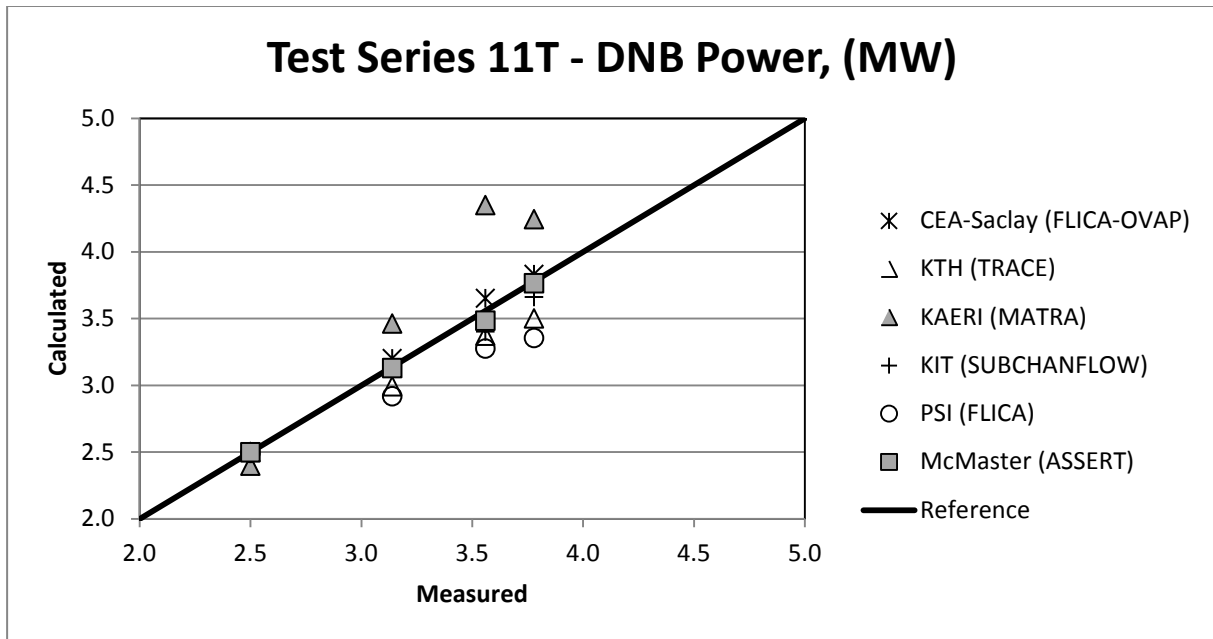
Figure AIII-6 Exercise 3 DNB Power Results (Test Series 12T)

Test Series 12T - DNB Power, (MW)

Legend:
- ✳ CEA-Saclay (FLICA-OVAP)
- ⌐ KTH (TRACE)
- ▲ KAERI (MATRA)
- + KIT (SUBCHANFLOW)
- ○ PSI (FLICA)
- ▢ McMaster (ASSERT)
- — Reference
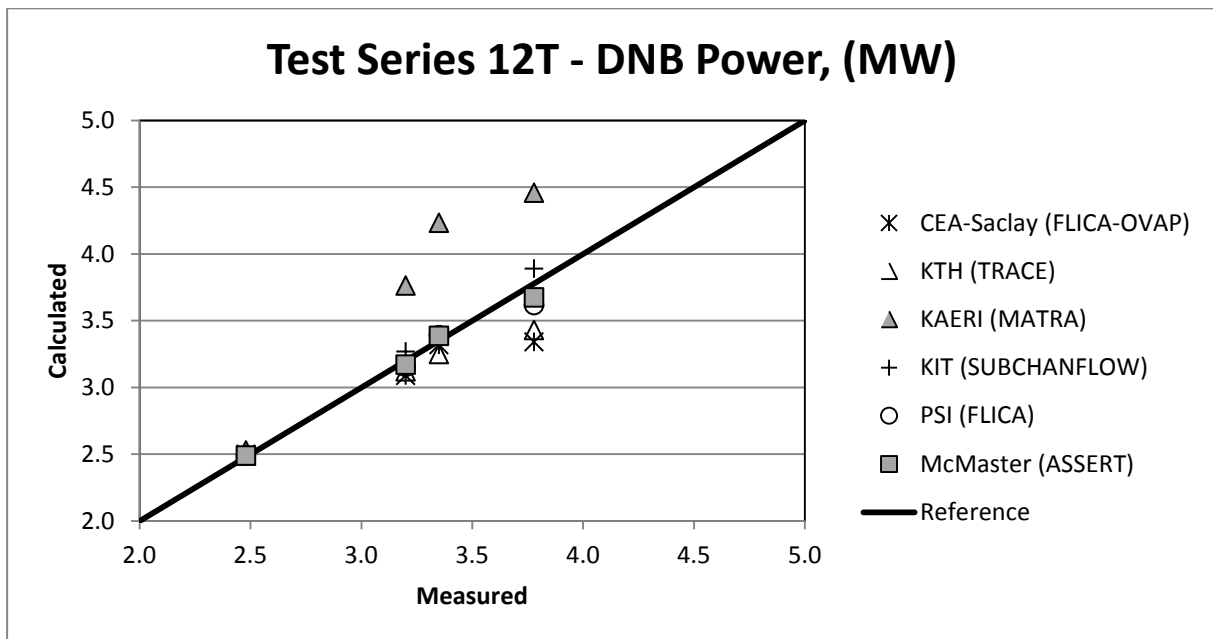
Appendix IV: Participant Questionnaires

Questionnaires were submitted for seven (7) of the codes for which results were submitted. These questionnaires are presented here as they were submitted to the benchmark team.

AIV.1 CEA-Grenoble (CATHARE 3)

AIV.1.1 Overall questionnaire

1. Specify the governing transport equations, assumptions and simplifications
See Phase I.

2. Specify the numerical algorithm used (fully implicit, fully explicit; semi-implicit)
See Phase I.

3. Specify the two-phase models and formulations used (HEM, drift flux model, two-fluid model, etc.)
See Phase I.

4. Specify any optimisations of the code predictions that were performed by adjusting the model parameters to the experimental database
Standard CATHARE 3 current version (V1 alpha) with adjustment of the liquid temperature turbulent dispersion based on Phase II ex 1 results; this adjustment was used for the phase II ex 2 simulations.

AIV.1.2 Phase II – Exercise 1

1. Specify the cross-flow models used (diversion flow, void drift and turbulent mixing models)
See Phase I.

2. Specify the flow regime map used
See Phase I.

3. Specify the interfacial mass, momentum and energy exchange models
See Phase I.

4. Specify the wall drag and heat transfer models
See Phase I.

5. Specify the spacer grid modelling
No answer provided.

6. If symmetry used, specify the symmetry applied in the model
See Phase I.

7. Specify the nodalisation and boundary conditions used
See Phase I.

AIV.1.3 Phase II – Exercise 2

1. Specify the DNB modelling approach (mechanistic model or empirical correlation)
Smoothed look-up tables (based on Groeneveld CHF original tables) are compared to local heat flux and allow locating the limit between nucleate boiling region and post dry-out region. The look up table parameters are: pressure, mass velocity and quality. The quality local value in a three-dimensional calculation is assessed assuming no slip and depends only on the local void fraction. The mass velocity is assessed locally, taken into account both the horizontal and vertical components of velocity.

2. Specify the cross-flow models (diversion flow, void drift and turbulent mixing models)
See Phase I.

3. If symmetry used, specify the kind of symmetry applied in the model
See Phase I.

4. Specify the nodalisation and boundary conditions used
See Phase I.

AIV.1.4 Phase II – Exercise 3

1. Specify the DNB modelling approach (mechanistic model or empirical correlation)
No answer provided.

2. Specify the cross-flow models (diversion flow, void drift and turbulent mixing models)
No answer provided.

3. If symmetry used, specify the kind of symmetry applied in the model
No answer provided.

4. Specify the nodalisation and boundary conditions used
No answer provided.

AIV.2 CEA-Saclay (FLICA-OVAP)

AIV.2.1 Overall questionnaire

1. Governing transport equations, assumptions and simplifications

A three-dimensional four-equation drift-flux model has been used, including the mixture mass balance equation, the mixture momentum balance equation, the mixture energy balance equation and the steam mass balance equation[1]:

mixture mass

$$\frac{\partial}{\partial t}\left(\sum_{k=v,l}\alpha_k\rho_k\right) + \nabla\cdot\left(\sum_{k=v,l}\rho_k\mathbf{u}_k\right) = 0 \qquad (2.1.1)$$

where α_k, ρ_k, $\mathbf{u}_k$ are the volume fraction, the density and the velocity:

mixture momentum

$$\frac{\partial}{\partial t}\left(\sum_{k=v,l}\alpha_k\rho_k\mathbf{u}_k\right) + \nabla\cdot\left(\sum_{k=v,l}\alpha_k\rho_k\mathbf{u}_k\otimes\mathbf{u}_k\right) + \nabla P - \nabla\cdot\left(\sum_{k=v,l}\alpha_k\underline{\underline{\tau_k}}\right) = \rho\mathbf{g} + \mathbf{F}_w \quad (2.1.2)$$

where P is the pressure, $\mathbf{g}$ the gravity and $\mathbf{F}_w$ the friction forces. The tensor $\underline{\underline{\tau_k}}$ represents the viscous and the Reynolds stress terms for the phase k. The mixture density ρ is defined as:

$$\rho = \sum_{k=v,l}\alpha_k\rho_k \qquad (2.1.3)$$

---

[1] Porosities are omitted for the sake of simplicity.

mixture energy

$$\frac{\partial}{\partial t}\left(\sum_{k=v,l}\alpha_k\rho_k E_k\right) + \nabla \cdot \left(\sum_{k=v,l}\alpha_k\rho_k H_k\mathbf{u}_k\right) - \nabla \cdot \left(\sum_{k=v,l}\alpha_k\mathbf{q}_k\right) = q_w + \rho\mathbf{g}\cdot\mathbf{u} \qquad (2.1.4)$$

where E_k and H_k are the total energy and the total enthalpy of the phase k, $\mathbf{q}_k$ includes molecular and turbulent heat fluxes and q_w is the volumetric source term of thermal power.

steam mass

$$\frac{\partial}{\partial t}(\alpha_v\rho_v) + \nabla \cdot (\alpha_v\rho_v\mathbf{u}_v) - \nabla \cdot (K_c\nabla c) = \Gamma_v \qquad (2.1.5)$$

where c is the vapour concentration, defined as

$$c = \frac{\rho_v\alpha_v}{\rho} \qquad (2.1.6)$$

and K_c is the corresponding diffusion coefficient. The term Γ_v represents the source terms for the vapour phase, including vapour generation on the walls or mass transfer within the bulk flow.

The model is closed by a drift flux correlation and a general equation of state with the assumption that, in presence of liquid, the vapour is in saturation conditions at the pressure of the system.

Models adopted for the void distribution benchmark

The drift-flux correlation:

FLICA-OVAP includes several Zuber-Findlay type correlations in order to estimate the relative velocity $\mathbf{u}_r$ between the vapour velocity $\mathbf{u}_v$ and the liquid velocity $\mathbf{u}_l$. The general form of these correlations is:

$$u_v = C_0\langle\mathbf{j}\rangle + \langle\langle\mathbf{v}_{g,j}\rangle\rangle = C_0\langle\mathbf{j}\rangle + \langle\mathbf{V}_{g,j}\rangle \qquad (2.1.7)$$

where C_0 is the distribution parameter, $\langle\mathbf{j}\rangle = \alpha\mathbf{u}_v + (1-\alpha)\mathbf{u}_l$ is the area-averaged total volumetric flux and $\mathbf{V}_{g,j}$ is the void-weighted area-averaged drift velocity. The Chexal-Lellouche correlation was used in the PSBT calculations.

Pressure drop

Friction forces are given by the sum of distributed and singular pressure drops.

$$\mathbf{F}_w = \mathbf{F}_{sing} + \mathbf{F}_{fric} \tag{2.1.8}$$

Singular friction due to spacer or mixing grids or other pressure drops are given by:

$$\mathbf{F}_{sing} = -\frac{1}{2}\rho\underline{\underline{\mathbf{K}}}_{sing}\|\mathbf{u}\|\mathbf{u} \tag{2.1.9}$$

where $\underline{\underline{\mathbf{K}}}_{sing}$ is an antisymmetric tensor. Distributed friction at walls is instead accounted for by:

$$\mathbf{F}_{fric} = -\frac{1}{2D_h}\rho\begin{pmatrix} f_w^X & & \\ & f_w^Y & \\ & & f_w^Z \end{pmatrix} \tag{2.1.10}$$

Where the different friction terms f_w are given by the product of the isothermal friction factor f_{iso}, the heating wall correction f_{heat} and the two-phase flow multiplier $f_{2\phi}$. In this analysis, the Chisholm correlation was used for $f_{2\phi}$, whereas the heating wall correction was estimated by an in-house model already used in the FLICA-4 code.

Diffusion effects

To account for viscous and turbulent diffusion effects, the tensor $\underline{\underline{\tau_k}}$ is introduced in the momentum equation, given by:

$$\tau_k^{ij} = \mu_k\big(1 + M_{t,k}^{ij}\big)\left(\frac{\partial u_k^i}{\partial x_j} + \frac{\partial u_k^j}{\partial x_i} - \frac{2}{3}\sum_{l=x,y,z}\frac{\partial u_k^l}{\partial x_l}\delta_{ij}\right) \tag{2.1.11}$$

where $\mu_k M_{t,k}^{ij}$ is the turbulent viscosity, which is limited to the liquid phase. An anisotropic formulation is used for turbulent viscosity:

$$M_{t,l}^{ij} = M_{t0}^{ij}(\text{Re} - \text{Re}_t)^{b_M}f_M(f_{2\varphi}) \tag{2.1.12}$$

where $\text{Re} = GD_h/\mu_l$ is the Reynolds number, M_{t0}^{ij}, b_M, Re_t are parameters and $f_M(f_{2\varphi})$ is a function of the two-phase flow multiplier.

Similarly, molecular and turbulent heat fluxes are given by:

$$\sum_{k=v,l} \alpha_k \mathbf{q}_k = \frac{\lambda_l}{c_{p_l}} \left(\underline{\underline{\mathbf{1}}} + \underline{\underline{\mathbf{K}}}_{t,l} \right) \nabla h_x \tag{2.1.13}$$

where $h_x = x h_v + (1 - x) h_l$ is the flow enthalpy based on the actual quality x. The turbulent conductivity is given by:

$$K_{t,l}^{ij} = K_{t0}^{ij} (\text{Re} - \text{Re}_t)^{b_K} f_K \left(f_{2\varphi} \right) \tag{2.1.14}$$

where K_{t0}^{ij}, b_K, Re_t are parameters and $f_K \left(f_{2\varphi} \right)$ is a function of the two-phase flow multiplier.

In this analysis, the value of M_{t0}^{ij} and K_{t0}^{ij} was varied as a function of the axial position. Two different values have been adopted for each parameter depending whether the considered axial position was downward a mixing or a spacer grid.

Wall temperature

Wall temperatures are estimated on the basis of the bulk temperature and the heat transfer coefficient as:

$$T_w = T_b + \frac{q''}{h} = T_b + \frac{q''}{\text{Nu} \, \lambda / D_h} \tag{2.1.15}$$

The Nusselt number and the bulk temperature depend on the heat transfer regime. Four different regimes can be distinguished: single-phase convection heat transfer, sub-cooled nucleate boiling (SNB), saturated nucleate boiling (SANB) and post-critical heat flux heat transfer (post-CHF). In single-phase heat transfer and SNB, the bulk temperature is equal to the liquid phase temperature, whereas in SANB it is equal to the saturation temperature. The single phase heat transfer coefficient is estimated by the Dittus-Boelter correlation. The onset of significant void (OSV), which is the transition between single-phase heat transfer and SNB can be predicted with the Forster and Grief correlation in low pressure conditions or the Jens and Lottes correlation in high pressure conditions. Both correlations allow estimating the minimum wall superheating required to achieve net vapour generation. Vapour generation starts when wall temperature estimated with Dittus-Boelter correlation exceeds this value. In the present analysis, the onset of vapour generation and the corresponding wall temperatures are estimated by the Jens and Lottes correlation. Finally, in post-CHF conditions, the choice of correlation depends on the boiling characteristics, whether it is IAFB (inverted annular film boiling) or DFFB (dispersed flow film boiling).

The mass transfer term Γ_v

The mass transfer term Γ_v appearing the steam mass balance equation is given by the sum of two contributions: the vapour generation on walls Γ_{wv} and the mass transfer between the liquid and the vapour phase Γ_{vl}. In sub-cooled nucleate boiling, only a portion χ_v of the heat flux transferred from the wall to the mixture is used to vapourise the liquid phase, whereas the remaining part is used to heat the liquid phase up. The vapour generation at walls is thus given by:

$$\Gamma_{wv} = \frac{\chi_v q''}{h_{lv}} \frac{4}{D_{\text{heat}}} \tag{2.1.16}$$

where χ_v is a function of the saturation temperature, the liquid phase temperature, and the wall superheat demanded to have sub-cooled nucleate boiling.

The mass transfer between the two phases Γ_{vl} is instead given by:

$$\Gamma_{lv} = \frac{q_{vl}}{h_v - h_l} \tag{2.1.17}$$

where q_{vl} is the heat transferred between the two phase, given by:

$$q_{vl} = K_{v0} \frac{G^2}{\log(1 + \text{Re}/\text{Re}_0)} f(P, \rho, \mu_l, \mathbf{u}, \mathbf{u}_r) \frac{\rho c(x_{eq} - c)}{1 - c} \tag{2.1.18}$$

Numerical Algorithm

The equations are solved with a collocated finite volume type scheme. This scheme allows solving the system on any type of structured or unstructured mesh that can be either conforming or non-conforming. The hyperbolic part of the system is approximated by a V FRoe-type scheme modified to be accurate at low Mach number. The diffusion part of the system is approximated with a diamond technique. An implicit time scheme used (Backward Euler) has been adopted for the convergence towards the steady-state or for the transient calculations.

Two-Phase models and Formulations used

See Section 1.1 for the models used in the void distribution benchmark.

Optimisation of the code predictions that were performed by adjusting the model parameters to the experimental database.

K_{v0} (see paragraph 1.1.5) was optimised based on the results obtained for the steady-state single channel void distribution available by Series 1 to 4. The selected value is 1.5E-4.

Prediction of the boiling crisis

To predict boiling crisis conditions, the Shah model has been used. This model consists of two separate correlations to determine the *boiling number* Bo, defined as:

$$\text{Bo} = \frac{q''_{\text{chf}}}{G\,h_{lv}}$$

(2.1.19)

The first correlation covers conditions where the critical heat flux depends on the upstream conditions, named UCC (*upstream conditions correlation*). The second, named LCC (*local conditions correlation*), depends only on local quantities.

The UCC correlation is:

$$\text{Bo} = 0.124 \left(\frac{D}{z_{eq}}\right)^{0.89} \left(\frac{10^4}{Y}\right)^n (1 - x_{i,eq})$$

(2.1.20)

with:

$$Y = \left[\frac{GDC_{p_f}}{\lambda_f}\right]\left[\frac{G^2}{\rho_f^2 gD}\right]^{0.4}\left[\frac{\mu_f}{\mu_g}\right]^{0.6}$$

(2.1.21)

In the previous equations, z_{eq} is the effective tube length and $x_{i,eq}$ is the effective inlet quality, defined as:

$$\begin{aligned} x_{i,eq} = x_i \quad & z_{eq} = z_{crit} \quad \text{for} \quad x_i < 0 \\ x_{i,eq} = 0 \quad & z_{eq} = z_{sat} \quad \text{for} \quad x_i > 0 \end{aligned}$$

Where z_{crit} is the distance from the inlet section and the location of the boiling crisis, where the critical heat flux is calculated, and z_{sat} is the boiling length, which for uniformly heated tubes is given by:

$$\frac{z_{sat}}{D} = \frac{z_{crit}}{D} + \frac{x_i}{4\text{Bo}}$$

(2.1.22)

For water flows, when $Y \leq 10^4$, $n = 0$, otherwise it is given by:

$$\begin{aligned} n &= \left(\frac{D}{z_{eq}}\right)^{0.54} \quad \text{for} \quad Y \leq 10^6 \\ n &= \frac{0.12}{(1 - X_{i,eq})^{0.5}} \quad \text{for} \quad Y > 10^6 \end{aligned}$$

(2.1.23)

The LCC correlation is expressed by:

$$Bo = F_E \, F_X \, Bo_0 \tag{2.1.24}$$

The entrance factor F_E is given by:

$$F_E = 1.54 - 0.032 \left(\frac{z_{crit}}{D}\right) \tag{2.1.25}$$

When the previous correlation gives $F_E < 1$, it is used $F_E = 1$.

Bo_0 is defined as the boiling number at $x_{crit} = 0$, given by the maximum value obtained by the following equations:

$$
\begin{aligned}
Bo_0 &= 15Y^{-0.612} \\
Bo_0 &= 0.082Y^{-0.3}\left(1 + 1.45P_r^{4.03}\right) \\
Bo_0 &= 0.0024Y^{-0.105}\left(1 + 1.15P_r^{3.39}\right)
\end{aligned}
\tag{2.1.26}
$$

where P_r is the reduced pressure given by $P_r = P/P_c$ where P_c is the critical pressure, that is 22.064 MPa for water.

The value of F_X depends on the quality at the location of the boiling crisis x_{crit}. When $x_{crit} > 0$, the following equation is used:

$$F_X = F_3 \left[1 + \frac{\left(F_3^{-0.29}-1\right)(P_r - 0.6)}{0.35}\right]^c \tag{2.1.27}$$

When $P_r > 0.6$, $c = 1$, otherwise $c = 0$. F_3 is instead given by:

$$F_3 = \left(\frac{1.25 \times 10^5}{Y}\right)^{0.833\,x_{crit}} \tag{2.1.28}$$

When $x_{crit} < 0$, F_X is given by:

$$F_X = F_1 \left[1 - \frac{(1-F_2)(P_r - 0.6)}{0.35}\right]^b \tag{2.1.29}$$

As in the previous case, when $P_r > 0.6$, $b = 1$, otherwise $b = 0$. F_1 is given by:

$$
\begin{aligned}
F_1 &= 1 + 0.0052\left(-x_{crit}^{0.88}\right)Y^{0.41} &&\text{for } Y \le 1.4 \times 10^7 \\
F_1 &= 1 + 0.0052\left(-x_{crit}^{0.88}\right)(1.4 \times 10^7)^{0.41} &&\text{for } Y > 1.4 \times 10^7
\end{aligned}
\tag{2.1.30}
$$

Finally, F_2 is given by:

$$
\begin{aligned}
F_2 &= F_1^{-0.42} \quad \text{for } F_1 \leq 4 \\
F_2 &= 0.55 \quad\ \ \text{for } F_1 > 4
\end{aligned}
$$

(2.1.31)

Choice between UCC and LCC correlation

For water, the UCC correlation is used when $Y \leq 10^6$. When $Y > 10^6$, the correlation giving the lower value of the boiling number Bo is used, with the exception of cases where $z_{eq} > 160/P_r^{1.14}$, for which the UCC formulation is always adopted. In this analysis, the UCC correlation was used in all calculations.

Range covered by the Shah correlation

The Shah correlation was tested against 62 experimental databases with 23 different fluids, covering the following operating conditions:

- $0.315 \times 10^{-3} < D < 37.5 \times 10^{-3}$ m
- $1.3 < z / D < 940$
- $4 < G < 29051$ kg/m^2/s
- $-4 < x_i < 0.85$
- $-2.6 < x_{crit} < 1$

Only 15 tests over the whole database are not included in the range covered by the Shah correlation. In the following table, the values of experimental quantities relevant for the Shah model are reported.

Table AIV.2.1-1 Range of parameters for the Shah model covered by NUPEC tests

	D [m]	z/D	G (max / min)	x_i (max / min)	x_{crit} (max / min)
Series 0	0.009711	376.67	4944.4/1408.3	-0.062/-0.96	0.49/-0.20
Series 2	0.009711	376.67	4769.4/316.7	-0.053/- 0.97	1.00/-0.06
Series 3	0.009989	366.21	4702.8/1361.1	-0.045/- 0.87	0.58/-0.05
Series 4	0.009711	376.67	4725.0/566.7	-0.058/-0.98	1.00/0.06
Series 13	0.009711	376.67	3861.1/1361.1	-0.057/-0.50	0.50/0.20
Series 8	0.008867	412.55	4816.7/575.0	-0.058/-0.97	1.00/0.11

AIV.3 KAERI (MATRA)

AIV.3.1 Overall questionnaire

1. Specify the governing transport equations, assumptions and simplifications

The governing transport equations for sub-channel geometry were derived from integral balances on an arbitrary fixed control volume.

The flow is a transient, single component, two-phase mixture of liquid and vapour in thermodynamic equilibrium state.

Governing transport equations for the mixture can be written as:

Continuity:

$$A_i \frac{\partial \langle\langle \rho_m \rangle\rangle_i}{\partial t} + \frac{\partial m_i}{\partial x} + \sum_j \left(w_{ij} + w'_{i \leftrightarrow j} \right) = 0$$

(3.1.1)

Energy:

$$A_i \frac{\partial}{\partial t} \langle\langle \rho_m \rangle\rangle_i \langle\langle h_m \rangle\rangle_i + \frac{\partial}{\partial x} \left(m_i \langle h \rangle_i \right) + \sum_j w_{ij} \langle h^* \rangle_i = Q$$

(3.1.2)

where,

$$Q = \frac{\partial}{\partial x} \left(\left\langle k \frac{\partial T}{\partial x} \right\rangle_i A_i \right) - \sum_j C_{ij} \left(T_i - T_j \right) - \sum_j w'_{ij} \left(h_i - h_j \right) + \sum_n \xi_n \langle q''_n \rangle$$

(3.1.3)

Axial momentum:

$$\frac{\partial m_t}{\partial t} + \frac{\partial}{\partial x} \left(\left\langle \sum_k \alpha_k \rho_k u_k^2 \right\rangle_i A_i \right) + \sum_j w_{ij} \langle u^* \rangle_i = -\overline{A} \frac{\partial P}{\partial x} - F_x$$

(3.1.4)

where,

$$F_x = \frac{1}{2} \left\{ \frac{f \phi^2}{d_{hy} \rho_m} + \frac{K}{\rho' \Delta x} \right\} \frac{m_i}{A_i} + f_T \sum_j w'_{ij} \left(u_i - u_j \right) + A_i \langle\langle \rho_m \rangle\rangle_i g \cos \theta$$

(3.1.5)

Lateral momentum:

$$\frac{\partial w_{ij}}{\partial t}+\frac{\partial}{\partial x}\left(w_{ij}\left\langle \overline{u}\right\rangle_i\right)+\frac{1}{l}\sum_j w_{ij}\left\langle \overline{v}\right\rangle_i = \frac{s_{ij}}{l}\left(P_i - P_j\right)-F_{ij}$$

(3.1.6)

where,

$$F_{ij}=\frac{1}{2}K_G\frac{w_{ij}\left|w_{ij}\right|}{\rho^* s_{ij} l}+s_{ij}\left\langle\left\langle \rho_m\right\rangle\right\rangle_i g\sin\theta$$

(3.1.7)

Important assumptions are:

- advection is allowed only across the fluid boundary;
- axial turbulent mixing is ignored;
- the work performed by viscous stress, and by body force are ignored;
- the internal heat generation in the fluid is ignored;
- the gravity is the only significant body force;
- fluid-to-fluid viscous force is ignored;
- the transverse linear momentum diffusion due to transverse turbulent mixing is ignored.

2. Specify the numerical algorithm used (fully implicit, fully explicit; semi-implicit)
Fully implicit.

3. Specify the two-phase models and formulations used (HEM, drift flux model, two-fluid model, etc.)
HEM

4. Specify any optimisations of the code predictions that were performed by adjusting the model parameters to the experimental database
None.

AIV.3.2 Phase II – Exercise 1

1. Specify the cross-flow models used (diversion flow, void drift and turbulent mixing models)
Diversion cross-flow was calculated by the lateral momentum equation.

Turbulent mixing model:

Single-phase turbulent mixing model:

$$w'_{ij} = \beta \cdot s_{ij} \cdot G_{avg}$$

(3.2.1)

Two-phase mixing and void drift model:

$$w'_{ij} = \beta \cdot s_{ij} \cdot G_{avg}$$

$$(3.2.2)$$

Turbulent mixing parameter, β=0.04

2. Specify the flow regime map used
None.

3. Specify the interfacial mass, momentum and energy exchange models
None.

4. Specify the wall drag and heat transfer models
Wall drag model:

Single-phase pressure drop model:

$$\Delta P_f = f \left(\frac{L}{d_{hy}} \right) \frac{G^2}{2\rho} + \sum_{n=1}^{N} K_{grid,n} \frac{G^2}{2\rho}$$

$$(3.2.3)$$

$$f = 0.184 \times \text{Re}^{-0.2}$$

$$(3.2.4)$$

$K_{grid} = 1.0, \; 0.7, \; 0.4$ for MV, NMV, SS grid, respectively.

Two-phase pressure drop model:

$$\Delta P_f = \Phi \cdot f \left(\frac{L}{d_{hy}} \right) \frac{G^2}{2\rho}$$

$$(3.2.5)$$

$$\Phi = \frac{(1-\chi)^2}{(1-\alpha)^{1.42}} \qquad \text{, for 0.0<α≤0.6}$$

$$\Phi = 0.478 \times \frac{(1-\chi)^2}{(1-\alpha)^{2.2}} \qquad \text{, for 0.6<α≤0.9}$$

$$\Phi = 1.73 \times \frac{(1-\chi)^2}{(1-\alpha)^{1.64}} \qquad \text{, for 0.9<α≤1.0}$$

Heat transfer model: Not used

5. Specify the spacer grid modelling

None.

6. If symmetry used, specify the symmetry applied in the model

Not used (full assembly is considered).

7. Specify the nodalisation and boundary conditions used

- number of nodes = 70;
- node size = 52.3 mm;
- axial nodding scheme = uniform.

Table AIV.3.2-1 Nodalisation used

Axial distance (mm)	Node size (mm)	Number of axial nodes
0 ∼ 3658	52.3	70

Table AIV.3.2-2 Spacer grid location (except SS grids) w.r.t. axial nodding

Spacer grid	A1	
	Location(mm)	Type
1	457	MV
2	914	MV
3	1372	MV
4	1829	MV
5	2286	MV
6	2743	MV
7	3200	MV

Uniform inlet flow distribution and uniform exit pressure distribution

AIV.3.3 Phase II – Exercise 2

1. Specify the DNB modeling approach (mechanistic model or empirical correlation)
Empirical correlation (EPRI CHF correlation).

2. Specify the cross-flow models used (diversion flow, void drift and turbulent mixing models)
Diversion cross-flow was calculated by the lateral momentum equation.

Turbulent mixing model:

Single-phase turbulent mixing model:

$$w'_{ij} = \beta \cdot s_{ij} \cdot G_{avg}$$

(3.3.1)

Two-phase mixing and void drift model:

$$w'_{ij} = \beta \cdot s_{ij} \cdot G_{avg}$$

(3.3.2)

Turbulent mixing parameter, β=0.08

3. If symmetry used, specify the symmetry applied in the model
Not used (full assembly is considered).

4. Specify the nodalisation and boundary conditions used
- number of nodes = 70;
- node size = 52.3 mm;
- axial nodding scheme = uniform.

Table AIV.3.3-1 Nodalisation used

Axial distance (mm)	Node size (mm)	Number of axial nodes
0 ~ 3658	52.3	70

Table AIV.3.3-2 Spacer grid location with respect to axial nodding

Spacer grid	A0		A2, A3		A4, A8, A13	
	Location(mm)	Type	Location(mm)	Type	Location(mm)	Type
1	610	MV	457	MV	2.5	NMV
2	1219	MV	914	MV	471	MV
3	1829	MV	1372	MV	925	MV
4	2438	MV	1829	MV	1378	MV
5	3048	MV	2286	MV	1832	MV
6			2743	MV	2285	MV
7			3200	MV	2739	MV
8					3247	MV

Uniform inlet flow distribution and uniform exit pressure distribution

AIV.3.4 Phase II – Exercise 3

1. Specify the DNB modelling approach (mechanistic model or empirical correlation)
empirical correlation (EPRI CHF correlation).

2. Specify the cross-flow models used (diversion flow, void drift and turbulent mixing models)
Diversion cross-flow was calculated by the lateral momentum equation.

Turbulent mixing model:

Single-phase turbulent mixing model:

$$w'_{ij} = \beta \cdot s_{ij} \cdot G_{avg} \qquad (3.4.1)$$

Two-phase mixing and void drift model:

$$w'_{ij} = \beta \cdot s_{ij} \cdot G_{avg} \qquad (3.4.2)$$

Turbulent mixing parameter, β=0.04.

3. If symmetry used, specify the symmetry applied in the model

Not used (full assembly is considered).

4. Specify the nodalisation and boundary conditions used

- Number of nodes = 70
- Node size = 52.3 mm
- Axial nodding scheme = uniform

Table AIV.3.4-1 Nodalisation used

Axial distance (mm)	Node size (mm)	Number of axial nodes
0 ∼ 3658	52.3	70

Table AIV.3.4-2 Spacer grid location (except SS grids) with respect to axial nodding

Spacer grid	Location (mm)	Type
1	5	NMV
2	471	MV
3	925	MV
4	1378	MV
5	1832	MV
6	2285	MV
7	2739	MV
8	3247	MV

Uniform inlet flow distribution and uniform exit pressure distribution

AIV.4 KIT (SUBCHANFLOW)

AIV.4.1 Overall questionnaire

1. Specify the governing transport equations, assumptions and simplifications.
Three-dimensional mass conservation equation – three-dimensional-enthalpy conservation equation – three-dimensional-momentum conservation equation without lateral transport of lateral momentum – Lumped volume approximation in lateral direction – Finite difference in axial direction

2. Specify the numerical algorithm used (fully implicit, fully explicit; semi-implicit)
Fully implicit axially upward flow only.

3. Specify the two-phase models and formulations used (HEM, drift flux model, two-fluid model, etc.)
HEM with vapour slip by empirical correlations.

4. Specify any optimisations of the code predictions that were performed by adjusting the model parameters to the experimental database
Constant lateral mixing coefficient: 0.06 using „equal mass mixing".

AIV.4.2 Phase II – Exercise 1

1. Specify the cross-flow models used (diversion flow, void drift and turbulent mixing models)
No answer provided.

2. Specify the flow regime map used
Diversion flow, simple equal mass, constant coefficient.
Bubbly, transition, annular, hidden in correlations.

3. Specify the interfacial mass, momentum and energy exchange models
HEM with slip correlation (Chexal Lellouche).

4. Specify the wall drag and heat transfer models
Blasius, Dittus-Boelter.

5. Specify the spacer grid modelling
Pressure loss coefficient dependent on grid type as recommended.

6. If symmetry used, specify the symmetry applied in the model
No symmetry assumptions used.

7. Specify the nodalisation and boundary conditions used
- 27 equal distance axial cells (heated zone plus distance to thermocouples);
- pressure boundary at the top;
- flow boundary at the bottom;
- constant velocity for all channels.

AIV.4.3 Phase II – Exercise 2

1. Specify the DNB modelling approach (mechanistic model or empirical correlation)
Empirical correlation (EPRI including power profile correction).

2. Specify the cross-flow models used (diversion flow, void drift and turbulent mixing models)
Diversion flow, simple equal mass, constant coefficient.

3. If symmetry used, specify the symmetry applied in the model
No symmetry assumptions used.

4. Specify the nodalisation and boundary conditions used
- 24 equal distance axial cells -Pressure boundary at the top;
- flow boundary at the bottom;
- constant velocity for all channels.

AIV.4.4 Phase II – Exercise 3

1. Specify the DNB modelling approach (mechanistic model or empirical correlation)
No answer provided.

2. Specify the cross-flow models used (diversion flow, void drift and turbulent mixing models)
- empirical correlation (EPRI including power profile correction);
- diversion flow;
- simple equal mass;
- constant coefficient.

3. If symmetry used, specify the symmetry applied in the model
No symmetry assumptions used.

4. Specify the nodalisation and boundary conditions used
- 24 equal distance axial cells – pressure boundary at the top;
- flow boundary at the bottom;
- constant velocity for all channels.

AIV.5 KTH (TRACE)

AIV.5.1 Overall questionnaire

1. Specify the governing transport equations, assumptions and simplifications

The answer is the same as the Phase I questionnaire.

2. Specify the numerical algorithm used (fully implicit, fully explicit; semi-implicit)

The answer is the same as the Phase I questionnaire.

3. Specify the two-phase models and formulations used (HEM, drift flux model, two-fluid model, etc.)

The answer is the same as the Phase I questionnaire.

4. Specify any optimisations of the code predictions that were performed by adjusting the model parameters to the experimental data

The answer is the same as the Phase I questionnaire.

AIV.5.2 Phase II – Exercise 1

1. Specify the cross-flow models used (diversion flow, void drift and turbulent mixing models)

This is not applicable for TRACE 1D component.

2. Specify the flow regime map used

The answer is the same as the Phase I questionnaire.

3. Specify the interfacial mass, momentum and energy exchange models

The answer is the same as the Phase I questionnaire.

4. Specify the wall drag and heat models

The answer is the same as the Phase I questionnaire.

5. Specify the spacer grid modelling

The spacer grid is modelled as a pressure loss coefficient K = 1.

6. If symmetry used, specify the symmetry applied in the model

This is not applicable for TRACE 1D component.

7. Specify the nodalisation and boundary conditions used

All tests are discretised with 24 uniform axial nodes 0.15241667 m long. The node hydraulic diameter is 9.7042E-3 m, the volume is 3.7189E-4 m^3 and the flow area is 2.439956E-3 m^2.

The boundary conditions are the same as in the Phase I questionnaire.

AIV.5.3 Phase II – Exercise 2

1. Specify the DNB modelling approach (mechanistic model or empirical correlation)

TRACE uses a look-up table based on [1] to determine the DNB. The CHF temperature is determined through iterative solution of the following equation:

$$q''_{NB}(T_{CHF}) = q''_{CHF} \tag{5.3.1}$$

The database of the look-up table spans the following range of conditions:

$$3 \leq D \leq 40 \ (mm) \tag{5.3.2}$$

$$0.1 \leq P \leq 20 \ (MPa) \tag{5.3.3}$$

$$6 \leq G \leq 8000 \ \left(\frac{kg}{m^2 s}\right) \tag{5.3.4}$$

$$-0.5 \leq x \leq 1 \tag{5.3.5}$$

$$80 \leq L/D \leq 2485 \tag{5.3.6}$$

The critical heat flux is found using:

$$q''_{CHF} = K_1 K_2 K_S fn\{P, G, x\} \tag{5.3.7}$$

Where:

- K_1 is the correction factor for tube diameter;
- K_2 is the correction factor for rod bundle geometry;
- K_s is the correction factor for low flow conditions;
- $f_n\{P,G,x\}$ is the table look-up value, which is a function of pressure, max flux and quality.

K_1 correction factor is calculated by:

$$K_1 = \text{Max}\left\{0.6, \sqrt{0.008/D_h}\right\} \qquad (5.3.8)$$

K_2 correlation factor is calculated by:

$$K_2 = \left[2\left(\frac{P}{D_R}\right) - 1.5\right] \exp\left(-\frac{x^{1/3}}{2}\right) \qquad (5.3.9)$$

where (P/D_R) is the pitch-to-diameter ratio for the bundle.

The low mass flux conditions a multiplicative correction factor, K_s, is not calculated directly. For low mass flux conditions, TRACE uses a set of correlations based on pool boiling [2,3,4].

2. Specify the cross-flow models (diversion flow, void drift and turbulent mixing models)

This is not applicable for TRACE 1D component.

3. If symmetry used, specify the type of symmetry applied in the model

This is not applicable for TRACE 1D component.

4. Specify the nodalisation and boundary conditions used

All tests were discretised with 24 uniform axial nodes, 0.15241667 m long. The node hydraulic diameter, volume and flow area depend on the test geometry (see Table 1).

The boundary conditions are the same as in the Phase I questionnaire.

Table AIV.5.3-1 Boundary conditions by test series

Test	D_h (m)	Volume (m³)	Flow area (m²)
0	9,70E-03	3,72E-04	2,44E-03
2	9,70E-03	3,72E-04	2,44E-03
3	9,98E-03	5,27E-04	3,45E-03
4	9,07E-03	3,72E-04	2,44E-03
8	9,43E-03	3,65E-04	2,39E-03

AIV.5.4 Phase II – Exercise 3

1. Specify the DNB modelling approach (mechanistic model or empirical correlation)

The answer is the same as in the previous section of this questionnaire.

2. Specify the cross-flow models (diversion flow, void drift and turbulent mixing models)

This is not applicable for TRACE 1D component.

3. If symmetry used, specify the type of symmetry applied in the model

This is not applicable for TRACE 1D component.

4. Specify the nodalisation and boundary conditions used

All tests were discretised with 24 uniform axial nodes, 0.15241667 m long. The node hydraulic diameter, volume and flow area depend on the test geometry (see Table 2).

The boundary conditions are the same as in the Phase I questionnaire.

Table AIV.5.4-1 Boundary conditions by test series

Test	D_h (m)	Volume (m³)	Flow area (m²)
11T	9,70E-03	3,72E-04	2,44E-03
12T	9,43E-03	3,65E-04	2,39E-03

Nomenclature

The nomenclature is the same as in Phase I questionnaire.

AIV.5.5 References

[1] D.C. Groeneveld et al. (1996), "The 1995 Look-Up Table for Critical heat Flux in Tubes," *Nuclear Engineering Design*, 163, 1-23.

[2] H.J. Ivey, D.J. Morris (1962), "On the Relevance of the Vapour-Liquid Exchange Mechanism for Subcooled Boiling Heat Transfer at High Pressure," AEEW-R-137, United Kingdom Atomic Energy Authority Research Group.

[3] P. Saha, N. Zuber (1974), "Point of Net Vapor Generation and Vapor Void Fraction in Subcooled Boiling," Heat Transfer 1974, Proceedings of the 5th International Heat Transfer Conference, Tokyo, Japan, Vol. 4, 175-179.

[4] US Nuclear Regulatory Commission (2010), "TRACE V5.0 Theory Manual".

AIV.6 McMaster (ASSERT-PV)

AIV.6.1 Overall questionnaire

1. Specify the governing transport equations, assumptions and simplifications

ASSERT assumes that the liquid and vapour phases in a flow have unequal velocity and unequal temperature (UVUT). The code models the sub-channels as a series of control volumes governed by a set of five conservation equations based on the two-fluid formulation of Ishii. Mass, momentum and energy conservation are solved for the flow as a "mixture". In addition, a set of equations specifically for the liquid and vapour energy are solved.

2. Specify the numerical algorithm used (fully implicit, fully explicit; semi-implicit)

The governing equations for the control volumes are solved using Newton's method – an implicit method.

3. Specify the two-phase models and formulations used (HEM, drift flux model, two-fluid model, etc.)

ASSERT utilises the drift-flux model based on both Zuber-Findlay and Ishii.

4. Specify any optimisations of the code predictions that were performed by adjusting the model parameters to the experimental database

The lateral mixing source terms are strongly influenced by the mixing vane geometry. In order to approximate their contributions, the diversionary cross-flow term was adjusted in the following manner:

1. CAD models of the simple spacer and mixing vanes were constructed based on the benchmark specifications;
2. The blocked area of each sub-channel was computed for the spacers/vanes:
   a. Equivalent k-factors for each sub-channel were approximated by using Idelchik's formula for a thin-edged orifice. Subscript "block" refers the area (A) or perimeter (P) at the blockage, while 'up' refers to the upstream value.

$$k_{equiv} = k_{loss} + k_{frict}$$

$$\epsilon = \frac{A_{block}}{A_{up}}$$

$$k_{loss} = \left(\frac{\sqrt{0.5\epsilon} + \epsilon}{1 - \epsilon} \right)^2$$

$$k_{frict} = \frac{fLP_{up}}{4A_{up}} \left[\frac{P_{block}}{P_{up}} \left(\frac{1}{\epsilon} \right)^3 - 1 \right]$$

(6.1.1)

3. Diversionary cross-flows are modelled using the Carlucci method [1] which applies an obstruction multiplier (F_{OBS}) to the Rogers & Tahir turbulent mixing correlation (w'_{hom}).

$$w'_{hom} = F_{OBS} \left[0.0018\mu \left(\frac{S}{D_h} \right)^{-0.4} Re^{0.9} \right]$$

$$F_{OBS} = \left(1 + A_{obs} k \exp \left(-B_{obs} \frac{z}{d_h} \right) \right)$$

(6.1.2)

    a. The k-factor in the F_{OBS} was derived based on the spacer/vane geometry as previously discussed. A_{obs} and B_{obs} scale the magnitude of the multiplier as a function of the number of hydraulic diameters downstream of the obstruction.

    b. Experiments with similar mixing vanes indicate that lateral momentum decays to ~50% of its initial value roughly 20 D_h downstream of the obstruction [2]. Based on this, B_{obs} was set to 0.033 in the model.

    c. A_{obs} was estimated using one case in the fluid temperature database (01-3233). The error between the predicted and experimental fluid temperature was minimised with A_{obs} = 49.50.

4. The same adjusted factors were used for both phases of the benchmark.

AIV.6.2 Phase II – Exercise 1

1. Specify the cross-flow models used (diversion flow, void drift and turbulent mixing models)

The procedure to determine the cross-flow terms is thoroughly documented by Carlucci [1]. Under single phase conditions, the Rogers and Tahir correlation defines the turbulent mixing rate. When the fluid encounters an obstruction, the diversionary effects are represented by applying a multiplier (F_{OBS}) to the turbulent mixing term. The values in Carlucci's F_{OBS} term were found using the method described in the previous section. Void drift is calculated using Rowe's equilibrium void correlation.

2. Specify the flow regime map used

- bubbly flow: $0.0 < \alpha \le 0.20$
- slug flow: $0.20 < \alpha \le 0.50$
- churn flow: $0.50 < \alpha \le 0.80$
- annular flow: $0.80 < \alpha < 1.00$

3. Specify the interfacial mass, momentum and energy exchange models

Interfacial energy exchange was facilitated by assuming the heat transfer coefficient between the liquid and vapour phases and was fixed at 22.7 kW/m^2°C.

Specific interfacial mass and momentum correlations were not explicitly used.

4. Specify the wall drag and heat transfer models

Wall drag was modelled using the Colebrook-White friction factor correlation in single-phase conditions. The Friedel two-phase multiplier was applied under two-phase conditions.

Under single phase conditions, wall heat transfer was determined using Dittus-Boelter. The Ahmad correlation was used under two-phase conditions.

5. Specify the spacer grid modelling

The spacer grids were modelled by calculating the blocked area of each sub-channel, and representing them as k-factors. Their effect on the lateral flows is adjusted in the method described in the previous section.

6. If symmetry used, specify the symmetry applied in the model

No symmetry was assumed in the model.

7. Specify the nodalisation and boundary conditions used

Seventy nodes of uniform size were used in the model. Mass flux and fluid temperature were specified at the inlet while system pressure was used as the outlet boundary condition. All external walls were assumed to be adiabatic.

AIV.6.3 Phase II – Exercise 2

1. Specify the DNB modelling approach (mechanistic model or empirical correlation)

DNB was predicted using the 1995 Groeneveld critical heat flux look-up table for tubes [3]. The correction factors for hydraulic diameter and gap size were applied.

2. Specify the cross-flow models (diversion flow, void drift and turbulent mixing models)

Same as in the fluid temperature benchmark.

3. If symmetry used, specify the type of symmetry applied in the model

No symmetry was assumed in the model.

4. Specify the nodalisation and boundary conditions used

Same as in the fluid temperature benchmark.

AIV.6.4 Phase II – Exercise 3

1. Specify the DNB modelling approach (mechanistic model or empirical correlation)

Same as in Phase II – Ex. 1.

2. Specify the cross flow models (diversion flow, void drift and turbulent mixing models)

Same as in Phase II – Ex. 1.

3. If symmetry used, specify the kind of symmetry applied in the model

No symmetry was assumed in the model.

4. Specify the nodalisation and boundary conditions used

Same as in the fluid temperature benchmark.

AIV.6.5 References

[1] L. N. Carlucci et al. (2004), "Two-phase turbulent mixing and void drift in rod bundles", *Nuclear Engineering and Design,* vol. 224, no. 1, pp. 65-84.

[2] H. L. McClusky et al. (2002), "Development of swirling flow in a rod bundle subchannel", *J. of Fluids Engineering,* vol. 124, no. 3, pp. 747–755.

[3] D. C. Groeneveld et al. (1996), "The 1995 look-up table for critical heat flux in tubes", *Nuclear Engineering and Design*, vol. 163, pp. 1-23.

AIV.7 PSI (FLICA)

AIV.7.1 Overall questionnaire

1. Specify the governing transport equations, assumptions and simplifications

Mixture mass conservation:

$$\frac{\partial \rho}{\partial t} + \frac{\partial \rho u_i}{\partial x_i} = 0,$$

(7.1.1)

Mixture momentum conservation:

$$\frac{\partial \rho u_i}{\partial t} + \frac{\partial \rho u_i u_j}{\partial x_j} = -\frac{\partial}{\partial x_j}\left[\rho c(1-c)u_{r_i}u_{r_j}\right] - \frac{\partial P}{\partial x_i} + \frac{\partial}{\partial x_j}\left(\sum_{k=v,l}\alpha_k \sigma_{ij}^k\right) + \tau_i + \rho g_i,$$

(7.1.2)

Mixture energy conservation:

$$\frac{\partial \rho E}{\partial t} + \frac{\partial}{\partial x_i}\left[\rho E u_i + P u_i\right] = -\frac{\partial}{\partial x_i}\left[\rho c(1-c)u_{r_i}(H_v - H_l)\right] - \frac{\partial q_i}{\partial x_i}$$
$$+ \frac{\partial}{\partial x_j}\left(\sum_{k=v,l}\alpha^k \sigma_{ij}^k u_{k_j}\right) + Q + \rho g_i u_i.$$

(7.1.3)

Balance equation for the vapour mass concentration:

$$\frac{\partial \rho c}{\partial t} + \frac{\partial \rho c u_i}{\partial x_i} = -\frac{\partial}{\partial x_i}\left[\rho c(1-c)u_{r_i}\right] + \frac{\partial}{\partial x_i}\left(K_T \frac{\partial c}{\partial x_i}\right) + \Gamma_v,$$

(7.1.4)

2. Specify the numerical algorithm used (fully implicit, fully explicit; semi-implicit)

Fully implicit algorithm (Implicit Roe / VF9 scheme).

3. Specify the two-phase models and formulations used (HEM, drift-flux model, two-fluid model, etc.)

Drift-flux model (Chexal-Lellouche model).

4. Specify any optimisations of the code predictions that were performed by adjusting the model parameters to the experimental database

- turbulence Multiplier $K_t = M_t = 0.01$;
- recondensation Coefficient $K_{v0} = 7.5e\text{-}4$.

AIV.7.2 Phase II – Exercise 1

1. Specify the cross-flow models used (diversion flow, void drift and turbulent mixing

models)

Turbulence mixing model based on mixing length approach:

$$\sigma_{ij}^k = -\mu^k(1 + M_T^k)\left(\frac{\partial u_{k_i}}{\partial x_j} + \frac{\partial u_{k_j}}{\partial x_i} - \frac{2}{3}\frac{\partial u_{k_l}}{\partial x_l}\delta_{ij}\right) \tag{7.2.1}$$

Turbulent viscosity:

$$\mu_l^t = \mu_l M_l^t = \mu_l M_l \left(\text{Re} - \text{Re}^t\right)^b \cdot Y_0^C \tag{7.2.2}$$

Turbulent conductivity:

$$k_l^t = \frac{\lambda_l}{C_{pl}} K_l^t = \frac{\lambda_l}{C_{pl}} K_t \left(\text{Re} - \text{Re}^t\right)^b \cdot Y_0^C \tag{7.2.3}$$

2. Specify the flow regime map used

Single-phase and nucleate boiling regimes were considered in this benchmark.

3. Specify the interfacial mass, momentum and energy exchange models

Interfacial mass:

$$\Gamma_{lv} \propto \frac{Kv_0 H_{lv} (T_l - T_v)}{h_{lv}}$$

(7.2.4)

4. Specify the wall drag and heat transfer models

- single phase friction: Blasius correlation;

- two-phase multiplier: Friedel correlation.

Heating wall corrector:

$$f_p = 1. - \frac{P_{ch}}{P_m} * a_1 * \frac{T_p - T_l}{1. + a_2 * (\frac{T_p + T_l - 2. * 273.15}{a_4})^{a_3}}$$

(7.2.5)

Single-phase heat transfer: Dittus-Boelter correlation.

Nucleate Boiling: Jens-Lottes correlation:

$$T_w - T_{sat} = a \cdot \Phi^b \cdot \exp(\frac{-P}{p_0})$$

(7.2.6)

Nucleation on heating wall (for sub-cooled boiling):

$$\Gamma_{pv} \propto \frac{\chi \Phi}{h_{lv}}$$

(7.2.7)

where, χ is the ratio of heat flux used for nucleate boiling

5. Specify the spacer grid modelling

Spacers are located at the relevant elevation and the pressure drop by the spacer is modelled by using loss coefficients.

6. If symmetry used, specify the symmetry applied in the model.

Half symmetry was applied.

7. Specify the nodalisation and boundary conditions used.

- number of axial nodes: 100;
- axial nodding: uniform;
- number of sub-channels: 18;
- inlet: mass flux, enthalpy;
- outlet: pressure;
- heater: power.

AIV.7.3 Phase II – Exercise 2

1. Specify the DNB modelling approach (mechanistic model or empirical correlation)

Groeneveld CHF table.

2. Specify the cross-flow models used (diversion flow, void drift and turbulent mixing models)

Same as Exercise 1.

2. Specify the flow regime map used

Same as Exercise 1.

3. If symmetry used, specify the kind of symmetry applied in the model

Same as Exercise 1.

4. Specify the nodalisation and boundary conditions used

- same as Exercise 1;
- number of sub-channels for assembly A3: 28.

AIV.7.4 Phase II – Exercise 3

Questions 1 – 4: same as Exercise 2.